NUREG/IA-0466

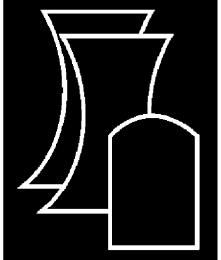

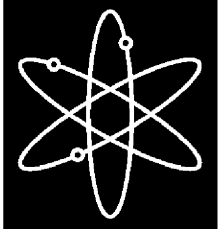

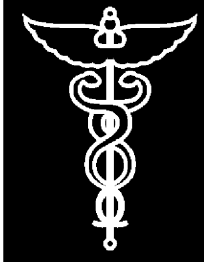

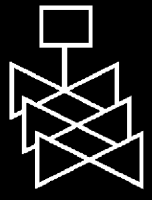

Analysis of the OSU-MASLWR 001 and 002 tests by using the TRACE code

U.S. Nuclear Regulatory Commission
Office of Nuclear Regulatory Research
Washington, DC 20555-0001

AVAILABILITY OF REFERENCE MATERIALS IN NRC PUBLICATIONS

NRC Reference Material

As of November 1999, you may electronically access NUREG-series publications and other NRC records at NRC's Public Electronic Reading Room at http://www.nrc.gov/reading-rm.html. Publicly released records include, to name a few, NUREG-series publications; *Federal Register* notices; applicant, licensee, and vendor documents and correspondence; NRC correspondence and internal memoranda; bulletins and information notices; inspection and investigative reports; licensee event reports; and Commission papers and their attachments.

NRC publications in the NUREG series, NRC regulations, and *Title 10, Energy*, in the Code of *Federal Regulations* may also be purchased from one of these two sources.

1. The Superintendent of Documents
   U.S. Government Printing Office
   Mail Stop SSOP
   Washington, DC 20402-0001
   Internet: bookstore.gpo.gov
   Telephone: 202-512-1800
   Fax: 202-512-2250
2. The National Technical Information Service
   Springfield, VA 22161-0002
   www.ntis.gov
   1-800-553-6847 or, locally, 703-605-6000

A single copy of each NRC draft report for comment is available free, to the extent of supply, upon written request as follows:

Address: Office of the Chief Information Officer,
Reproduction and Distribution
Services Section
U.S. Nuclear Regulatory Commission
Washington, DC 20555-0001
E-mail: DISTRIBUTION@nrc.gov
Facsimile: 301-415-2289

Some publications in the NUREG series that are posted at NRC's Web site address http://www.nrc.gov/reading-rm/doc-collections/nuregs are updated periodically and may differ from the last printed version. Although references to material found on a Web site bear the date the material was accessed, the material available on the date cited may subsequently be removed from the site.

Non-NRC Reference Material

Documents available from public and special technical libraries include all open literature items, such as books, journal articles, and transactions, *Federal Register* notices, Federal and State legislation, and congressional reports. Such documents as theses, dissertations, foreign reports and translations, and non-NRC conference proceedings may be purchased from their sponsoring organization.

Copies of industry codes and standards used in a substantive manner in the NRC regulatory process are maintained at—

The NRC Technical Library
Two White Flint North
11545 Rockville Pike
Rockville, MD 20852-2738

These standards are available in the library for reference use by the public. Codes and standards are usually copyrighted and may be purchased from the originating organization or, if they are American National Standards, from—

American National Standards Institute
11 West 42nd Street
New York, NY 10036-8002
www.ansi.org
212-642-4900

Legally binding regulatory requirements are stated only in laws; NRC regulations; licenses, including technical specifications; or orders, not in NUREG-series publications. The views expressed in contractor-prepared publications in this series are not necessarily those of the NRC.

The NUREG series comprises (1) technical and administrative reports and books prepared by the staff (NUREG–XXXX) or agency contractors (NUREG/CR–XXXX), (2) proceedings of conferences (NUREG/CP–XXXX), (3) reports resulting from international agreements (NUREG/IA–XXXX), (4) brochures (NUREG/BR–XXXX), and (5) compilations of legal decisions and orders of the Commission and Atomic and Safety Licensing Boards and of Directors' decisions under Section 2.206 of NRC's regulations (NUREG–0750).

NUREG/IA-0466

Analysis of the OSU-MASLWR 001 and 002 tests by using the TRACE code

Manuscript Completed: October 2015
Date Published: March 2016

Prepared by: Fulvio Mascari[1], Brian G. Woods[2], Kent Welter[3], Giuseppe Vella[4], Francesco D'Auria[5], Felice De Rosa[1]

[1]ENEA- Via Martiri di Monte Sole 4, Bologna, Italy
[2]Department of Nuclear Engineering and Radiation Health Physics, Oregon State University, 116 Radiation Center, Corvallis, OR 97331-5902, USA.
[3]NuScale Power Inc., 1100 NE Circle Blvd, Suite 200, Corvallis, OR 97330, USA.
[4]Dipartimento dell'Energia, Università degli Studi di Palermo,90128 Palermo, Italia
[5]San Piero a Grado – Nuclear Research Group (SPGNRG), University of Pisa, Italy

K. Tien, NRC Project Manager

Prepared for:
Division
Office
U.S. Nuclear Regulatory Commission
Washington, DC 20555-0001

ABSTRACT

The Oregon State University (OSU) has constructed, under a U.S. Department of Energy grant, a scaled integral test facility to examine natural circulation phenomena characterizing the Multi-Application Small Light Water Reactor (MASLWR) design. The MASLWR is a small modular PWR relying on natural circulation during both steady-state and transient operation, which includes an integrated helical coil steam generator within the reactor pressure vessel. Testing has been conducted in order to assess the operation of the prototypical MASLWR under normal full pressure and full temperature conditions and to assess the passive safety systems performance. The experimental data produced are useful also for the assessment of the computational tools necessary for the operation, design and safety analysis of nuclear reactors.

This report describes the assessment of TRACE code predictions, conducted under the NRC CAMP program, against the MASLWR tests OSU-MASLWR-001 and the OSU-MASLWR-002, respectively. This activity has been conducted in collaboration with the Italian National Agency for the New Technologies, Energy and Sustainable Economic Development (ENEA), the Department of Energy of the University of Palermo, the Gruppo di Ricerca Nucleare San Piero a Grado (GRNSPG) of University of Pisa, the Department of Nuclear Engineering and Radiation Health Physics at OSU and NuScale Power Inc. In particular the OSU-MASLWR-001 test, an inadvertent actuation of one submerged ADS valve, investigates the primary system to containment coupling under design basis accident conditions; the OSU-MASLWR-002 test, a natural circulation test, investigates the primary system flow rates and secondary side steam superheat for a variety of core power levels and feed water flow rates. The assessment against experimental data shows that the TRACE code predicts the main phenomena of interest of the selected tests reasonably well for most conditions.

CONTENTS

FIGURES

TABLES

ABBREVIATIONS

ADS	Automatic Depressurization System;
BIC	Boundary and Initial Condition
CL	Cold Leg;
CPV	Cooling Pool Vessel;
FW	Feed Water;
HL	Hot Leg;
HPC	High Pressure Containment;
IAEA	International Atomic Energy Agency;
ICSP	International Collaborative Standard Problem;
LOCA	Loss of Coolant Accident;
LP	Lower Plenum;
LWR	Light- Water Reactor;
MASLWR	Multi-Application Small Light Water Reactor;
OSU	Oregon State University;
PRZ	Pressurizer;
PWR	Pressurized Water Reactor;
RPV	Reactor Pressure Vessel;
SBLOCA	Small Break Loss of Coolant Accident;
SG	Steam Generator;
SOT	Start of the Transient;
SNAP	Symbolic Nuclear Analysis Package;
TRAC	Transient Reactor Analysis Code;
TRACE	TRAC/RELAP Advanced Computational Engine;
UP	Upper Plenum;
USNRC	U.S. Nuclear Regulatory Commission.

1. INTRODUCTION

The Oregon State University (OSU) has constructed, under a U.S. Department of Energy grant, an integral test facility called MASLWR. The purpose of this integral test facility is to examine the natural circulation phenomena characterizing the MASLWR design in steady and transient conditions.

The MASLWR [1][1] reactor concept is shown in Fig. 1 and was developed by Idaho National Engineering and Environmental Laboratory, OSU and NEXANT–Bechtel. It is a small modular Pressurized Water Reactor (PWR) relying on natural circulation for steady-state and transient operation. The design includes an integrated Steam Generator (SG) consisting of banks of vertical helical tubes contained within the Reactor Pressure Vessel (RPV) and located in the upper region of the vessel outside of the Hot Leg (HL) chimney. During steady-state conditions the primary fluid, in single phase natural circulation, removes the core power and transfers it to the secondary fluid via shell-side of the SG. Then the Feed Water (FW) is fully vaporized in the tube-side of SG resulting in superheated steam at the SG outlet.

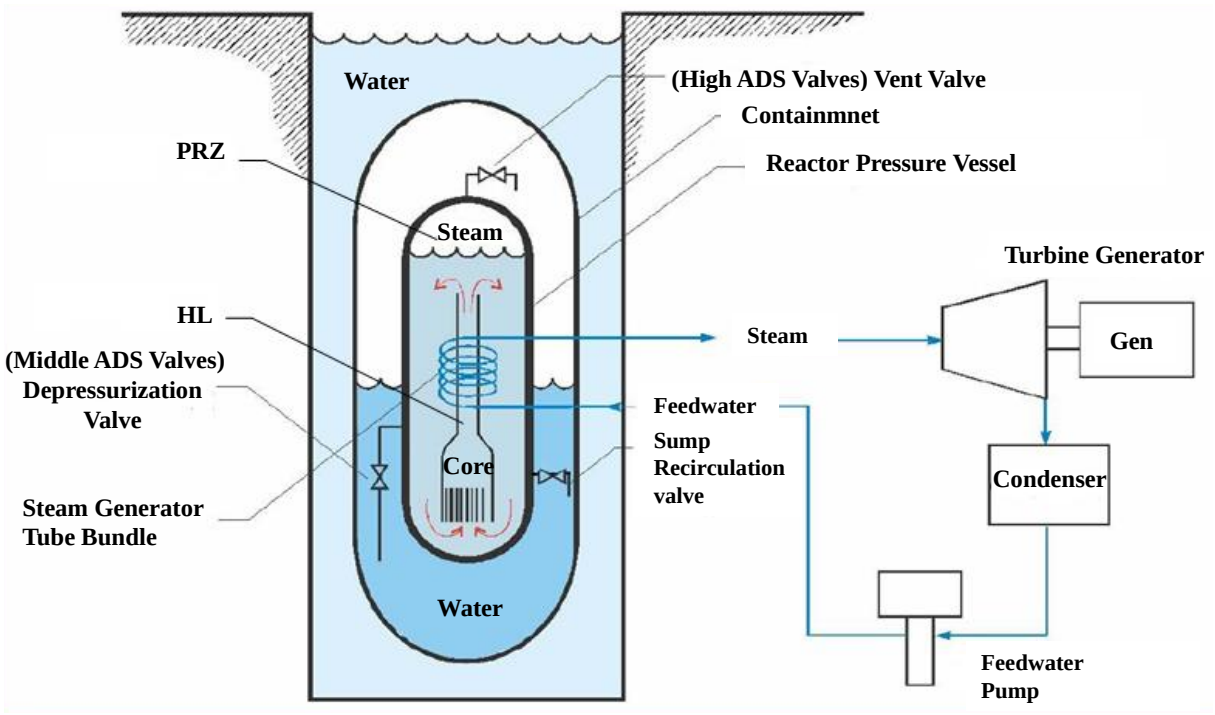

Figure 1 MASLWR Conceptual Design Layout [1,3,18,19,20]

The RPV is surrounded by a cylindrical containment partially filled with water that provides pressure suppression and liquid makeup capabilities during design basis events. The containment is submerged in a pool of water that acts as the ultimate heat sink. The RPV can be depressurized using the Automatic Depressurization System (ADS) which consists of six valves discharging into various locations within the containment. Specifically, the ADS design includes two independent vent valves (high ADS valves), two independent depressurization valves (middle ADS valves) and two independent sump recirculation valves (low ADS valves).

The integral arrangement of the MASLWR reactor allows avoiding pressurized primary components outside the RPV eliminating the possibility of large break Loss of Coolant Accident (LOCA) and reducing the potential for Small Break LOCA (SBLOCA) events. Of particular interest is the SBLOCA mitigation strategy based on a passive primary/containment coupling and natural circulation. For example, given an inadvertent opening of an ADS valve, the primary side blows down into the containment takes place. The RPV blowdown causes a primary pressure decrease and a consequent containment pressure increase causing a safety injection signal. When a safety signal is received, the high ADS valves automatically actuate, along with the middle ADS valves and the sump recirculation valves. As the primary and the containment pressures equalize, the blowdown is terminated, and a natural circulation flow path is established between the containment and primary system. When the sump recirculation valves are opened the vapor produced in the core travels to the upper RPV and exits through the high ADS valve. The vapor is then condensed on the inside surface of the containment with the condensate being captured in the lower part of the containment. The condensate in the lower part of the containment is then returned to the primary system via recirculation valves. The containment is also submerged in a pool and acts as the ultimate heat sink [2,4,19,20] for design basis events.

A scaling analysis of the OSU-MASLWR experimental facility was performed in order to evaluate potential scaling distortions in the test facility compared to the prototype reactor. The scaling method used for the design of the facility was the Hierarchical Two-Tiered Scaling (H2TS) Methodology [2, 4, 5, 6]. The detailed OSU-MASLWR scaling analyses is reported in [2,4]. Some of the main facility scaling parameters are reported in Table 1 [1,34].

A testing program has been conducted in order to assess the operation of the MASLWR design under full pressure and full temperature conditions and to assess the passive safety system performance. The experimental data produced are useful also for the assessment of the computational tools necessary for the operation, design and safety analysis of nuclear reactors [1-4,19].

After the completion of the first test series, through a grant from the International Atomic Energy Agency (IAEA), the OSU-MASLWR test facility core was reconfigured to eliminate a recurring grounding problem and improve facility reliability in anticipation of conducting an IAEA International Collaborative Standard Problem (ICSP) on "Integral PWR Design Natural Circulation Flow Stability and Thermohydraulic Coupling of Primary System and Containment During Accidents". This ICSP was hosted at OSU with experimental data from the OSU-MASLWR facility. The data provides insights into single/two-phase flow instability phenomena under natural circulation conditions and coupled containment/reactor vessel behavior in integral type light water reactors [33-43].

Table 2 shows the test performed in the OSU-MASLWR and available at the international community.

[1]The MASLWR design is the basis for the NuScale Power integral reactor design [9,10].

Table 1 OSU-MASLWR Main Scaling Parameters [1,34]

Parameter	MASLWR	OSU-MASLWR	Note
Time Scale	1:1	1:1	Time preserved facility
Volumetric Scale	1:1	1:254.7	Reduced volume facility
Height Scale	1:1	1:3	Reduced height facility
Design Primary Pressure (MPa)	8.6	11.4	Full pressure facility
Loop Number	1	1	Integral test facility
Hot Leg Riser D (mm)	914.4	102.3	
Power (MW)	150	0.6	Full power facility
Core Rod Number	6336	56	
Core Rod DIA (mm)	9.5222	15.9	
Heated Length (m)	1.35	0.686	
SG Type	Vertical once-through helical tubes	Vertical once-through helical tubes	
SG Bundle	2	3	
SG Tubes Number For Bundle	506	5, 5, 4	
SG OD Tube (mm)	15.9	15.9	

Table 2 Test Performed in the OSU-MASLWR Test Facility Available at the International Community [1,43]

	Test	Test Type
DOE	OSU-MASLWR-001	Inadvertent Actuation of 1 Submerged ADS Valve
	OSU-MASLWR-002	Natural Circulation at Core Power up to 210 kW
	OSU-MASLWR-003A	Natural Circulation at Core Power of 210 kW
	OSU-MASLWR-003B	Inadvertent Actuation of 1 High Containment ADS Valve
IAEA	ICSP test SP-2	Loss of Feedwater Transient
	ICSP test SP-3	Power Maneuvering

2. OSU-MASLWR TEST FACILITY DESCRIPTION

2.1 OSU-MASLWR Overview

As a result of the scaling analyses the OSU-MASLWR [1- 7,19, 34,35] test facility, shown in Fig. 2, is scaled at 1:3 length scale, 1:254.7 volume scale and 1:1 time scale, is constructed entirely of stainless steel, and is designed for full pressure and full temperature prototype operation. It includes the primary circuit, consisting of the RPV and ADS lines, the secondary circuit and the containment structures. In addition to the physical structures that comprise the test facility, there are data acquisition, instrumentation and control systems. Auxiliary lines and systems are present in the facility. The OSU-MASLWR test facility process and instrumentation diagram are shown in Fig. 3. Table 3 shows the OSU-MASLWR test facility instrumentation; Table 4 shows the OU-MASLWR instrumentation type.

Figure 2 OSU-MASLWR Experimental Facility Photo [3,18,19,20]

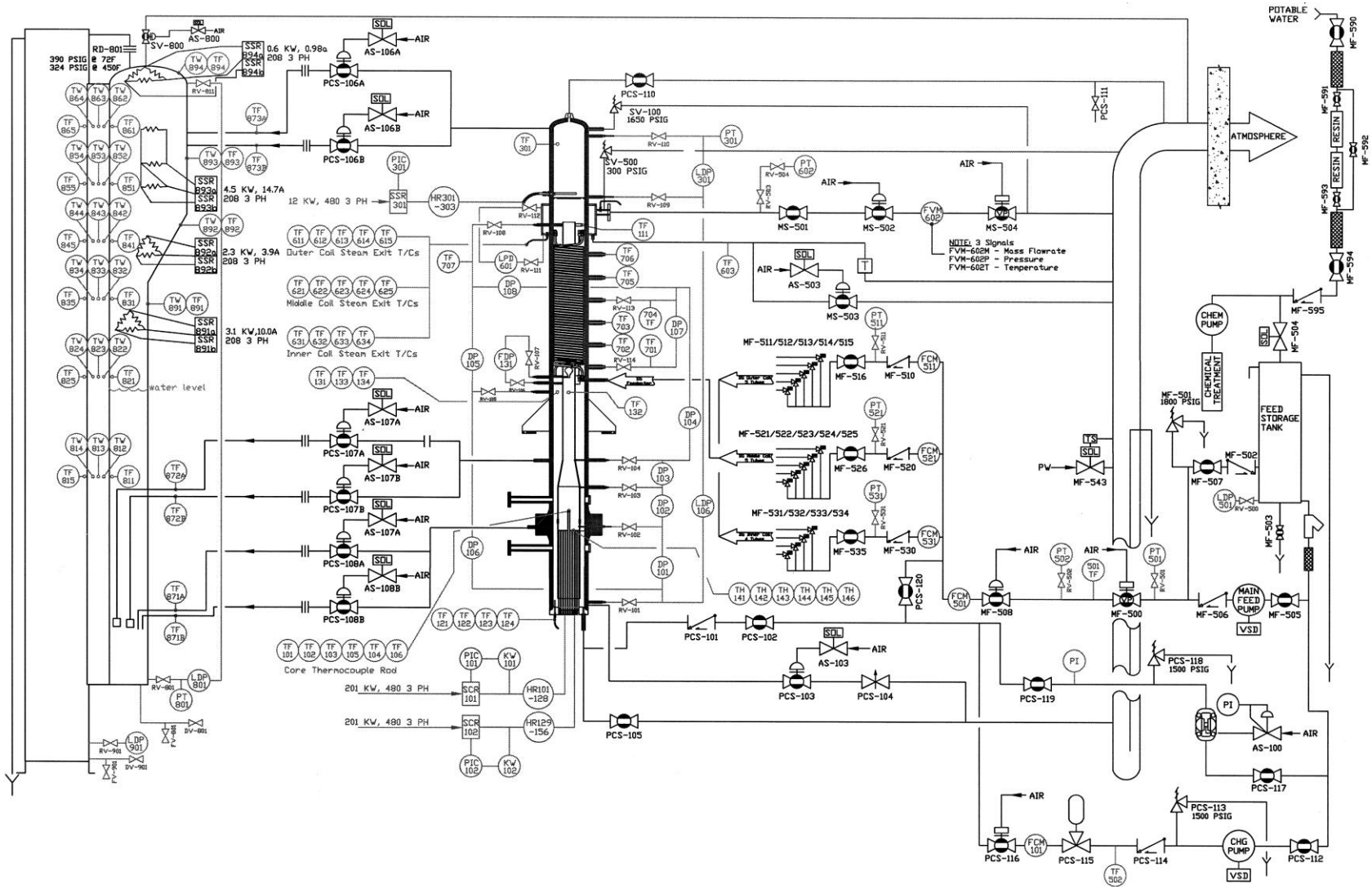

Figure 3 OSU-MASLWR Test Facility Process and Instrumentation Diagram [19,35]

Table 3 OSU-MASLWR Test Facility Instrumentation [34]

Tag number	Description
LDP-501	Feed water storage tank level
FMM-501	Feed water mass flow rate
TF-501	Feed water temperature
FCM-511	Feed water supply in the steam generator outer coil mass flow rate
PT-511	Feed water pressure in the steam generator outer coil supply pipe
FCM-521	Feed water supply in the steam generator middle coil mass flow rate
PT-521	Feed water pressure in the steam generator middle coil supply pipe
FCM-531	Feed water supply in the steam generator inner coil mass flow rate
PT-531	Feed water pressure in the steam generator inner coil supply pipe
LDP-601	Feed water supply collector level
PT-602	Main steam pressure
FVM-602-P	Main steam pressure
FVM-602-T	Main steam temperature
FVM-602-M	Main steam mass flow rate
TF-603	Steam drain line temperature
TF-611, 612, 613, 614, 615	Thermocouples inside the outer coil pipe of the steam generator exit
TF-621, 622, 623, 624, 625	Thermocouples inside the middle coil pipe of the steam generator exit
TF-631, 632, 633, 634	Thermocouples inside the inner coil pipe of the steam generator exit
TF-101, 102, 103, 104, 105, 106	Center of core thermocouple rod, six thermocouples spaced 6 inches apart, measuring water temperatures
TH-141, 142, 143, 144, 145, 146	Core heater rod temperatures
TF-121, 122, 123, 124	Core inlet temperatures
TF-131, 133, 134	Primary containment water down flow temperatures after steam generator coils
TF-132	Primary containment water temperature inside chimney below steam generator coil
TF-111	Primary containment water temperature at top of chimney
TF-301	Steam temperature in pressurizer
PT-301	Steam pressure in pressurizer
LDP-301	Primary containment water level in the pressurizer
DP-101	Pressure loss in the core
DP-102	Pressure loss between core top and riser cone
DP-103	Pressure loss in the riser cone
DP-104	Pressure loss in the chimney
DP-105	Pressure loss across steam generator
DP-106	Pressure loss in the annulus below steam generator
LDP-106	Primary containment water level
TF-811, 821, 831, 841, 851, 861	Water temperatures located inside the HPC near the heat transfer plate
TF-815, 825, 835, 845, 855, 865	Water temperatures located inside the CPV near the heat transfer plate
TW-812, 822, 832, 842, 852, 862	Wall temperatures within the heat transfer plate between the CPV and the HPC, nearest to the HPC
TW-813, 823, 833, 843, 853, 863	Wall temperatures at the midpoint of the heat transfer plate between the CPV and the HPC
TW-814, 824, 834, 844, 854, 864	Wall temperatures within the heat transfer plate between the CPV and the HPC, nearest to the CPV
TH-891, 892, 893, 894	Temperatures of Heaters located on the walls of the HPC
TW-891, 892, 893, 894	Temperatures within the walls of the HPC, between the heaters and the water

TF-871A, 871B, 872A, 872B, 873A, 873B	Water temperatures inside the automatic depressurization system (ADS) lines outside of the HPC vessel
PT-801	HPC pressure
LDP-801	HPC level
LDP-901	CPV level
TF-882	CPV water temperature
FDP-131	Differential pressure from V-Cone flowmeter within hot leg chimney
KW-101, 102	Measures power to the core heater rod bundles
KW-301	Measures power to pressurizer heater

Table 4 OSU-MASLWR Instrumentation Type [34]

Instrumentation type	Tag number
Vortex flow meter	FVM-602
Coriolis flow meter	FCM-511, -521, -531
Magnetic flow meter	FMM-501
Thermocouple	TW-xxx, TF-xxx, TH-xxx
Pressure meter	PT-511, -521, -531
Pressure meter	PT-301
Pressure meter	PT-602
Pressure meter	PT-801
Differential pressure meter	DP-101, -103, -105
Differential pressure meter	DP-102
Differential pressure meter	DP-104
Differential pressure meter	DP-106
Differential pressure meter	DP-107
Differential pressure meter	DP-108
Flow differential pressure meter	FDP-131
Level differential pressure meter	LDP-106
Level differential pressure meter	LDP-301
Level differential pressure meter	LDP-501, -801
Level differential pressure meter	LDP-901
Level differential pressure meter	LDP-601
Power meter	KW-101, -102

2.2 OSU-MASLWR RPV Description

The internal components of the RPV, Fig. 4, are the core, the HL riser, the Upper Plenum (UP), the Pressurizer (PRZ), the SG primary side, the Cold Leg (CL) downcomer and the Lower Plenum (LP).

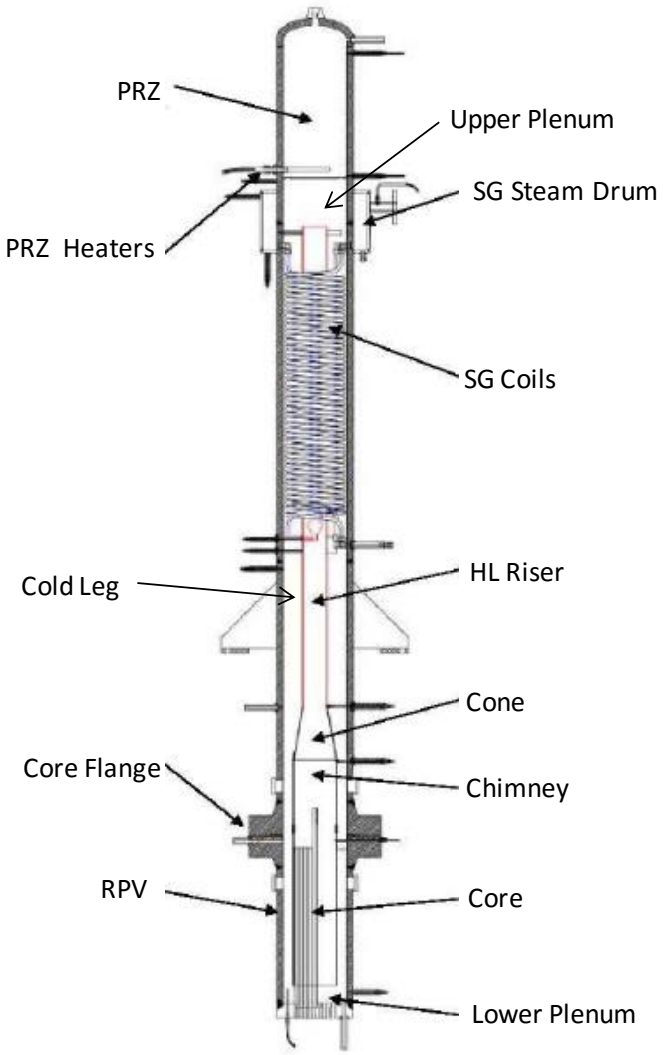

Figure 4 RPV Internals Component [3,18,19,20]

The core is modelled with 56 cylindrical heater rods distributed in a 1.86 cm pitch square array with a 1.33 pitch to diameter ratio. The nominal power of each heater rod is 7.1 kW resulting in a maximum core power of 398 kW. The diameter of the core rod is 1.59 cm. A lower core flow plate, Fig. 5, contains 76 auxiliary flow holes of 0.635 cm of diameter, arranged at 1.86 cm pitch square array, and 57 core rod flow holes. In order to create a flow annulus between the flow plate and the core rod, the holes of the rodded lower core flow plate are oversized at 1.72 cm. The core is shrouded, Fig. 6, to ensure all flow enters the core via the bottom and travels the entire heated length. The shroud is shaped to partially block the primary coolant flow through the outermost auxiliary flow holes in order to ensure that each heated rod receives approximately equal axial coolant flow. The amount of blockage is dependent on the number and location of heated rods

adjacent to each auxiliary flow hole. At mid elevation a core grid wires, Fig. 7, is considered in order to maintain the radial alignment of the core rods. Four thermocouples for measuring the core inlet temperatures are located at the bottom CL entering the core. The core heater rod temperatures are measured. Six thermocouples vertically spaced every 15.24 cm measuring water temperatures, are located in the center of core thermocouple rod. The pressure loss in the core is measured; the power to the core heater rod bundles is measured as well.

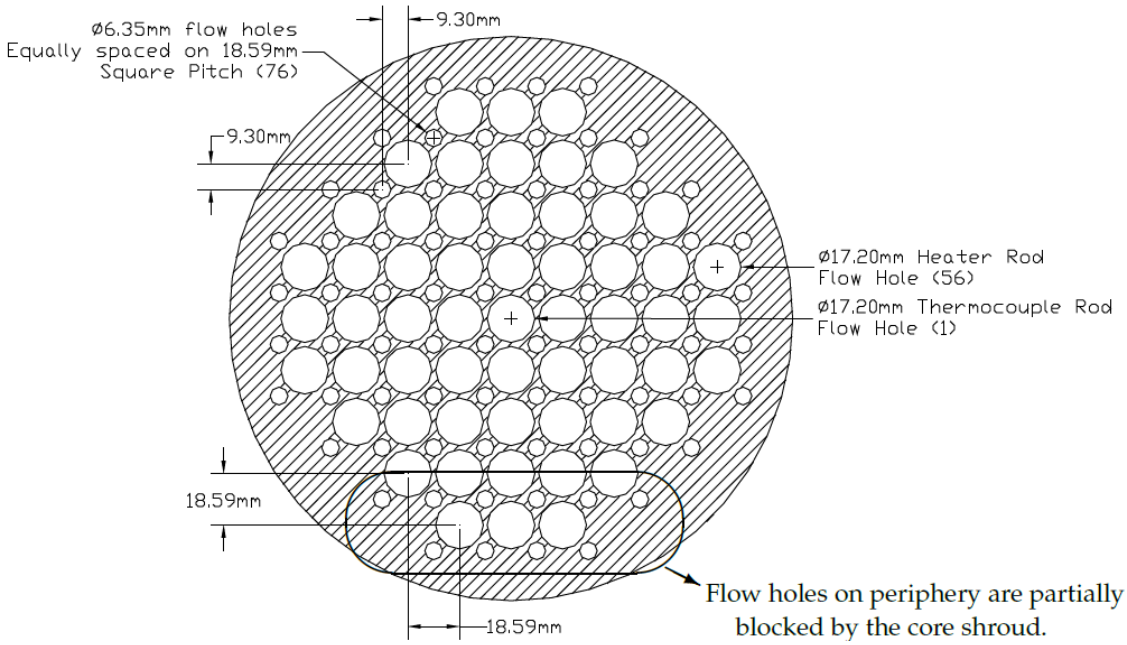

Figure 5 Lower Core Flow Plate Layout [7,19,20] See Figure 6 for Flow Blockage Detail

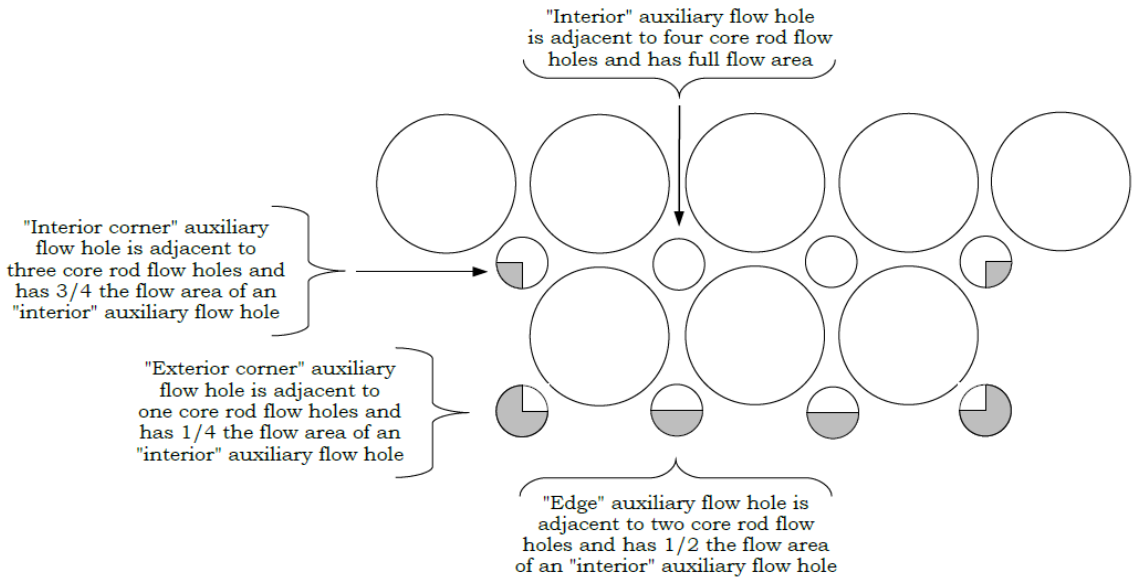

Figure 6 Auxiliary Flow Hole Blockage by Core Shroud [7,19,20]

The HL riser, Fig. 4, consists of a lower region, an upper region and a transition region. The lower region consists of a pipe with an outside diameter of 20.32 cm, an inside diameter of 19.71 cm and a wall thickness of 0.305 cm. The upper region consists of a pipe with an outside diameter of 11.43 cm, an inside diameter of 10.23 cm, and a wall thickness of 0.602 cm. The transition region consists of a cone with a 0.305 cm thickness and an half angle of 20.61°. The pressure loss between core top and riser cone, the pressure loss in the riser cone and the pressure loss in the chimney, from the exit of the transition cone to the UP, are measured. Along the riser a thermocouple measures the water temperature inside chimney below SG coil and another one measures the water temperature at top of chimney. The flow rate within the HL chimney is measured with a differential pressure cell used to measure flow. The primary containment water level is measured as well.

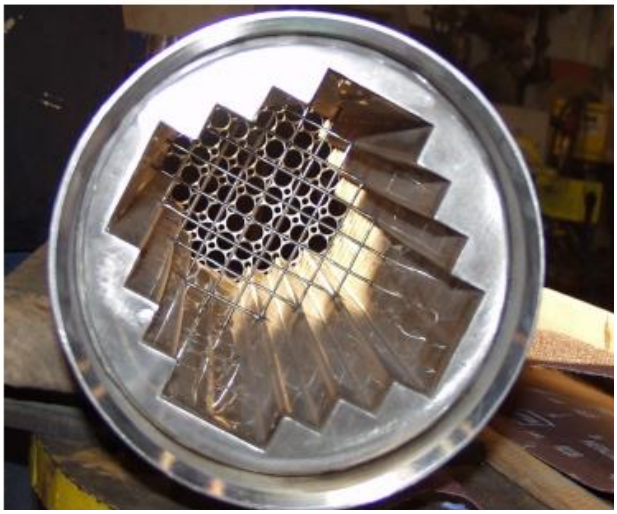

Figure 7 Core Shroud Photo [7,19,20]

The UP is separated from the heated upper PRZ section by a thick baffle plate having eight 2.54 cm holes, spaced uniformly around the baffle plate periphery, which allow free communication of the PRZ to the remainder of the RPV during normal operation and for volume surges into and/or out of the PRZ due to transients.

The PRZ is integrated in the RPV and is located in its upper part. In the PRZ are located three heater elements, each 4 kW, that are modulated by the test facility control system to maintain nominal primary system pressure at the desired value. The PRZ steam temperature and pressure are measured. The PRZ level is measured as well.

The CL downcomer region, Fig. 4, is an annular region bounded by the RPV wall on the outside and the HL riser on the inside, and the flow area reduces at the HL riser cone. In the SG primary side section is inserted the SG helical coil bundle, Fig. 8 and 9. Thermocouples are located in the CL downcomer region to measure water down flow temperatures after SG coils. The primary side pressure loss across SG and the pressure loss in the annulus below SG are measured. The RPV shell is covered by Thermo-12 hydrous calcium silicate insulation.

2.3 OSU-MASLWR Secondary Side

The secondary circuit includes the FW treatment and storage system, the Main FW Pump (MFP), the Main FW (MFW) system supply lines, the SG secondary side internal to the vessel, the Main Steam (MS) system and associated FW and steam valves.

Potable water, coming from the city water supply, passes through a mechanical filter and a resin bed to remove impurities and flows to the FW storage tank. The MFW system supplies deionized and demineralized water to the SG. The MFP is a positive displacement pump and can be isolated from the downstream main FW system supply lines by pneumatic motor operated globe valve MF-508 (FW supply valve). The MFP controller is interlocked with the MFP discharge isolation valve MF-508 position, to ensure that the MFP is not energized unless MF-508 is fully open. The single MFW line splits into three supply lines, one for each coil bank of SG tubes.

Figure 8 Helical Coil SG Bundle Photo [18,19,34]

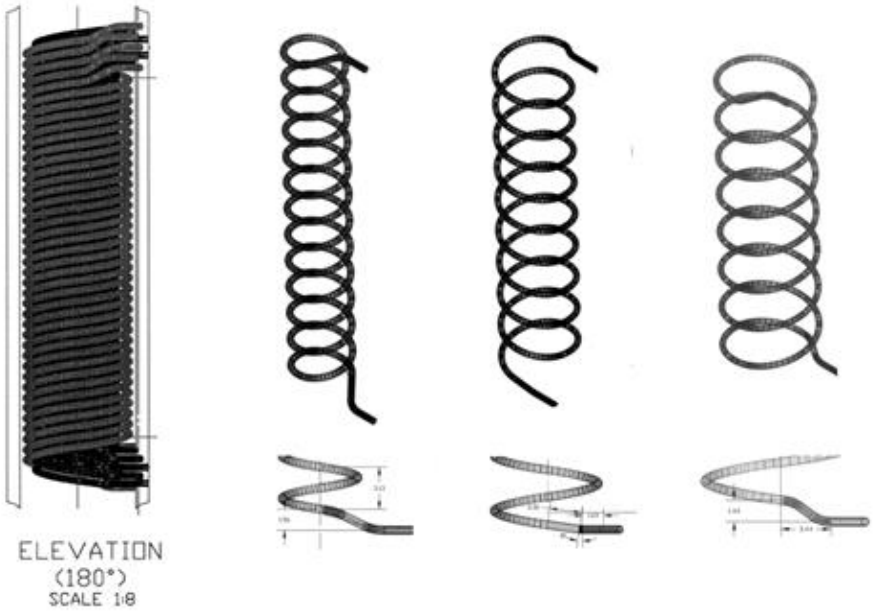

Figure 9 Helical Coil SG Bundle [19,35]

The SG of the facility is a once through heat exchanger and is located within the RPV in the annular space between the HL riser and the inside surface of the RPV. The tube bundle, Fig. 8 and 9, is a helical coil consisting of fourteen tubes. There are three separate parallel coils of stainless steel tubes. The outer and middle coils consist of five tubes each while the inner coil consists of four

tubes. Some SG geometrical data are reported in Table 5.

Table 5 SG Geometrical Data [18]

	Inner	Mid	Outer
Number of Tubes in Bank	4	5	5
Number of Rotations From Feed Inlet to Steam Outlet	13	9.5	7.5
Average Tube Length of The Bank (m)	6.05	6.15	6.21
Total Average Tube Length (m)	6.21	6.30	6.36
Total Tube Bank Surface Area (m^2)	1.209	1.532	1.550
Individual Tube Outside Diameter (m)	0.0159	0.0159	0.0159
Individual Tube Wall Thickness (m)	0.00165	0.00165	0.00165

Each coil is joined at a common inlet header and each of them exhausts the superheated steam into a common steam drum from where it is subsequently exhausted to atmosphere via the MS system. The FW, enters at the bottom of the SG and boils off after travelling a certain length in the SG. This boil off length is a function of both core power and MFW flow rate. Nominally, the boil off length is approximately 40% shorter than the actual length of the SG tubes so the steam will leave the SG superheated. The value of the degree of the steam superheat is changed in order to control the facility.

The steam received in the SG steam drum goes to the MS line, Fig. 10, and that exhausts the SG superheated steam to atmosphere. A pneumatic motor operated globe valve MS-502 (MS header drain line isolation valve) is immediately downstream of the SG steam drum. Another motor operated globe valve, MS-503 (MS header isolation valve), isolates the MS header from the steam header drain line. In order to have always an open discharge for the SG, the MS-502 and MS-503 are interlocked to prevent them both from being simultaneously commanded shut.

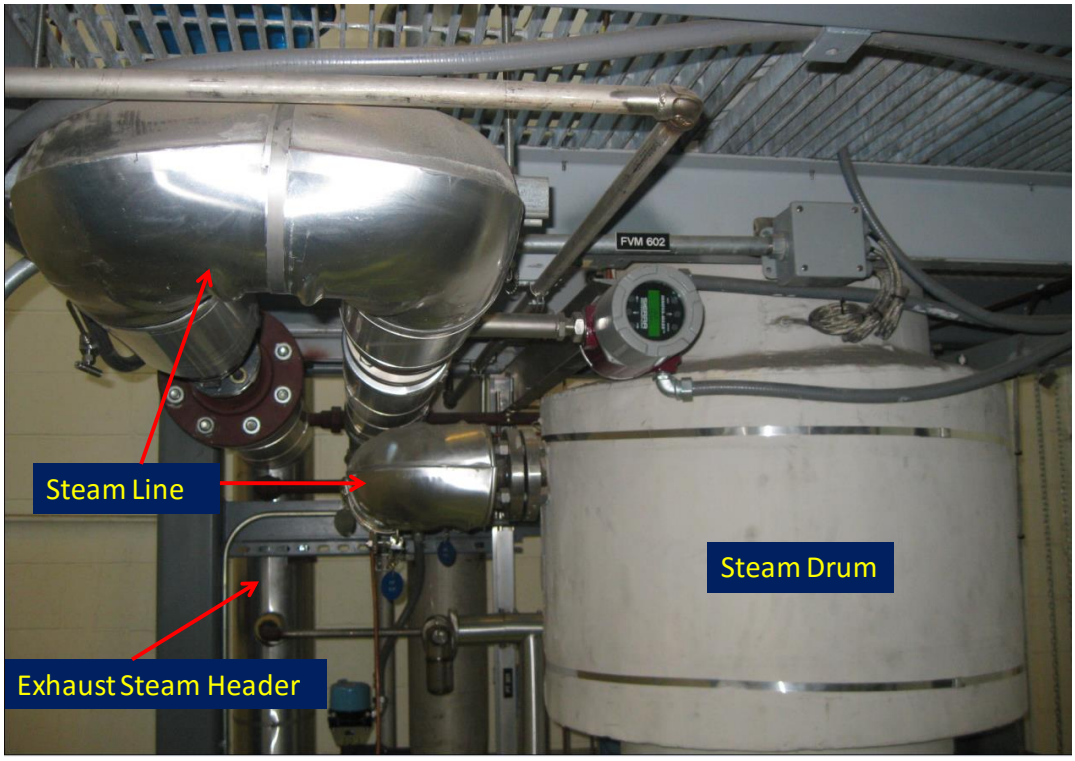

Figure 10 Main Steam Line Photo [19]

2.4 OSU-MASLWR Containment Structures

The HPC, Fig. 11, consists of a lower cylindrical section, an eccentric cone section, an upper cylindrical section and an hemispherical upper end head. For scaling reasons, in order to have an adiabatic boundary condition in all the wall of the HPC except through the heat transfer plate wall where the condensation has to take place, four groups of containment heaters have been installed permitting the heat transfer takes place only between the CPV and HPC containment. These heaters are located in the exterior surface of the HPC, under the insulation, and above the containment water level. The temperatures of the heaters located on the walls of the HPC and the temperatures within the walls of the HPC, between the heaters and the water, are measured. The HPC level and pressure are measured. The entire HPC is covered by Thermo-12 hydrous calcium silicate insulation.

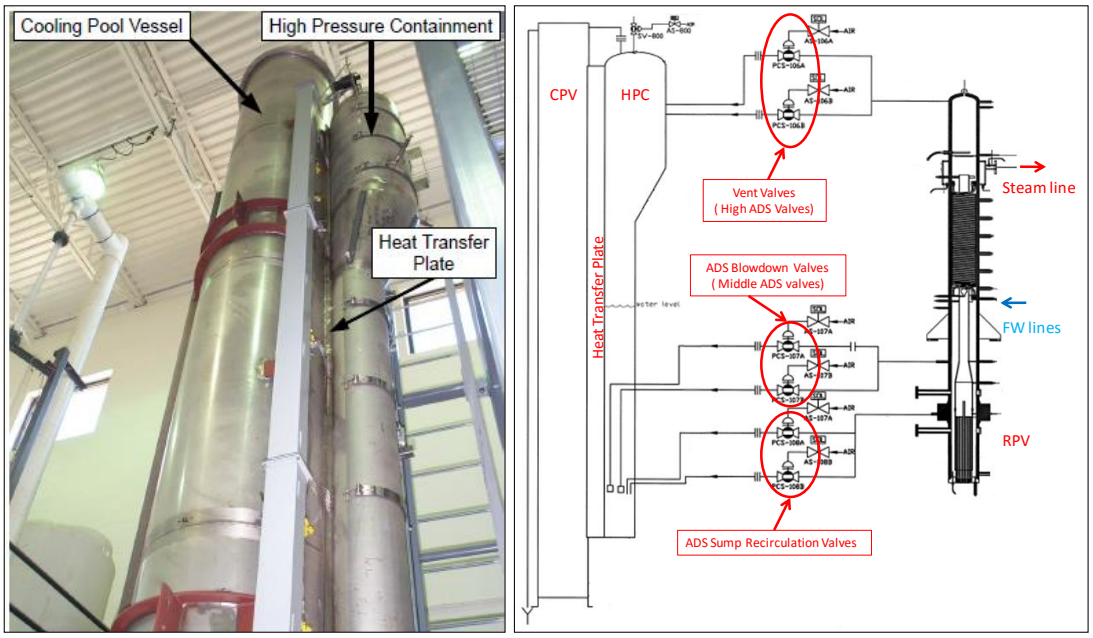

Figure 11 OSU-MASLWR Containment Structures [3,17,19,20]

The CPV consists of a tall right cylindrical tank. One disk rupture is connected between the HPC and the CPV. The CPV level and water temperature are measured. The CPV is covered by Thermo-12 hydrous calcium silicate insulation.

The heat transfer plate, having the same height of the HPC without the hemispherical head, provides the heat conduction between the HPC and CPV. The heat transfer plate is scaled in order to model the heat transfer area between the MASLWR design high pressure containment vessel and the cooling pool in which it sits.

Five thermocouples are located at six different elevations to measure the temperature distribution from the HPC to the CPV. In particular one group of thermocouples measures the water temperatures located inside the HPC near the heat transfer plate, one measures the water temperatures located inside the CPV near the heat transfer plate, one measures the wall temperatures at the midpoint of the heat transfer plate between the CPV and the HPC, one measures wall temperatures within the heat transfer plate between the CPV and the HPC nearest to the HPC and one measures wall temperatures within the heat transfer plate between the CPV and the HPC nearest to the CPV.

2.5 OSU-MASLWR ADS Lines

The high ADS lines, Fig. 12, are horizontally oriented and connect the PRZ steam space with the HPC. A pneumatic motor operated globe valve is located in each line. Downstream from each isolation valve is a transition piece with an internal square-edge orifice. The two high ADS lines enter the HPC above the waterline, penetrate it and then terminate with a sparger.

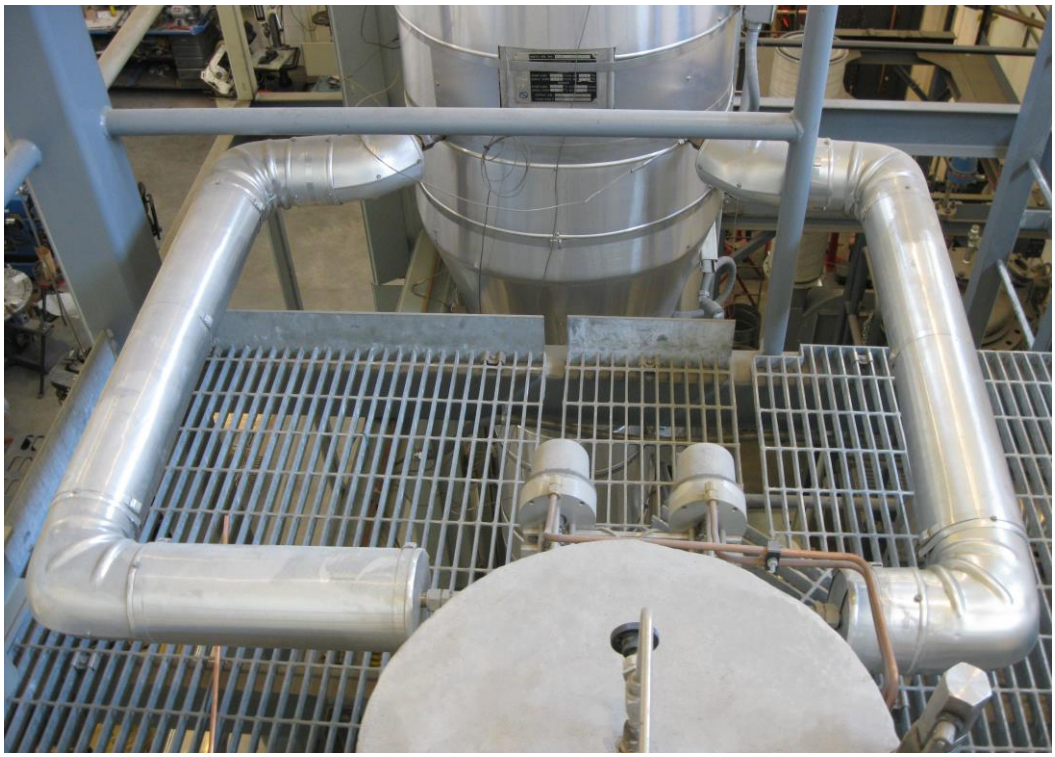

Figure 12 High ADS Lines Photo [20]

The middle ADS lines are horizontally oriented and connect the RPV CL to the HPC. A pneumatic motor operated globe valve is located in each line. Downstream from each isolation valve is a transition piece with an internal square-edge orifice. These two lines enter the HPC, penetrate it and then turn downward before terminating below the HPC waterline. A sparger is considered at the end of these lines.

The ADS sump recirculation lines are horizontally oriented and connect the RPV lower CL to the HPC. A pneumatic motor operated globe valve is located in each line. Downstream from each isolation valve is a transition piece with an internal square-edge orifice. These two lines enter the HPC, penetrate it and then turn downward before terminating below the HPC waterline. No sparger is considered for these lines.

The water temperatures inside the ADS lines outside of the HPC are measured. The penetration elevation of the HPC and CPV are shown in Fig. 13.

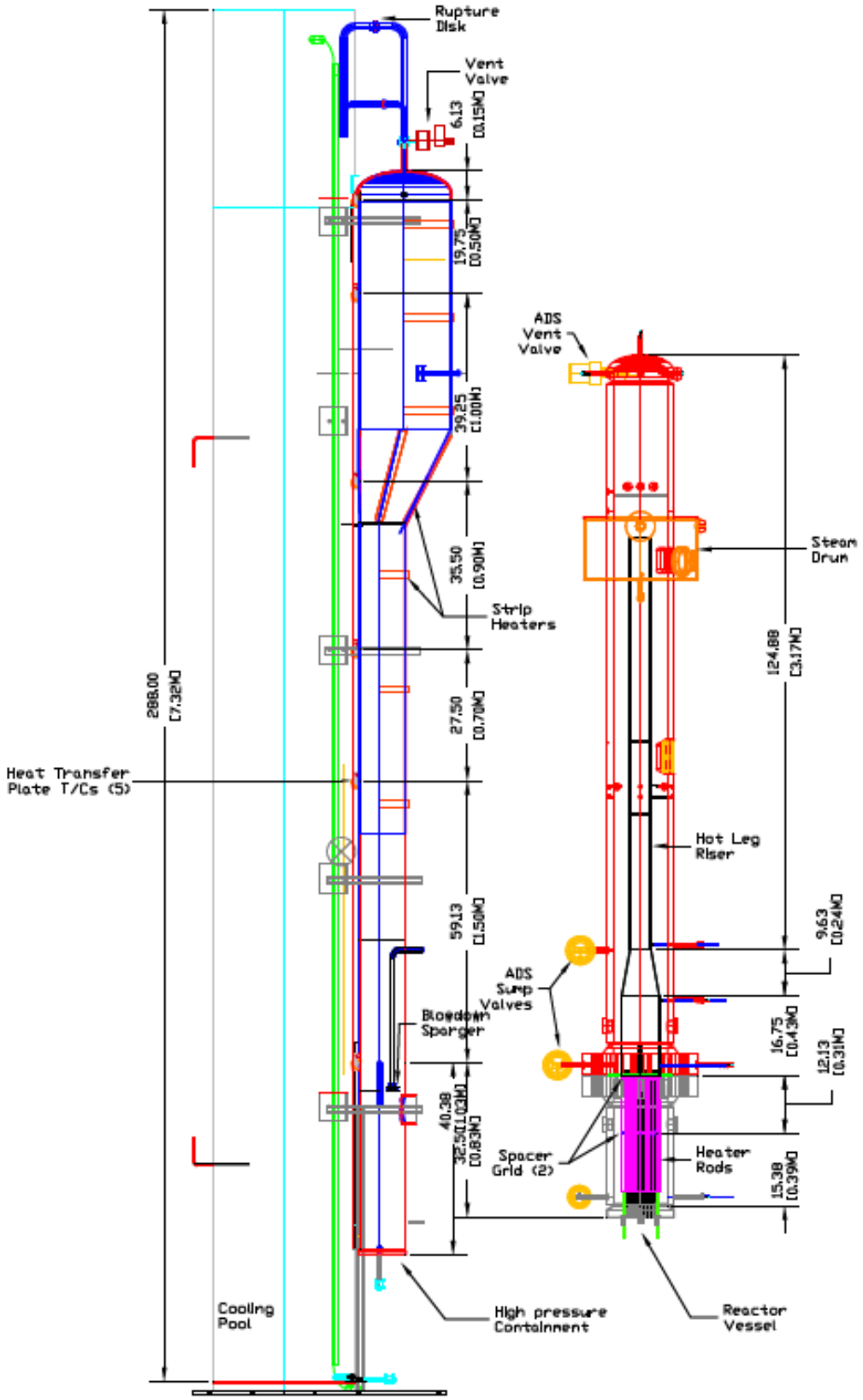

Figure 13 HPC and CPV Penetration Elevation [34]

2.6 OSU-MASLWR Data Acquisition and Control Subsystem Overview

The data acquisition and control system, Fig. 14 and 15, consists of various field input/output modules, a programmable logic controller module, and a desktop computer. The data acquisition and control subsystem processes input signals from system components, generates control signals as determined by the control logic, and applies those control signals to applicable system components. The operator can monitor parameters and alarms in the main control screen, via a graphical user interface. Individual system component operation algorithms are considered in the facility.

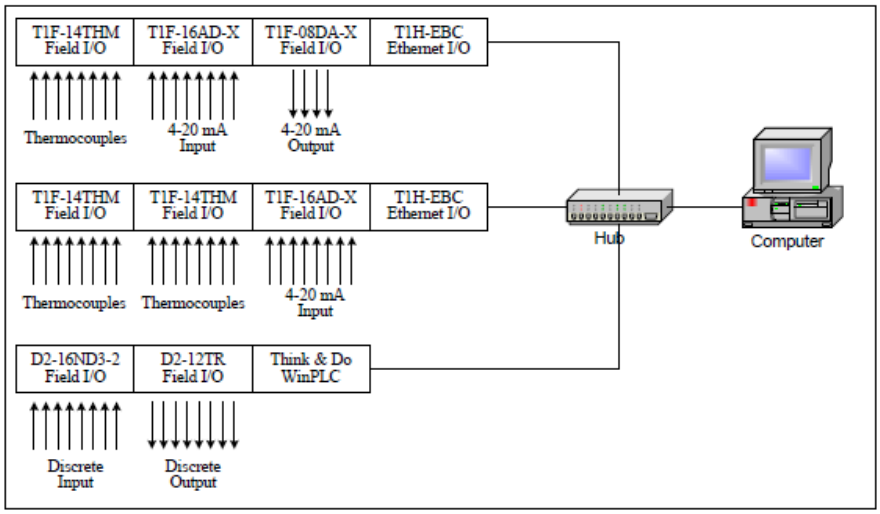

Figure 14 Data Acquisition and Control System [34]

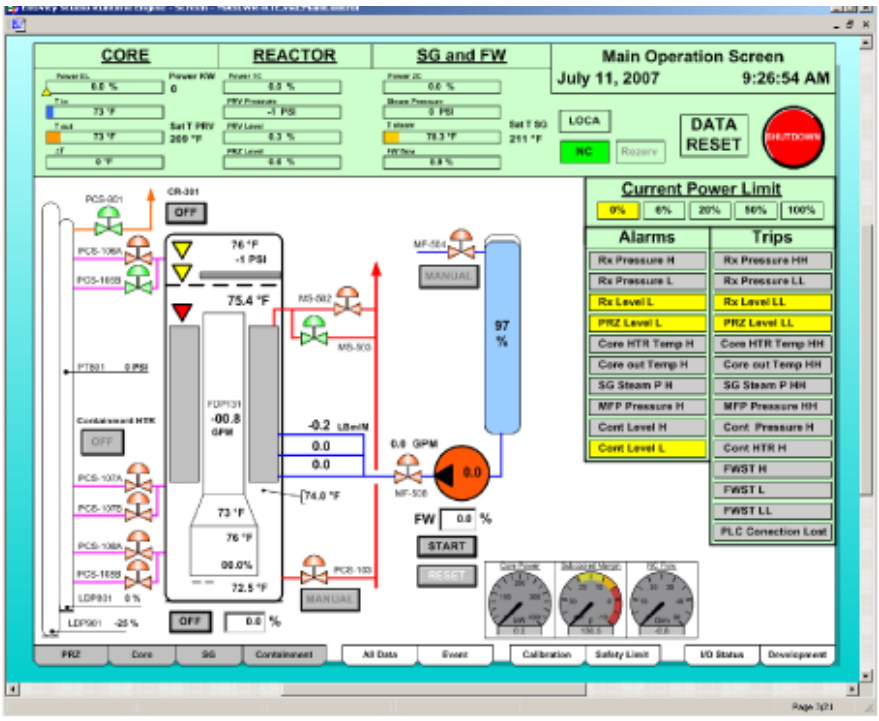

Figure 15 Data Acquisition and Control System Main Control Screen [34]

2.7 OSU-MASLWR Testing Campaign

The first tests conducted on the OSU-MASLWR facility [1, 3, 19] were in support of the MASLWR concept design verification and are shown in Table 6.

Table 6 Summary of the Previous DOE Tests Conducted in the OSU-MASLWR [1,3,19]

Name of the test	Type of test	ADS line configuration					
		Middle ADS 1 (%)	Middle ADS 2 (%)	High ADS 1 (%)	High ADS 2 (%)	Sump Recirc 1 (%)	Sump Recirc 2 (%)
OSU-MASLWR-001	Inadvertant actuation of 1 submerged ADS valve.	Failed Shut	100	100	100	100	100
OSU-MASLWR-002	Natural circulation at core power up to 210 kW.	N/A	N/A	N/A	N/A	N/A	N/A
OSU-MASLWR-003A	Natural circulation at core power of 210 kW. (Continuation of test 002, establishing the initial conditions for the 003B test)	Failed Shut	N/A	N/A	N/A	N/A	N/A
OSU-MASLWR-003B	Inadvertant actuation of 1 high containment ADS valve	Failed Shut	100	Failed Shut	100	100	100

The purpose of the test OSU-MASLWR-001, a design basis accident for MASLWR concept design, was to determine the behavior of the RPV and containment pressure following an inadvertent actuation of one middle ADS valve. The test successfully demonstrated the behavior of the MASLWR during one of its design basis accident. The normal opening sequence used in the MASLWR for the ADS valves is the middle submerged lines first, after the high containment lines and finally the sump recirculation lines. This sequence minimizes the rise in containment pressure since a large fraction of the energy transferred to the containment is direct into the subcooled containment coolant. However, if the high containment lines are actuated first, the rise in containment pressure will be larger than the previous. Also the chocked flow in the high containment line will limit the rate at which the containment and vessel pressure equalize. Therefore the purpose of the OSU-MASLWR-003B test is to study the pressure transient in the containment and in the primary system during the inadvertent actuation of the high containment ADS vent line. This test represents a beyond design basis accident scenario for the MASLWR and demonstrates the vessel containment coupling and containment vessel condensation phenomena during the transient.

The test OSU-MASLWR-002 and OSU-MASLWR-003A investigated the primary system flow rates and secondary side steam superheat for a variety of core power levels and FW flow rates. OSU-MASLWR-002 test stepped power level incrementally up to 165 kW, varying FW flow rate at each power level, and OSU-MASLWR-003A test was an extended 210 kW steady-state test establishing initial conditions for the OSU-MASLWR-003B test. During these two tests seven different core powers as well as nine different FW flow rates were used. Since the slope of the MS superheat curve increases if the value of the core power increases and decreases if the value of the FW flow rate increases, the target of these tests was to acquire primary system flow rates and secondary side steam superheat for different core powers and FW flow rates.

2.7.1 OSU-MASLWR-001 Test Description

The purpose of the OSU-MASLWR-001 test [1,3,4,7,19,20], a design basis accident for MASLWR concept design, was to determine the pressure behavior of the RPV and containment following an inadvertent actuation of one middle ADS valve. The test successfully demonstrated the blowdown behavior of the MASLWR test facility during one of its design basis accident. The main phenomena of interest in this kind of transient are [43,49-52]:

- RPV:
  - Single phase natural circulation;
  - Two-phase natural circulation;
  - Heat transfer in covered core;
  - Distribution of pressure drop through primary system;
  - Primary containment coupling during blowdown and long term cooling typical of the MASLWR design;
  - Structural heat and heat losses;

- HPC:
  - Thermal stratification;
  - Steam condensation;
  - Effect of non-condensable gases on condensation heat transfer;
  - Primary containment coupling during blowdown and long term cooling typical of the MASLWR design;
  - Condensation on containment structures - HPC/CPV thermal coupling through the heat transfer plate;
  - Structural heat and heat losses.

- CPV:
  - Thermal stratification;
  - HPC/CPV thermal coupling through the heat transfer plate.

Following the inadvertent middle ADS actuation the blowdown of the primary system takes place. A subcooled blowdown, characterized by a fast RPV depressurization, takes place after the Start Of the Transient (SOT). A two-phase blowdown occurs when the differential pressure, at the break location, results in fluid flashing. A choked two-phase flow condition prevails and a decrease in depressurization rate of the primary system is experimentally observed. When the PRZ pressure reaches saturation, single phase blowdown occurs and the depressurization rate increases. The RPV and HPC pressure experimentally detected and the primary saturation temperature are shown in Fig. 16. The P_{sat}, saturation pressure, is based on the temperature at the core outlet.

At 539s after the SOT the pressure difference between the RPV and the HPC reaches a value less than 0.517 MPa, one of the high ADS valve is opened and, with approximately 10s of delay, the other high ADS valve is opened equalizing the pressure of the primary and HPC system.

At 561s after the SOT the pressure difference between the RPV and the HPC reaches a value less than 0.034 MPa, one of the sump recirculation valves is opened and, with approximately 10s of delay, the other sump recirculation valve is opened terminating the blowdown period and starting the refill period. The refill period takes place for the higher relative coolant height in the HPC compared to the RPV. Fig. 17 shows the RPV level evolution experimentally detected during the test. The RPV water level never fell below the top of the core during the execution of the test 1. Fig. 18 shows the HPC level behavior experimentally detected.

During the saturated blowdown period, the inlet and the outlet temperature of the core are equal each other assuming the saturation temperature value. A core reverse flow and a core coolant boiling off at saturation is present in the facility during this period. When the refill takes place the core normal flow direction is restarted and a delta T core is observed depending on the refill rate and core power, Fig. 19.

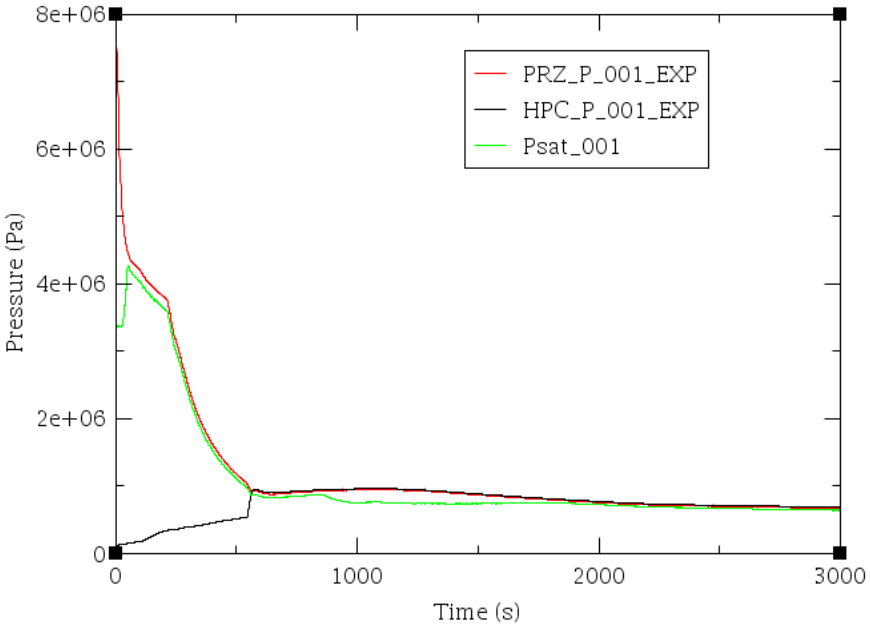

Figure 16 RPV and HPC Pressure Behavior during the OSU-MASLWR-001 Test [1,3,19,20]

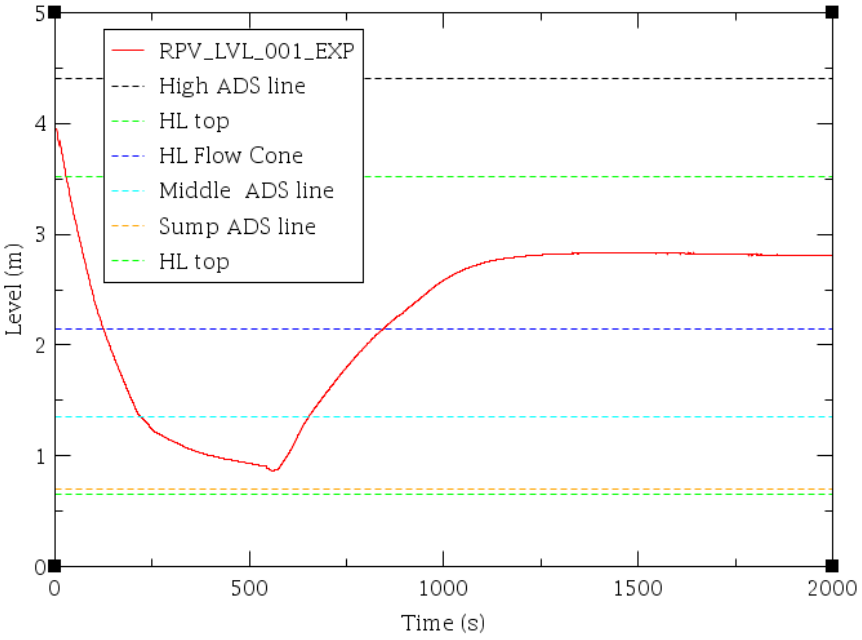

Figure 17 RPV Water Level Behavior during the OSU-MASLWR-001 Test [1,3,19,20]

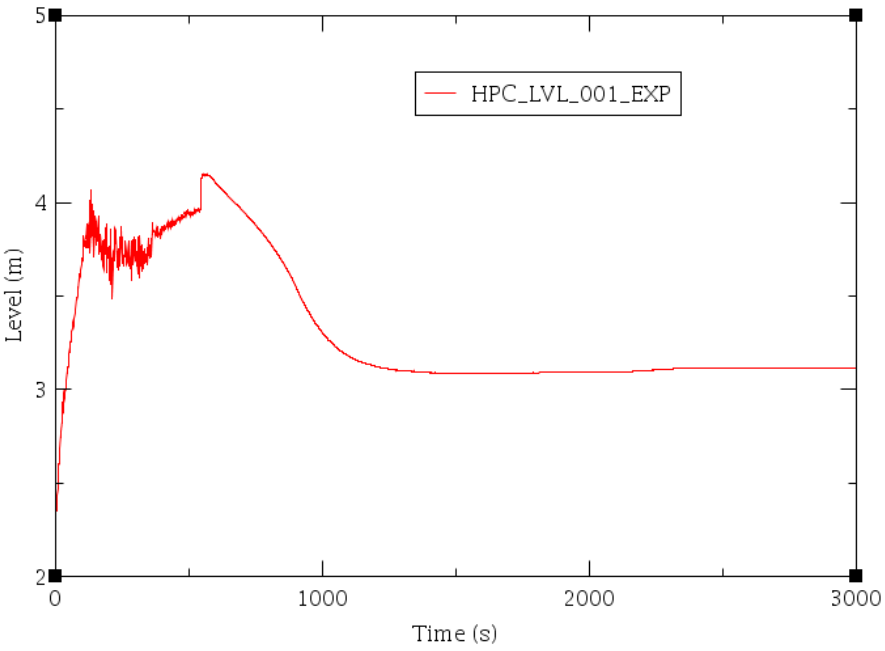

Figure 18 HPC Water Level Behavior during the OSU-MASLWR-001 Test [20]

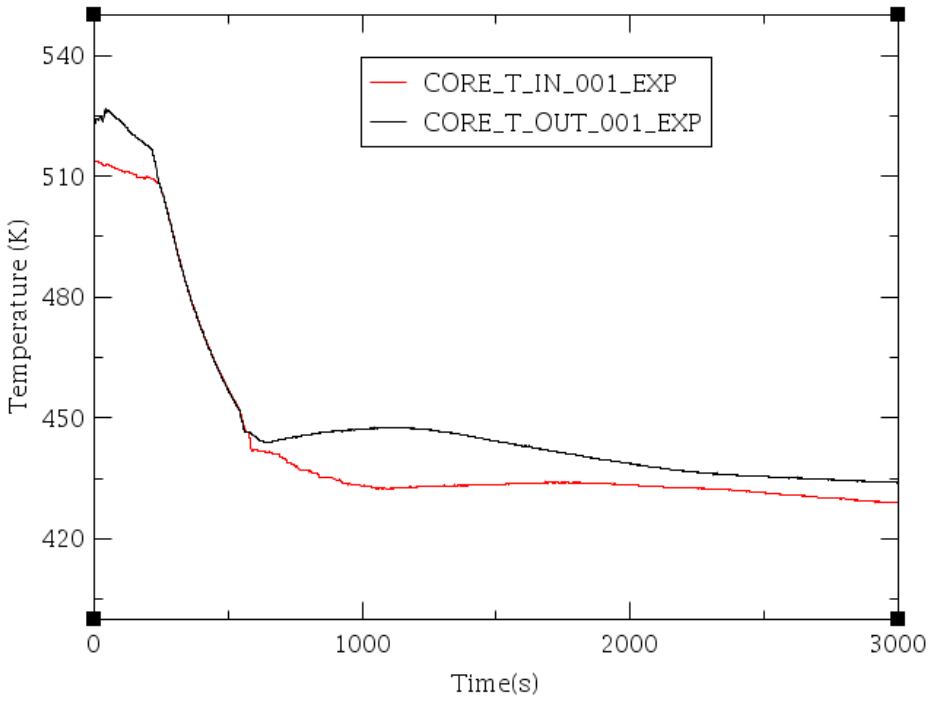

Figure 19 Inlet/Outlet Core Temperature Behavior during the OSU-MASLWR-001 Test [1,19,20]

When the refill of the reactor takes place the level of the coolant reaches the location of the flow rate HL measurement point, therefore a “large” increase of the RPV flow rate is detected for this phenomenon, Fig. 20.

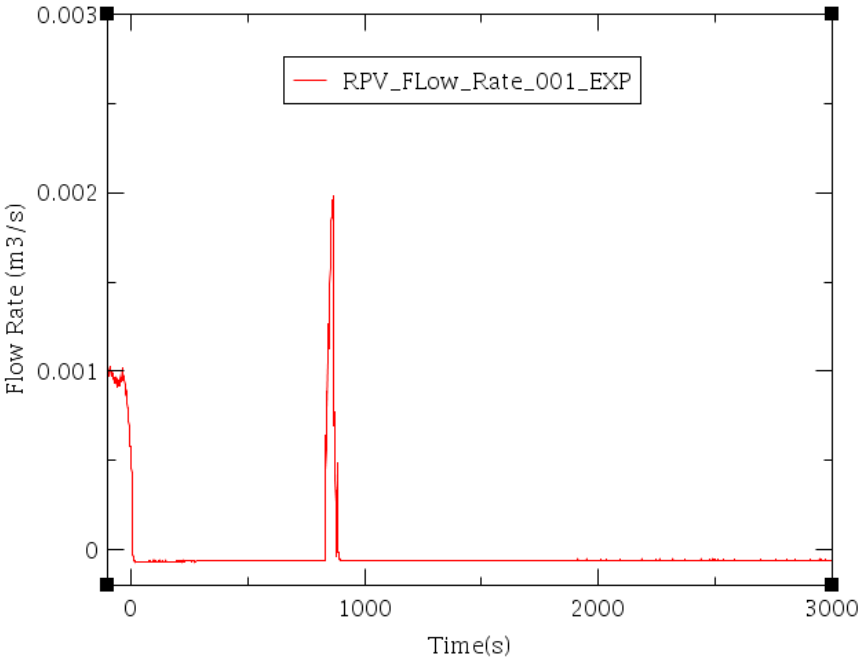

Figure 20 RPV Flow Rate during the OSU-MASLWR-001 Test [1,19,20]

2.7.2 OSU-MASLWR-002 Test Description

The test OSU-MASLWR-002 and OSU-MASLWR-003A [1,3,7,18,19] investigated the primary system flow rates and secondary side steam superheat for a variety of core power levels and FW flow rates. Table 7 shows the OSU-MASLWR-002 and OSU-MASLWR-003A test conditions. The main phenomena of interest in this kind of transient are [43, 49-52]:

- RPV:
  - Single phase natural circulation;
  - Heat transfer in covered core;
  - Distribution of pressure drop through primary system;
  - Direct heat exchange between riser and downcomer (by pass heat transfer [18, 43]);
  - Heat transfer in SG primary side;
  - Structural heat and heat losses.

- RPV-SG:
  - Heat transfer in SG secondary side;
  - Steam superheated on secondary side.

The OSU-MASLWR-002 stepped power level incrementally up to 165 kW, varying FW flow rate at each power level. Since the 210 kW data in OSU-MASLWR-002 was not used, because of a liquid carry over in the SG, the OSU-MASLWR-003A was an extended 210 kW steady-state test establishing initial conditions for the OSU-MASLWR-003B. During these two tests seven different core powers were used as well as nine different FW flow rates. Fig. 21 shows the inlet/ outlet core and the top of the HL temperature during the OSU-MASLWR-002 test.

In general the value of the degree of the steam superheat is changed in order to control the facility. Since the slope of the MS superheat curve increases if the value of the core power increases and decreases if the value of the FW flow rate increases, the target of these tests was to acquire primary system flow rate and secondary side steam superheat for different core powers and FW flow rates. The difference between the MS saturation temperature and the measured MS temperature is used to estimate the value of the MS superheat. Fig. 22 shows the steam superheat data for the test OSU-MASLWR-002.

By analysing the experimental data, related to the flow temperature after the SG coils primary side section and the core inlet temperature, it is evident that the direct heat exchange, by pass heat transfer, through the internal shell, between the fluid ascending the HL and the fluid descending the CL, is a crucial parameter for the evaluation of the core inlet temperature and, therefore, the core outlet temperature. In fact, the experimental data show that, along the downcomer region, the fluid increases its temperature between the end of the SG primary side section and the core inlet . Fig. 23 shows the difference of fluid temperature at the inlet of the core and at the exit of the SG primary side for the OSU-MASLWR-002 test.

Table 7 OSU-MASLWR-002 and OSU-MASLWR-003A Test Conditions [1,3,7,19]

Test	Start time (s)	End Time (s)	Primary					Secondary			
			Core Power (kW)	T_in (K)	T_out (K)	Flow (L/min)	Vel (m/s)	T_in (K)	T_Out (K)	P (MPa)	Feed Water (kg/min)
002	0	127	80.0	489	506	65.6	0.13	292	482	1.41	1.13
	250	550	100.0	491	509	77.9	0.16	292	488	1.40	1.81
	750	1200	100.0	490	508	80.0	0.16	292	494	1.38	2.14
	1380	1570	100.0	486	505	81.9	0.17	292	494	1.37	2.50
	1670	1920	110.0	483	503	84.9	0.17	292	493	1.36	2.49
	2060	2250	125.0	482	503	88.5	0.18	292	493	1.35	2.50
	2450	2600	160.0	481	505	104.1	0.21	292	488	1.36	3.85
	2700	2930	165.0	478	503	105.0	0.21	293	482	1.35	3.83
003A	0	450	210.0	501	528	118	0.24	293	507	1.581	4.14
	550	1000	210.0	499	526	120	0.24	293	509	1.567	4.56

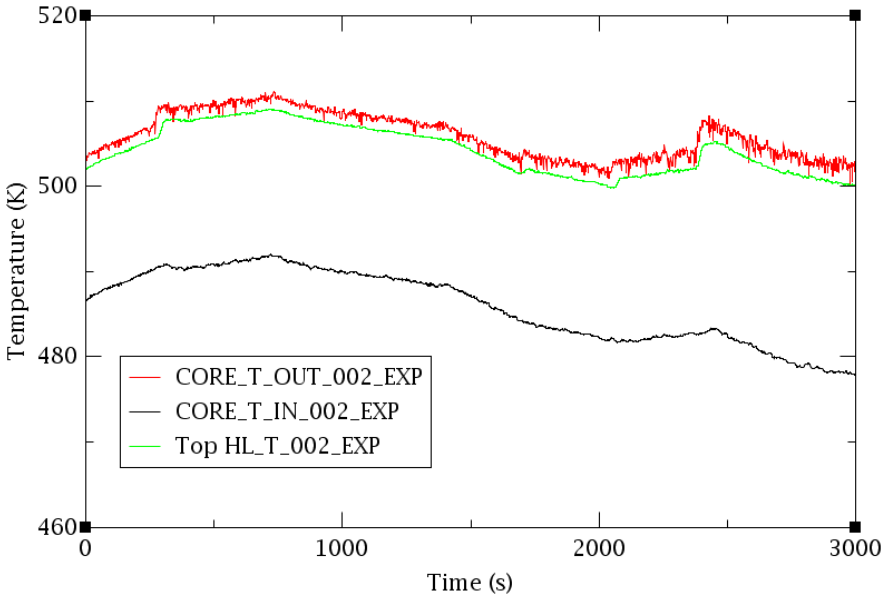

Figure 21 Inlet, Outlet Core and Top of the Hot Leg Temperature Behavior during the OSU-MASLWR-002 Test [1,18,19]

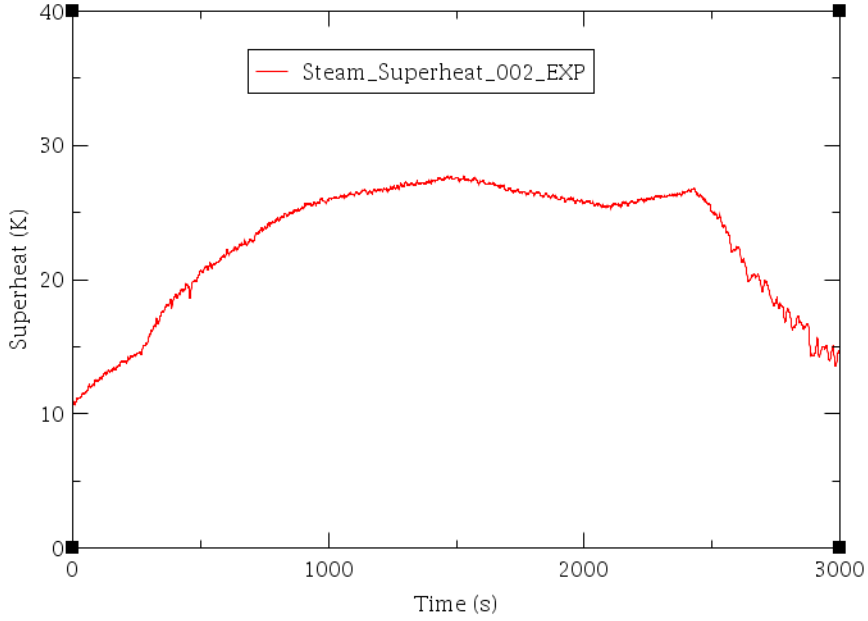

Figure 22 Steam Superheat at the SG Outlet Behavior during the OSU-MASLWR-002 Test [3,19]

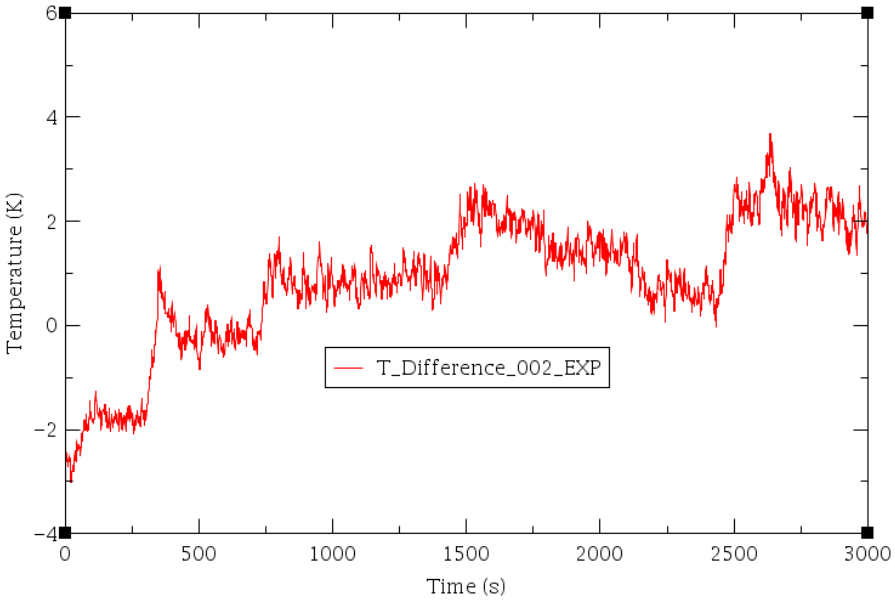

Figure 23 Difference of Fluid Temperature at the Inlet of the Core and at the Exit of the SG Primary Side during the OSU-MASLWR-002 Test [18,19]

3. CODE APPLICATION

3.1 TRACE Code Description

In the past, to support independent vendor review of reactor LWR designs, the USNRC has maintained four separate computer codes (RAMONA, the RELAP5, the TRAC-B and the TRAC-P) for analysing system thermal hydraulic response.

Over the past ten years, the NRC has developed an advanced best estimate thermal hydraulic system code, by merging, among other things, the capability of the previous codes into a single code. This new code is called TRAC/RELAP Advanced Computational Engine or TRACE [44], and is a component-oriented code designed to perform best estimate analyses for LWR. In particular TRACE is developed to simulate operational transient, LOCA, other transient typical of the LWR and to model the thermal hydraulic phenomena taking place in the experimental facilities used to study the steady state and transient behavior of reactor systems.

TRACE is a finite volume, two-fluid, code with 3D capability which gives user the ability to model heat structures and control systems that interact with component models. It can be run coupled with the 3D reactor kinetics code PARCS as well. TRACE can be used together with a user-friendly front end, Symbolic Nuclear Analysis Package (SNAP) [45], which allows direct visualization of selected calculated data using the animation model capability, visualization of models, and accepts existing RELAP5 and TRAC-P input. The computational complexity of a generic TRACE model is only limited by the availability of the computer memory. Fig. 24 shows the TRACE/SNAP environment architecture.

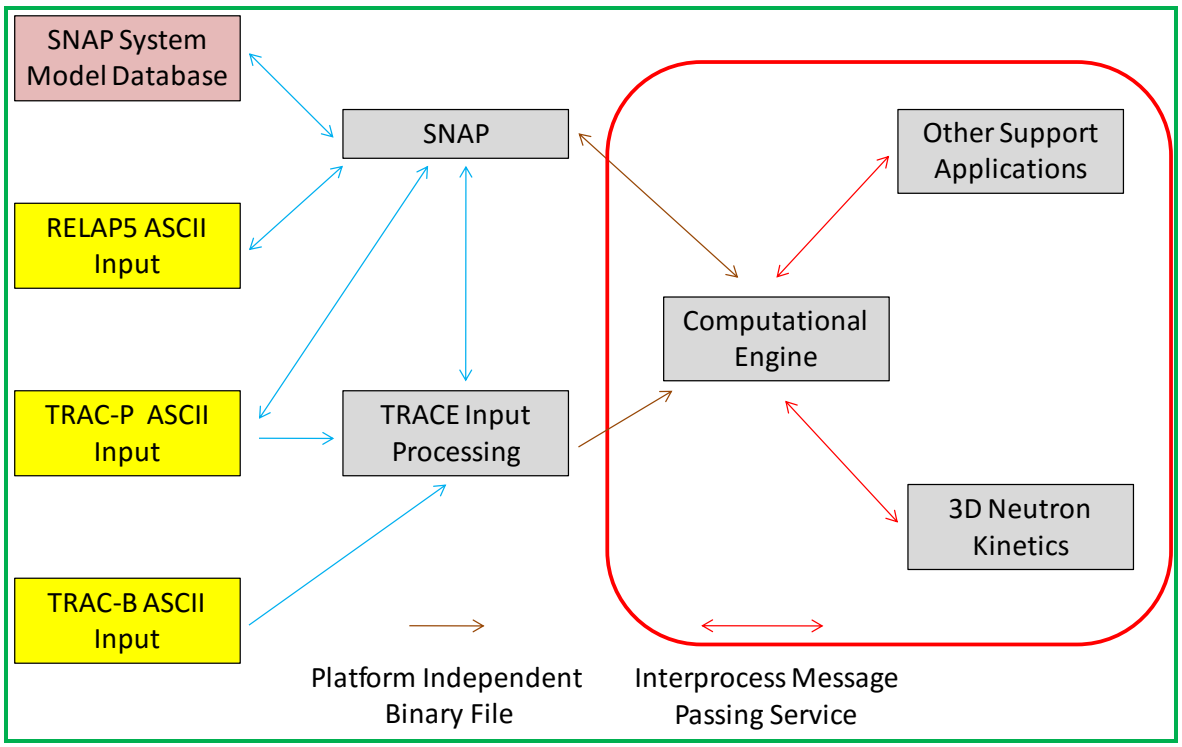

Figure 24 TRACE/SNAP Environment Architecture [18,20,46]

The code is based on two fluid, two-phase field equations. This set of equations consists of the conservation laws of mass, momentum and energy for liquid and gas fields. The resulting equation set is coupled to additional equations for non-condensable gas, dissolved boron, control systems and reactor power. Relations for wall drag, interfacial drag, wall heat transfer, interfacial heat transfer, equation of state and static flow regime maps are used for the closure of the field equations. The interaction between the steam-liquid phases and the heat flow from solid structures is also considered. These interactions are in general dependent on flow topology and for this purpose a special flow regime dependent constitutive-equation package has been incorporated into the code. TRACE uses a pre-CHF flow regime, a stratified flow regime and a post-CHF flow regime. In order to study the thermal history of the structures the heat conduction equation is applied to different geometry. A 2D(r and z) treatment of conduction heat transfer is taken into account as well. A finite volume numerical method is used to solve the partial differential equations governing the two-phase flow and heat transfer. By default, a multi-step time-differencing procedure that allows the material Courant-limit condition to be exceeded is used to solve the fluid-dynamics equations [8,11-32,44].

3.2 TRACE Model Description

The OSU-MASLWR TRACE model [11-32,37-43] was developed using SNAP and is shown in Fig. 25. This model has been revised and applied for the simulation of the IAEA-ICSP test SP-2 and SP-3 [37-43]. In particular, a complete review of the facility geometry has been implemented (height VS volume plot, mass and surface of the heat structures, etc); a first estimation of the heat losses of the facility has been completed. The IAEA-ICSP SP-3 value of about 5 kW has been assumed for the heat losses calibration [37-43].

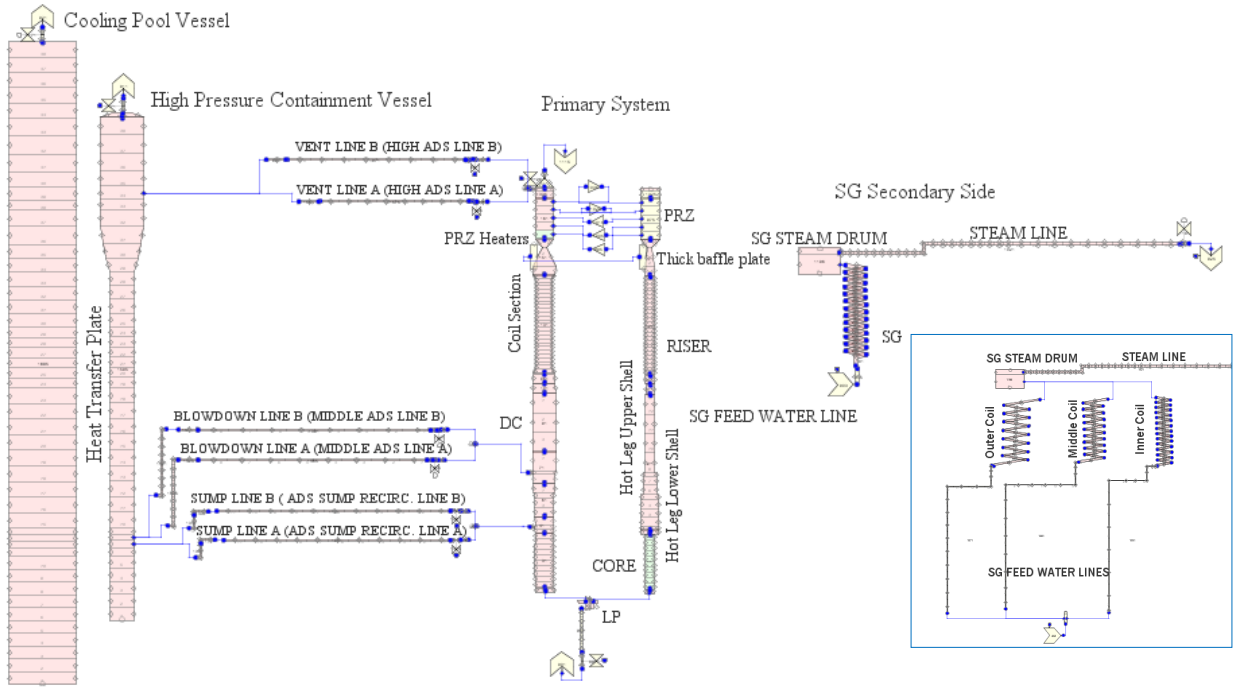

Figure 25 OSU-MASLWR Model [11-32,37-43]

The nodalization models the primary and the secondary circuit, the HPC, the heat transfer plate and the CPV. The ADS blowdown lines, vent lines and sump recirculation lines are modelled as well.

The “slice nodalization” technique is adopted in order to improve the capability of the code to reproduce natural circulation phenomena. This technique considers mesh cells of different nodalization zones, at the same elevation, with the same cell length. In this way errors due to the position/elevation of the cell nodalization center that can influences the results of the calculated data when natural circulation regime is present are reduced. If the “slice nodalization” technique is not used, this error has to be taken into account and its effect increases if larger nodalization cells are used. In this case it can be reduced by using a “fine nodalization”. In general, its effect on the results is less important when forced circulation regimes are simulated. However the “slice nodalization” technique could require nodes of small length which would increase the numerical error and the computational time. The “code user” has to take into account these disadvantages during the nodalization development [20].

The primary circuit of the TRACE model comprises the core, the HL riser, the UP, the PRZ, the SG primary side, the CL downcomer and the LP. After leaving the top of the HL riser, the flow enters the UP which is divided into two thermal hydraulic regions connected to the PRZ. After leaving the UP the flow continues downward through the SG primary section and into the CL downcomer region. The core is modelled with one thermal hydraulic region thermally coupled with one equivalent active heat structure simulating the 56 electric heaters. The PRZ is modelled with two hydraulic regions, connected by different single junctions, in order to allow for simulation of potential natural circulation/convection phenomena. The three different PRZ heater elements are modelled with one equivalent active heat structure. The thick baffle plate is modelled as well. Fig. 26 shows the heat structures considered in the TRACE nodalization. The direct heat exchange by the internal shell between the hotter fluid in the hot leg riser and the colder fluid in the descending annular downcomer is modelled by heat structures thermally coupled with these two different hydraulic regions. Fig. 27 shows the correspondence between the TRACE model and the facility lower shell section.

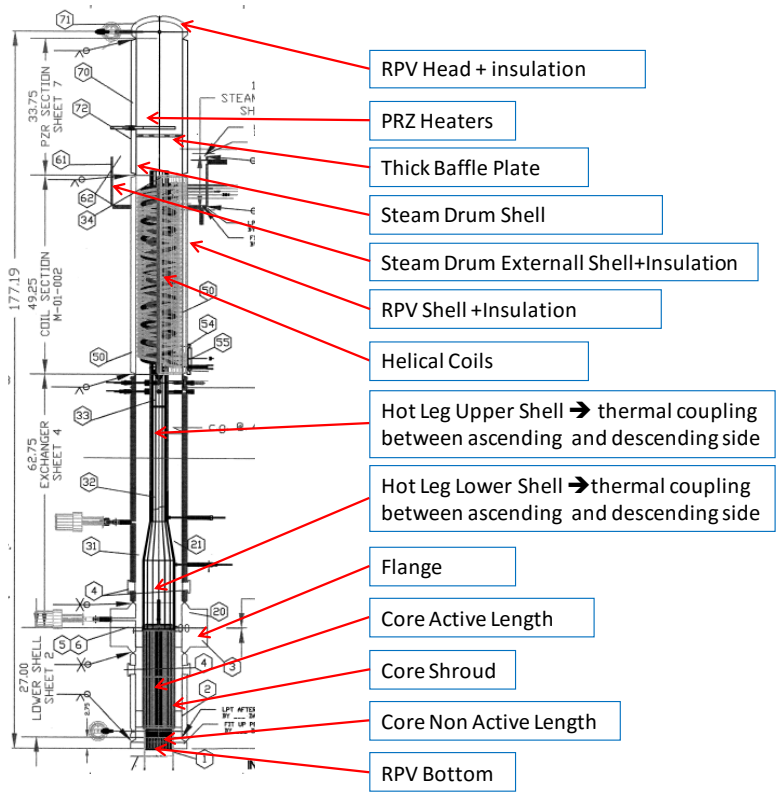

Figure 26 Heat Structures Modeled in the TRACE Nodalization [11-32,37-43]

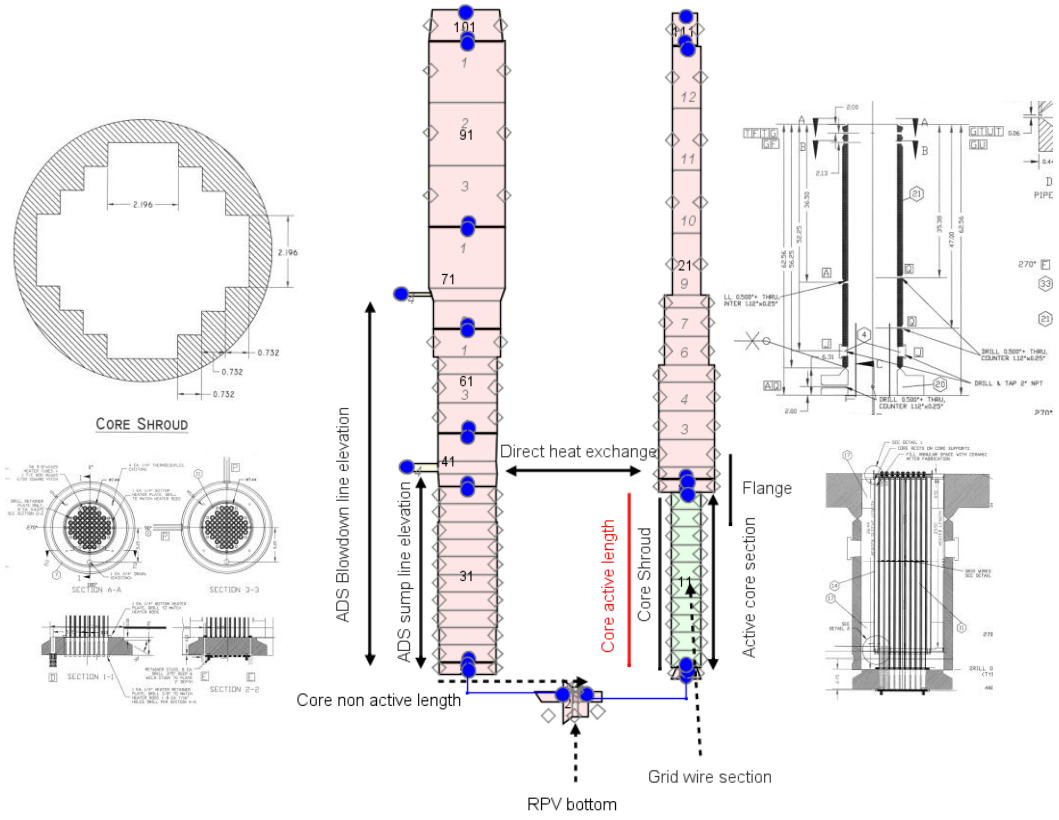

Figure 27 Correspondence Between the TRACE Model and the Facility Lower Shell Section [11-32,37-43]

SG coils are modelled with only one “equivalent” vertical group of pipes thermally coupled by an equivalent heat structure with the SG primary side section. A model with three different equivalent oblique groups of pipes has been implemented as well. Previous analyses, based on the TRACE simulation of the OSU-MASLWR-002 test [18], show that the instabilities of the superheat condition of the fluid at the outlet of the SG, observed in previous analysis [11] as well, are also related to the equivalent SG model. Since in these analyses a model with one equivalent vertical group of pipes shows a more stable fluid temperature at the SG outlet, this model is used as reference for the analysis of the OSU-MASLWR 001 and 002 test presented in this document. Since no specific helical coil heat transfer correlations have been implemented in the TRACE V5 patch 3, considering the results reported in [21, 22, 23, 43], in order to reach the initial conditions of the OSU-MASLWR-001 and 002 tests, the heat transfer area of the equivalent helical coil SG heat structure is incremented.

The RPV, HPC and CPV shell and the connected insulation are modelled. In particular the HPC is modelled with one hydraulic region connected by a heat structure, representing the heat transfer plate, to the CPV simulated with another hydraulic region. The ADS lines are modelled separately in order to simulate the OSU-MASLWR-001 test logic. The sparger (vent and blowdown ADS lines) is modelled in the ADS line along with the orifice (sump return, vent and blowdown lines) and the heat structure with related insulation [13, 20]. The heat losses of these lines are taken into account. The RPV, HPC and CPV shell and the connected insulation are modelled.

The list of the facility instrumentation versus TRACE model measurement points is shown in the Table 8 and it is presented in the Fig. 28.

Table 8 Facility Instrumentation vs TRACE Nodalization Measurement Points[37-43]

Facility Instrumentation	TRACE model measurement points
PT 301	1325 cell 2
TF 121, 122, 123, 124	51 cell 1 - sv 175
TF 106	21 cell 2 – sv 176
FDP 131	111 edge 1 - cb15
TF 111	141 cell 2 - sv 177
TF 131, 133, 134	91 cell 1 – sv 178
TF 132	21 cell 12 – sv 195
TF-301	1325 cell 2 – sv 196
DP 101 [RV 101 - 102]	cb22 [1 cell 1 - 21 cell 2]
DP 102 [RV102 - 103]	cb23 [21 cell 2- 21 cell 5]
DP 103 [RV 103 - 104]	cb24 [21 cell 5 - 21 cell 8]
DP 104 [RV 104 - 108]	cb25 [21 cell 8 - 141 cell 2]
DP 105 [RV 105 - 108]	cb55 [141 cell 2 - 101 cell 1]
DP 106 [RV 101 - 105]	cb56 [101 cell 1 - 1 cell 1]
LDP 301	cb12
LDP 106	cb18
KW-101, 102	Heat structure 915 - Power 915
FCM 511	1071 edge 5
FCM 521	1061 edge 3
FCM 531	1051 edge 2
PT 511	1071 cell 5
PT 521	1061 cell 3
PT 531	1051 cell 2
PT-511-521-531 ave	903 cell 1
TF 611, 612, 613, 614, 615	771 cell 1
TF 621, 622, 623, 624, 625	621 cell 1
TF 631, 632, 633, 634	431 cell 1

Average SG Outlet T (611-634)	431 cell 1 (one equivalent SG) – sv 179 1196 cell 1 – sv 194
FVM 602 T	1021 cell 20 – sv 180
FVM 602 P	1021 cell 20
Secondary steam superheat	cb30
FMM-501	1315 edge 1
TF 501	1315 cell 1 – sv 181
Heat Losses	cb2
TF 811	1595 cell 9 – sv 182
TF 821	1595 cell 18 – sv 183
TF 831	1595 cell 24- sv 184
TF 841	1595 cell 30 – sv 185
TF 851	1595 cell 36 – sv 186
TF 861	1595 cell 38 – sv 187
TF 812, 822, 832, 842, 852, 862	1615 A9, 18,24,30,36,38 R02
TF 813, 823, 833, 843, 853, 863	1615 A9, 18,24,30,36,38 R03
TF 814, 824, 834, 844, 854, 864	1615 A9, 18,24,30,36,38 R04
TF 815	1605 cell 14 – sv 188
TF 825	1605 cell 23 - sv 189
TF 835	1605 cell 29- sv 190
TF 845	1605 cell 35 – sv 191
TF 855	1605 cell 41 – sv 192
TF 865	1605 cell 43 –sv 193
LDP 801	sv73
PT 801	1595 cell 1
LDP 901	sv74

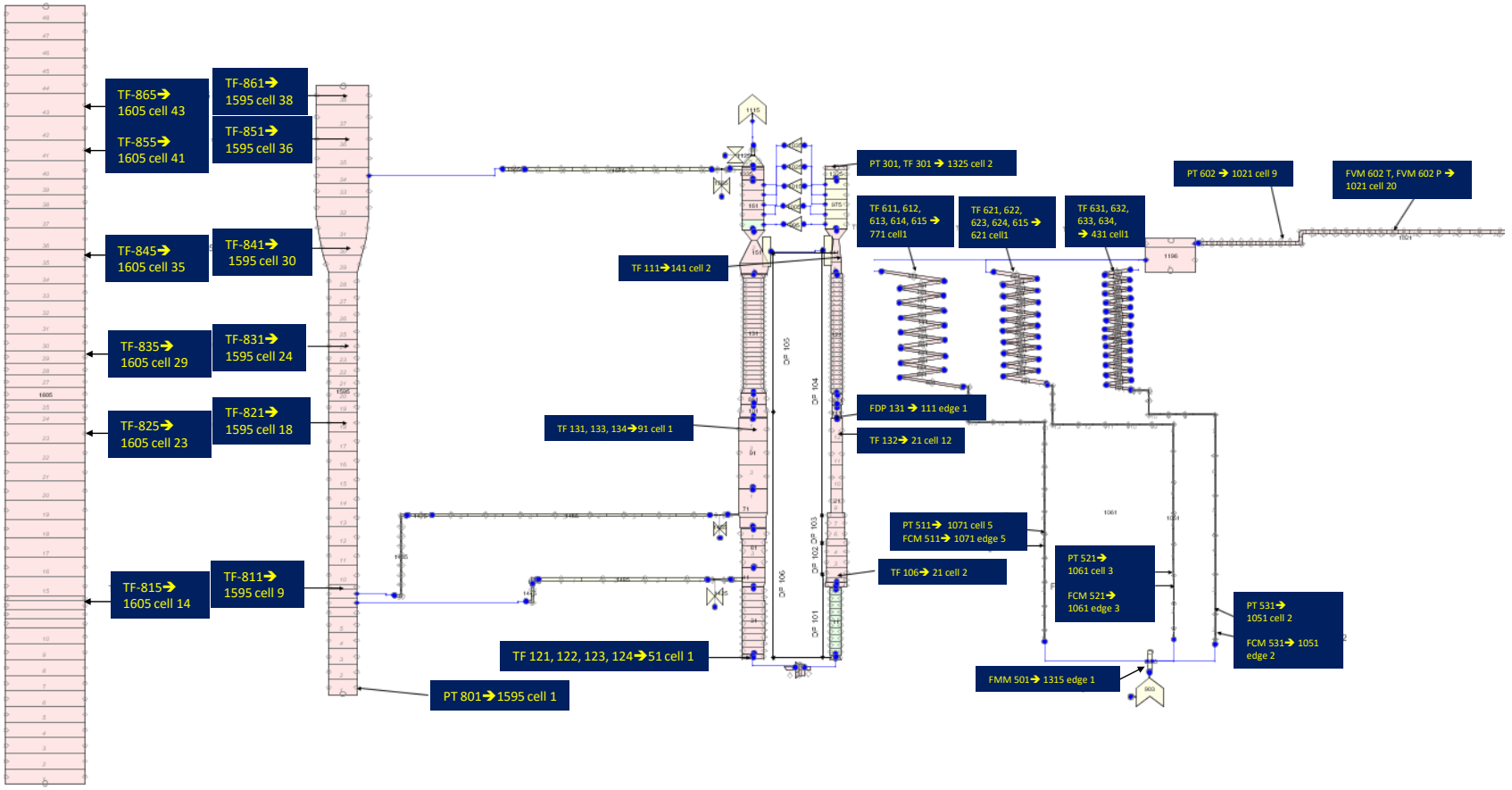

Figure 28 Measurement Points in the TRACE Nodalization [37-43]

3.3 Analyses of the OSU-MASLWR-001 Calculated Data

Starting from the calculated data developed in previous analyses [12, 13, 14, 16, 20] the target of this section is to give an expanded revised analyses of the TRACE V5 Patch 3 code capability in predicting the primary/containment coupling phenomena typical of the MASLWR prototypical design. For scaling reasons, in order to have an adiabatic boundary condition in all the walls of the HPC except through the heat transfer plate wall, containment heaters have been installed and are in operation during this test, two different calculations have been performed. In the reference case the HPC is assumed to be adiabatic in all the walls of the HPC except through the heat transfer plate wall and no heater operation has been considered during the transient simulation (REF plot reference); in the sensitivity case, no adiabatic conditions have been considered for the HPC walls and the HPC heaters were in operation during the transient simulation (SEN1 plot reference).

In order to reach the Boundary and Initial Condition (BIC) a pre-test phase has been conducted. The pre-test phase started at about 2814s before the SOT (-2814s) and the main facility procedures to reach the BIC, characterizing that time window (from -2814s to 0s) have been implemented in the TRACE model. The facility configuration before the SOT of the OSU-MASLWR-001 test is reported in Table 9. The core power time evolution and the FW time evolution are imposed as boundary conditions during this phase while the PRZ heaters are assumed to be in operation in order to maintain the primary pressure set-point; the HPC heaters are OFF in the reference case and are ON in the sensitivity case. The ADS valves are closed.

Table 9 Facility Configuration Before the SOT of the OSU-MASLWR-001 Test

System	Facility Operation	TRACE Model Operation		Note
		REF	SEN1	
Core Heaters	ON	ON	ON	
PRZ Heaters	ON	ON	ON	In order to maintain the primary pressure set-point.
HPC Heaters	ON	OFF	ON	In order to have an adiabatic boundary condition in all the walls of the HPC except through the heat transfer plate wall.
Feed Water	ON	ON	ON	In order to remove the net primary power [primary power less ambient losses].
ADS Valves	Closed	Closed	Closed	

Before the SOT, the TRACE code predicts a primary system in sub cooled condition with single-phase natural circulation. The primary pressure is at about 7.6 MPa and the PRZ heaters are set up to maintain the primary pressure at the fixed set point. The secondary fluid, circulating inside the helical coil tubes removes the core power (less the facility heat losses from the primary fluid and goes out from the SG as superheated steam). The outlet SG secondary pressure is around 2.2e5 Pa. The ADS middle line valves, the ADS high line valves, and the ADS sump recirculation line valves are closed. Since no helical coil heat transfer correlation have been implemented in the TRACE V5.0 Patch 3, in agreement with previous analyses [21, 22, 23, 43], the heat transfer area of the equivalent helical coil SG heat structure is incremented in order to reach the initial conditions of the OSU-MASLWR-001 test.

Table 10 shows the initial conditions predicted by the TRACE code against the experimental initial conditions for the REF and SEN1 case. Figure 29 and 30 show the fluid condition of the facility at the SOT for the REF and SEN1 case respectively and the different fluid conditions in the upper part

of the HPC in the two different calculations. In general the initial conditions are predicted by the TRACE code in both REF and SEN1 case. The discrepancies related to TF 891, 892, 893, 894 (temperatures within the walls of the HPC, between the heaters and the water) in the REF case are due to the lack of the HPC heaters. The facility configuration for the simulation of the OSU-MASLWR-001 test is summarized in the Table 11. The experimental core power behavior is implemented in the TRACE model as a boundary condition. The experimental logic of the valves is implemented in the TRACE model as it is shown in Table 11. Table 12 shows the event sequence for the experimental test and that predicted by the TRACE code.

The analysis of the OSU-MASLWR-001 calculated data shows that the TRACE code is able to reasonably[2] predict the primary/containment coupling phenomena characterizing the test. The blowdown phenomena, the refill of the core and the long term core cooling, permitting of removing the decay power, are reasonably predicted by the code. In particular, following the inadvertent middle ADS actuation, the blowdown of the primary system takes place. A subcooled blowdown, characterized by a fast RPV depressurization, is predicted by the code after the SOT. When the differential pressure in the facility at the break location results in flashing, a two-phase blowdown, qualitatively predicted by the code, occurs. A decrease in depressurization rate of the primary system is then observed which is in agreement with the experimental data. When the PRZ pressure reaches saturation, single phase blowdown occurs and the depressurization rate increases again, in agreement with the experimental data. The RPV and HPC pressure versus code calculations are shown in Fig. 31.

Table 10 SOT Thermal Hydraulic Conditions Comparison (TRACE Calculated Data vs Experimental Data) for the OSU-MASLWR-001 Test

Parameter	EXP	TRACE (REF)	TRACE (SEN1)
Core Power (W)	39134	39200	39200
PRZ Pressure (Pa)	7718000	7645646	7643602
T Outlet Core (K)	523	522	521
T Inlet Core (average) (K)	514	511	511
Primary Volumetric Flow Rate (m3/s)	0.0005*	0.0007	0.0007
PRZ Level (m)	0.21	0.25	0.24
T In SG (K)	293	293	293
P Inlet SG (average) (Pa)	1.32e5	1.3e5	1.3e5
P Outlet SG (Pa)	2.17e5	2.2e5	2.2e5
T Outlet SG (K)	487	525	525
Secondary Mass Flow Rate (kg/s)	0**	0	0
HPC Level (m)	2.35	2.41	2.41
HPC Pressure (Pa)	1.22e5	1.16e5	1.22e5
TF-811(K)	284	286	286
TF-891(K)	400	321	401
TF-892(K)	475	362	475
TF-893(K)	478	360	478
TF-894(K)	489	361	485
CPV Level (m)	6.35	6.3	6.3
TF-815 (m)	283	283	283

* The primary flow rate starts to decrease at about -28s before the SOT (at 31s before the SOT the core power starts to decrease from about 65 kW); the value before starting the decrease is around 0.001m^3/s. The value predicted by the TRACE code is around 0.001 m^3/s.

**The FW starts to decrease at -10s of the SOT; the value before starting the decrease is around 0.0195 kg/s. The value predicted by the TRACE code is 0.0195 kg/s.

Table 11 Facility Configuration for the Simulation of the OSU-MASLWR-001 Test

System	Facility Operation	TRACE Model Operation		Note
		REF	SEN1	
Core Heaters	ON	ON	ON	
PRZ Heaters	OFF	OFF	OFF	
HPC Heaters	ON	OFF	ON	
Feed Water	OFF	OFF	OFF	
Middle ADS	Failed shut	Failed shut	Failed shut	
Middle ADS	100% following the logic	100% following the logic	100% following the logic	
High ADS	100% following the logic	100% following the logic	100% following the logic	Valve opens when the pressure difference between RPV and HPC (PT-301 minus PT 801) is less than 0.517 MPa.
High ADS	100% following the logic	100% following the logic	100% following the logic	Valve open with 10s of delay with respect to the other high ADS valve.
Sump Recirculation	100% following the logic	100% following the logic	100% following the logic	Valve opens when the pressure difference between RPV and HPC (PT-301 minus PT 801) is less than 0.034 MPa.
Sump Recirculation	100% following the logic	100% following the logic	100% following the logic	Valve open with 10s of delay with respect to the other sump recirculation ADS valve.

Table 12 Event Transient Sequence of the OSU-MASLWR-001

Parameter	Facility Operation	TRACE (REF)	TRACE (SEN1)
SOT*	0s	0s	0s
Middle ADS Opens	0s	0s	0s
Core Power Decrease	3s	3s	3s
First High ADS Valve Opens	539s	548s	511s
Second High ADS Valve Opens	549s	558s	521s
First Sump Recirculation ADS Valve Opens	561s	584s	537s
Second Sump Recirculation ADS Valve Opens	571s	594s	547s

The FW starts to decrease at -10s of the SOT.

[2]Qualitative analyses subjective judgment mark [47]:

- **Excellent** – calculation falls within experimental data uncertainty band –: the code predicts qualitatively and quantitatively the parameter;
- **Reasonable** – calculation shows only correct behavior and trends –: the code predicts qualitatively, but not quantitatively the parameter;
- **Minimal** – calculation does not lie within experimental data uncertainty band and at times does not have correct trends–: the code does not predict the parameter, but the reason is understood and predictable;
- **Unqualified** – calculations does not show correct trend and behavior, reasons are unknown and unpredictable–: the code does not predict the parameter and the reason is not understood;
- Not applicable (–).

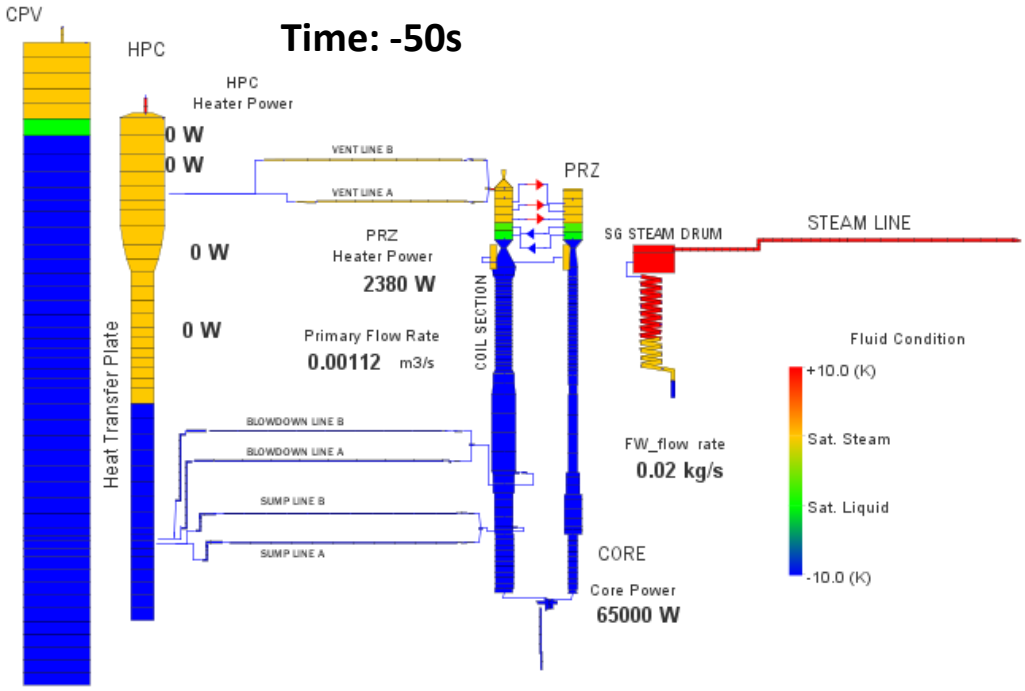

Figure 29 SNAP Animation Model Showing the Fluid Condition of the TRACE Model at 50s Before the SOT (REF Plot Reference - Cold HPC)

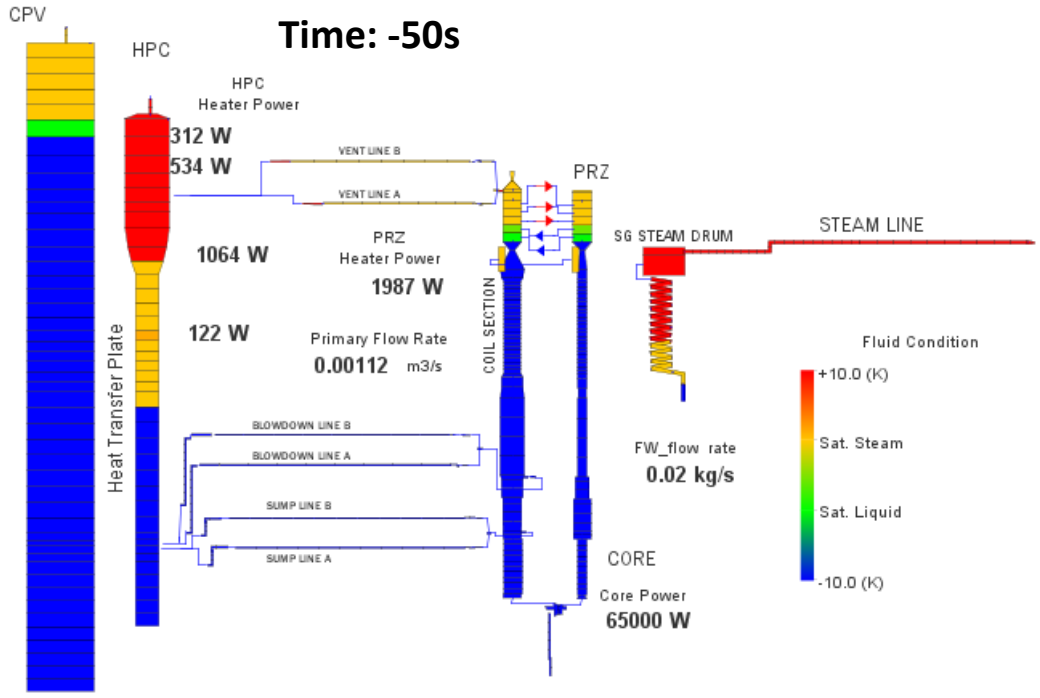

Figure 30 SNAP Animation Model Showing the Fluid Condition of the TRACE Model at 50s Before the SOT (SEN1 Plot Reference - Hot HPC)

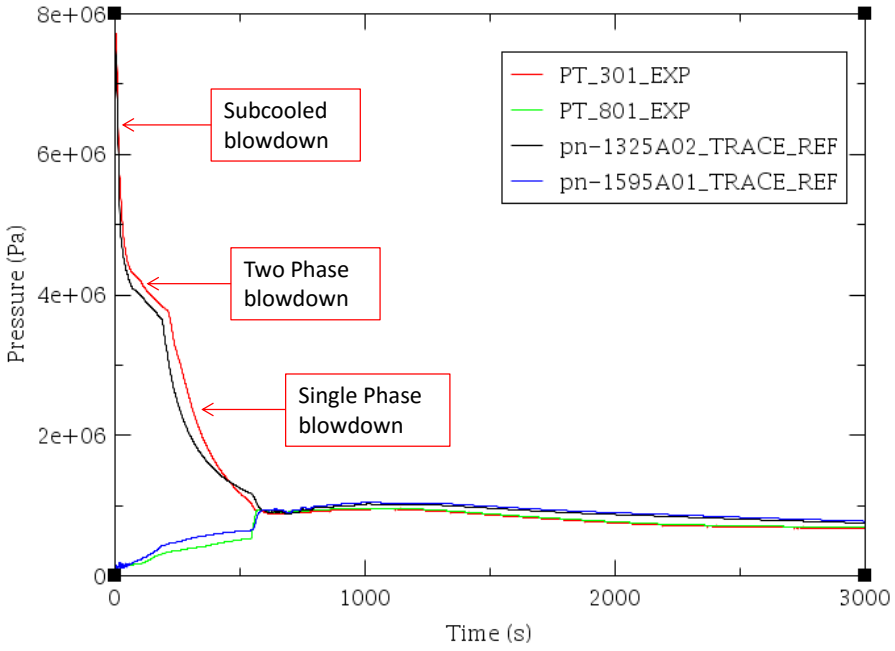

Figure 31 Experimental Data versus Code Calculation for PRZ (PT-301) and HPC (PT-801) Pressure

In agreement with the experimental data, when the pressure difference between the RPV and the HPC reaches a value less than 0.517 MPa [REF case 548s - EXP 539s], one of the high ADS valves is opened. After 10s, also in agreement with the experimental test logic, the other High ADS valve opens. This equalizes the RPV and HPC pressure. When the pressure difference reaches a value less than 0.034 MPa [REF case, 584s – EXP 561s], the sump recirculation valve is opened. After 10s the other sump recirculation valve opens. The consequent core refill phenomenon is predicted by the code. As in the experimental data, the refill period takes place for the higher relative coolant height in the HPC compared to the RPV. Fig. 32 shows the RPV level evolution experimentally recorded during the test versus the TRACE predictions. In agreement with the experimental data, the RPV water level never fell below the top of the core. Fig. 33 shows the HPC level versus code calculation, the qualitative behavior is well predicted by the TRACE code.

In agreement with the experimental data, during the saturated blowdown period the inlet and the outlet temperature of the core are equal to each other assuming the same saturation temperature. Both core reverse flow and a core boiling off at saturation are reasonably predicted by the code. When the refill takes place, the core normal flow direction is restarted. Fig. 34 and 35 shows the experimental data versus code calculation for outlet and the average inlet core temperature respectively. Fig. 36 shows the experimental data versus code calculation for RPV volumetric flow rate.

In agreement with the experimental data, when the sump recirculation valves are opened, the vapor produced in the core travels to the upper part of the RPV and through the high ADS valve goes to the HPC where it is condensed. At this point, the condensate travels through the sump recirculation line, into the down comer, and returns to the core. Fig. 37 shows the long term cooling flow path typical of the MASLWR design.

The analysis of the calculated data shows that the TRACE code is able to reasonably predict the primary/containment coupling during blowdown and long term cooling and the related single and two natural circulation phenomena taking place in the RPV/HPC coupled natural circulation loop. The

related heat transfer in covered core (the core is never uncovered during the experimental transient and calculated transient) is reasonably predicted as well.

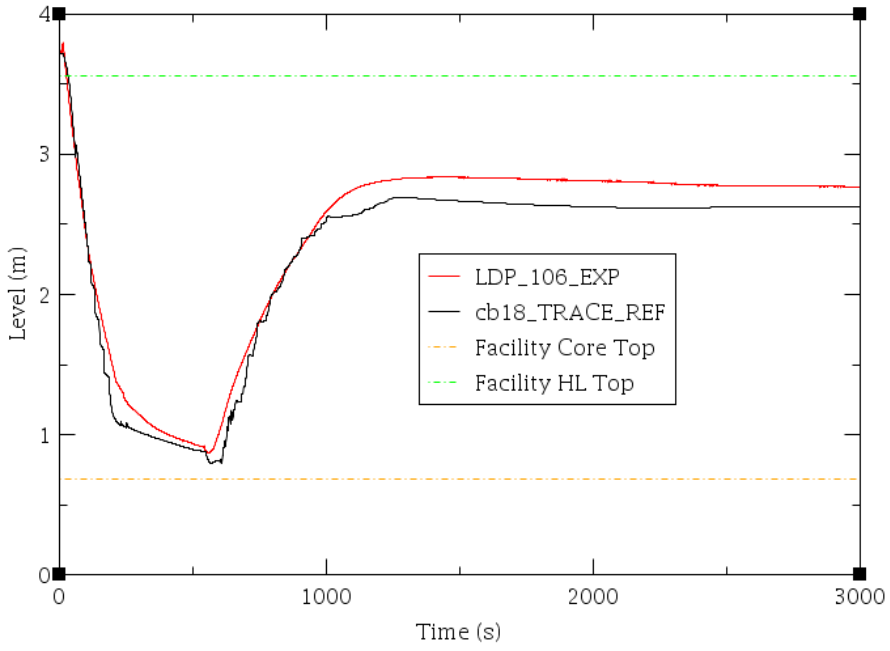

Figure 32 Experimental Data versus Code Calculation for RPV Level (LDP-106)

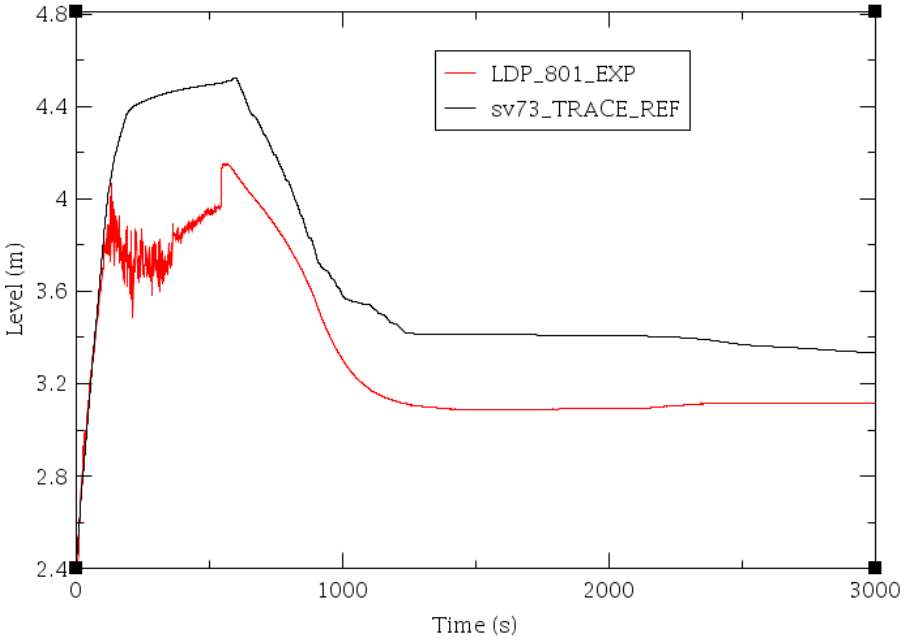

Figure 33 Experimental Data versus Code Calculation for HPC Level (LDP-801)

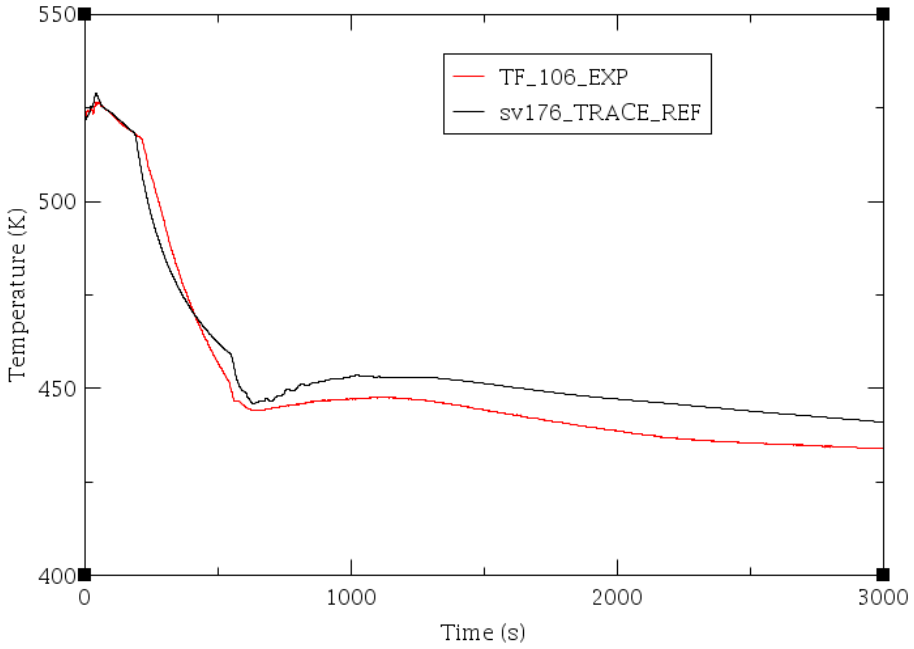

Figure 34 Experimental Data versus Code Calculation for Core Outlet Temperature (TF-106)

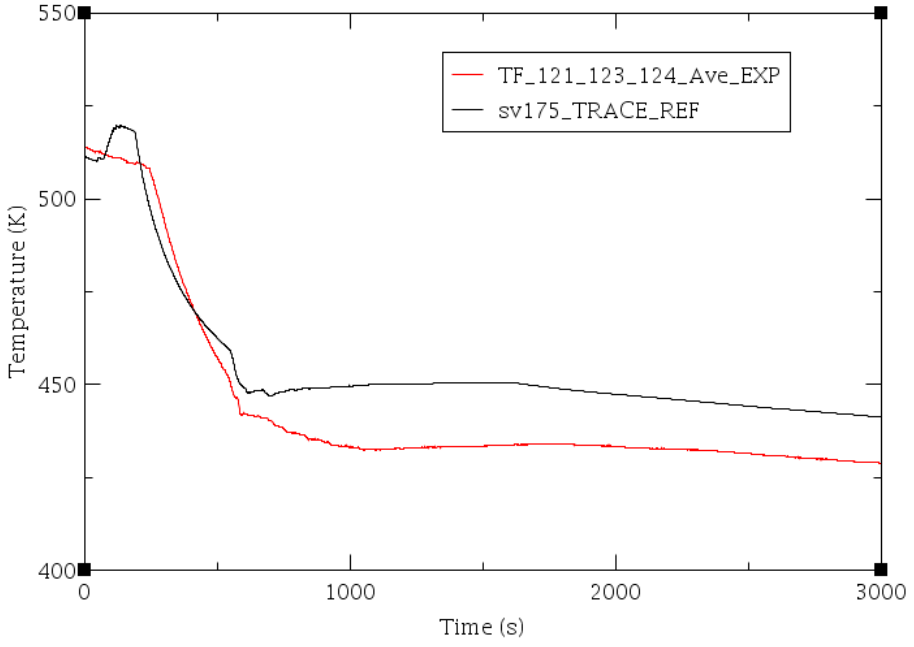

Figure 35 Experimental Data versus Code Calculation for the Average Core Inlet Temperature (Average value of TF-121, TF-123, TF-124)

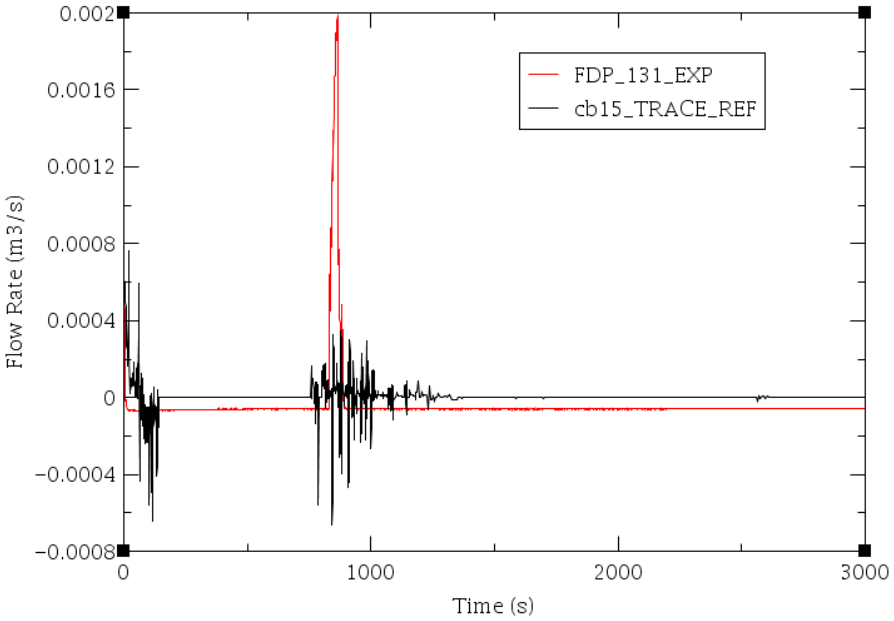

Figure 36 Experimental Data versus Code Calculation for RPV Volumetric Flow Rate (FDP-131)

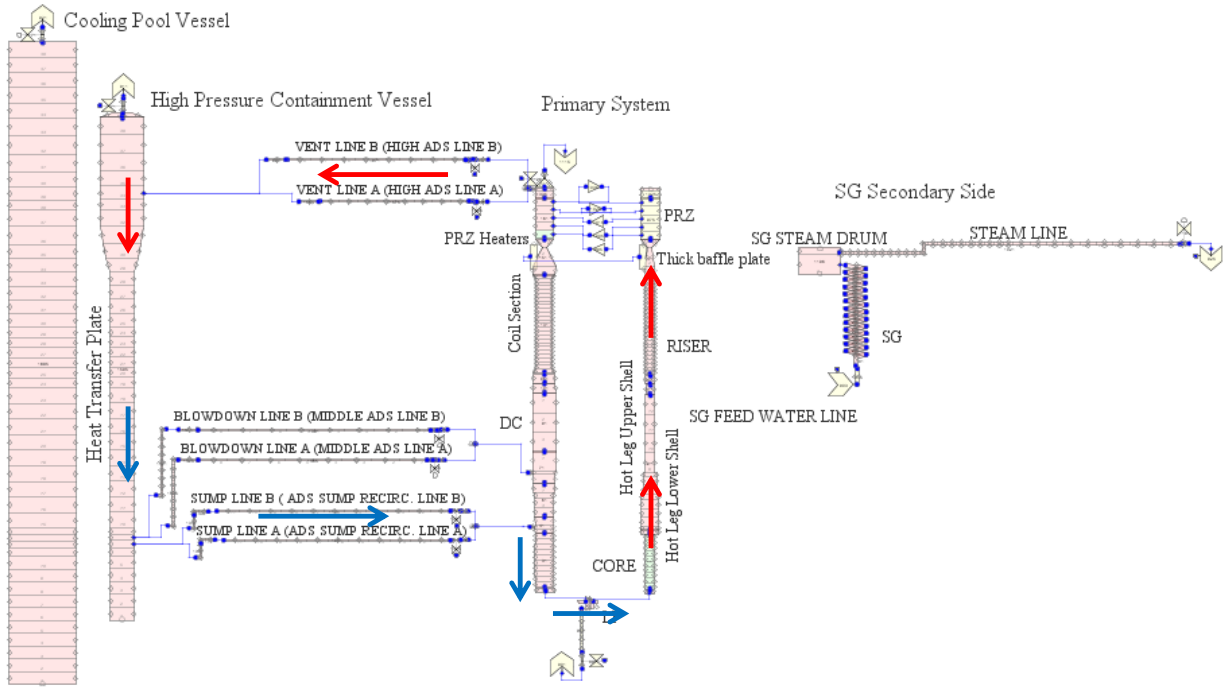

Figure 37 Long Term Cooling Flow Path Typical of the MASLWR Design

In order to characterize the thermal stratification in large containment cooling pool, the HPC temperatures (TF-811, TF- 821, TF-831, TF-841, TF-851, TF-861) were analyzed. In general, the qualitative experimental time trend is predicted by the code in the REF and SEN1 case though quantitative discrepancies exist. The TRACE results show a general overestimation of temperature in comparison with the experimental data. This could be due to the 1D model of the HPC that

doesn't allow the natural circulation and mixing phenomena in the HPC or the position of the thermocouples. The thermocouples are located very close to the heat transfer plate where the condensation takes place and do not represent the average bulk fluid temperature. The temperature calculated by the TRACE code is the average temperature related to the nodalization volume. The general qualitative behavior of the temperatures in the HPC, during the transient, is not affected by the initial condition of the HPC (Hot or Cold). In the SEN1 case a general greater overestimation, in comparison with the REF case, of the HPC temperatures is obtained. Greater discrepancies are observed in the TF-861 code prediction. This is related also to the nodalization strategy of using only one pipe to simulate the HPC, which doesn't simulate the mixing phenomena taking place in the upper part of the HPC. A more detailed 3D HPC model, by using the "vessel component" available in TRACE, may provide a better quantitative estimation of the HPC temperatures. In this way it is possible to simulate the natural circulation and the mixing phenomena in the upper part of the HPC. Fig. 38, as an example, shows the experimental data versus code calculation for TF-811. The comparisons between the calculated data and the experimental data in relation to the TF- 821, TF-831, TF-841, TF-851, TF-861 are reported in the Appendix A.

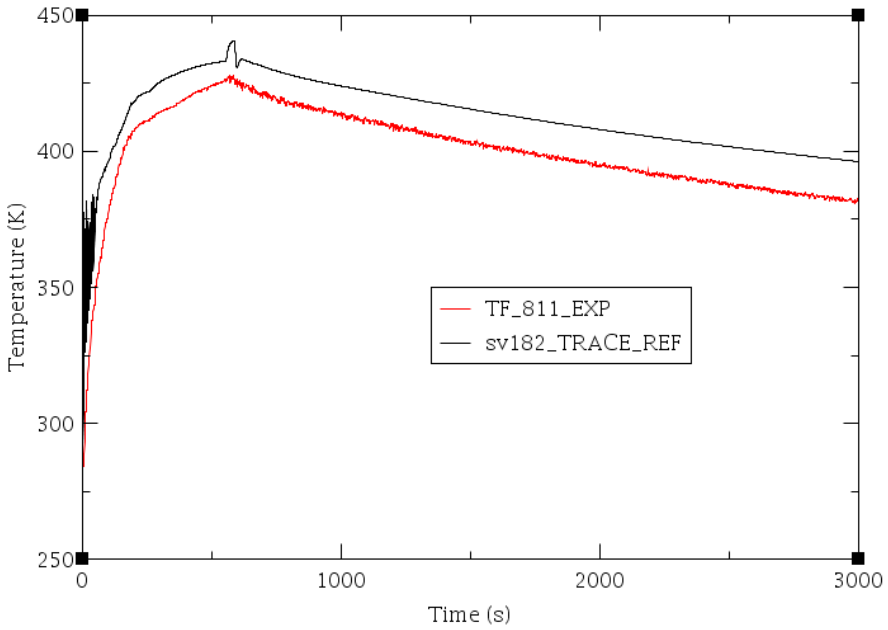

Figure 38 Experimental Data versus Code Calculation for TF-811

In order to characterize the thermal stratification in large containment cooling pool, the CPV temperatures (TF-815, TF-825, TF-835, TF-845, TF-855, TF-865) were analyzed. The TF-815, TF-825, TF-835, and TF-845 transient data are characterized by a slow temperature increase. TF-855 experimental data is characterized by temperature oscillations; TF 865 shows first a slow increase followed by a second more rapid increase (Appendix A). In general the TRACE calculation results show a constant temperature increase with a general underestimation compared to experimental data. This could be related also to the position of the thermocouples; in fact they are located very close to the heat transfer plate as well. No oscillations are predicted by the code for the TF 855 behavior. Fig. 39, as an example, shows the experimental data versus code calculation for TF-815. The comparison between calculated data and experimental data, in relation to the TF 825, TF 835, TF 845, TF 855, TF 865, is reported in the Appendix A.

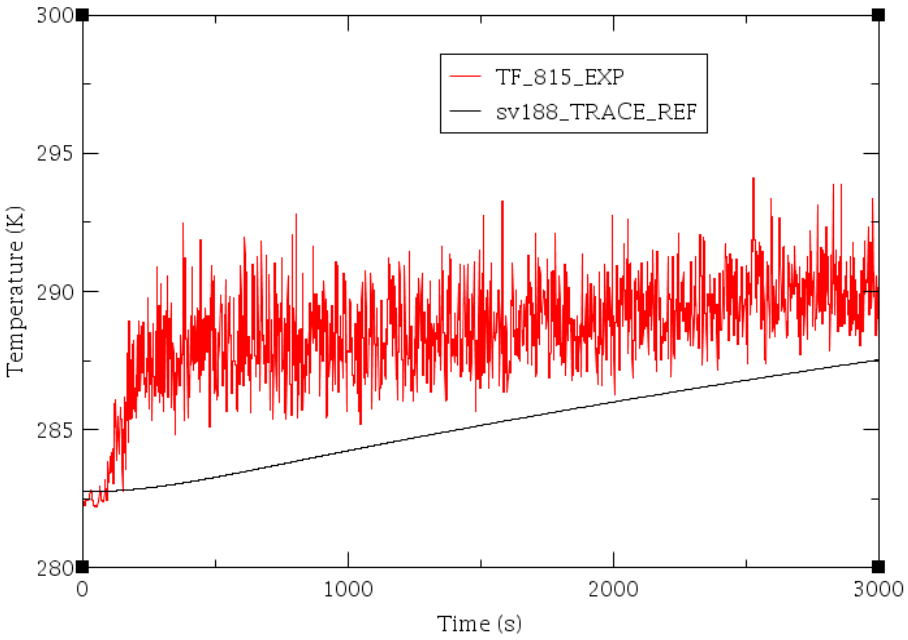

Figure 39 Experimental Data versus Code Calculation for TF-815

The results of the sensitivity study (SEN1 plot reference) shows that the qualitative trend of the calculated data is similar, as expected, but the RPV/HPC pressure, Fig. 40, and temperatures, Fig. 41 and 42, are in general over predicted by TRACE if the HPC heaters are in operation. Therefore the RPV/HPC coupled system stored energy calculated by TRACE is higher than the experimental data. This could be due to the 1D HPC TRACE nodalization. A 3D model, by using the "vessel component" available in TRACE, may better simulate the natural circulation and the mixing phenomena in the HPC. The sequence of events of the SEN1 case in comparison with the REF case, and the experimental data is shown in Table 12. The comparison of RPV level behavior is shown in Fig. 43. The temperature behavior and the fluid condition of the HPC, in different times of the transient, are shown in Figs. 44-51 for both REF and SEN1 case.

In the Appendix A the main parameter evolutions and comparison between calculated and experimental data are reported.

From a quantitative point of view the results of the calculated data show a general over prediction of the primary side pressure and temperatures compared with the experimental data. It is thought that this could be due to a combination of selection of vent valve discharge coefficients, condensation models applied to the inside surface of the containment, and to the 1D model of the HPC [12,16,20]. As it is shown in the [20] the correct prediction of the facility heat losses is an important parameter to accurately predict the transient evolution. The heat losses imposed as boundary condition has been calibrated considering the information's distributed during the IAEA ICSP [43].

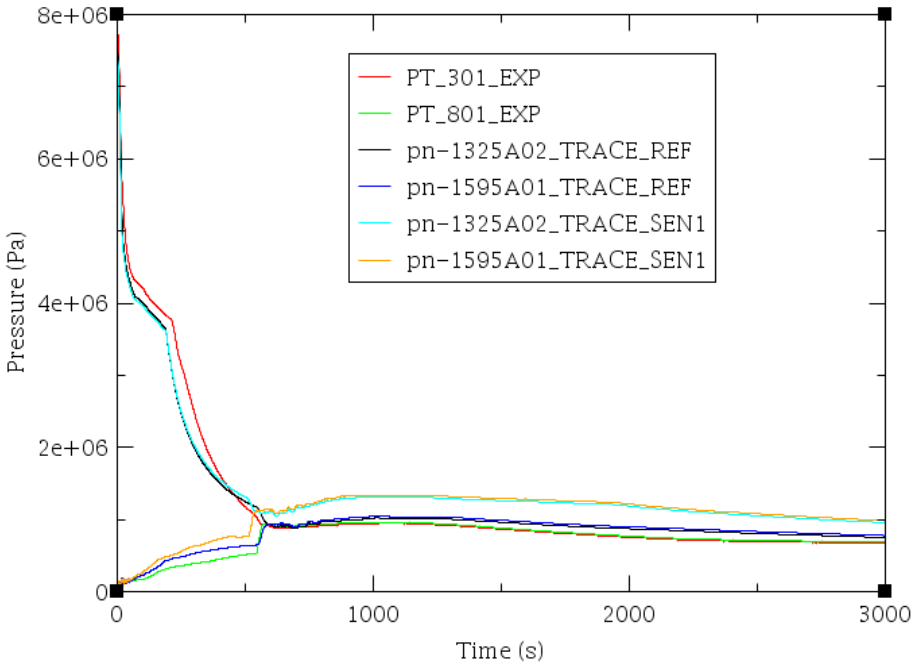

Figure 40 Experimental Data versus Code Calculation for PRZ (PT-301) and HPC Pressure (PT-801) for REF and SEN1 Case

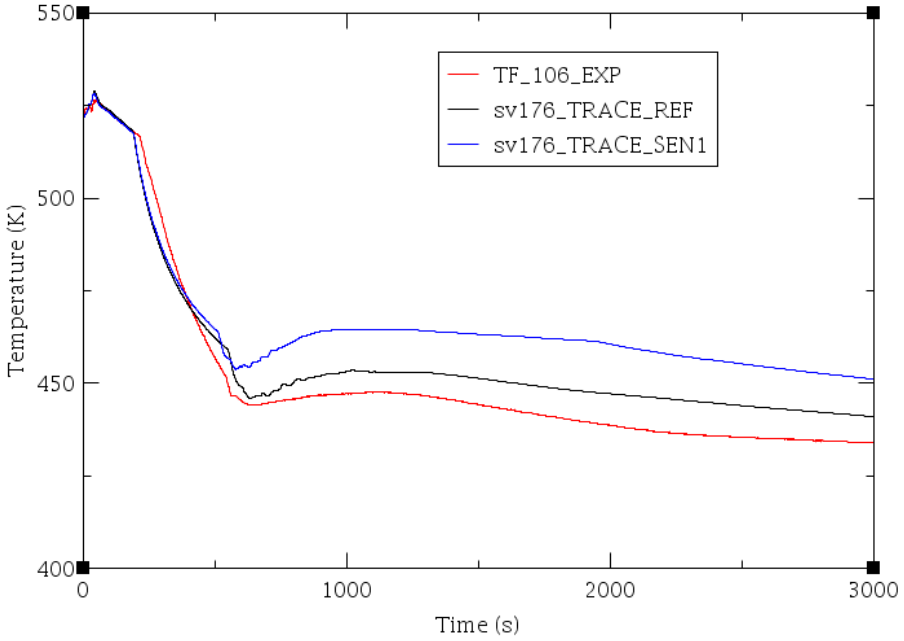

Figure 41 Experimental Data versus Code Calculation for Core Outlet T (TF-106) for REF and SEN1 Case

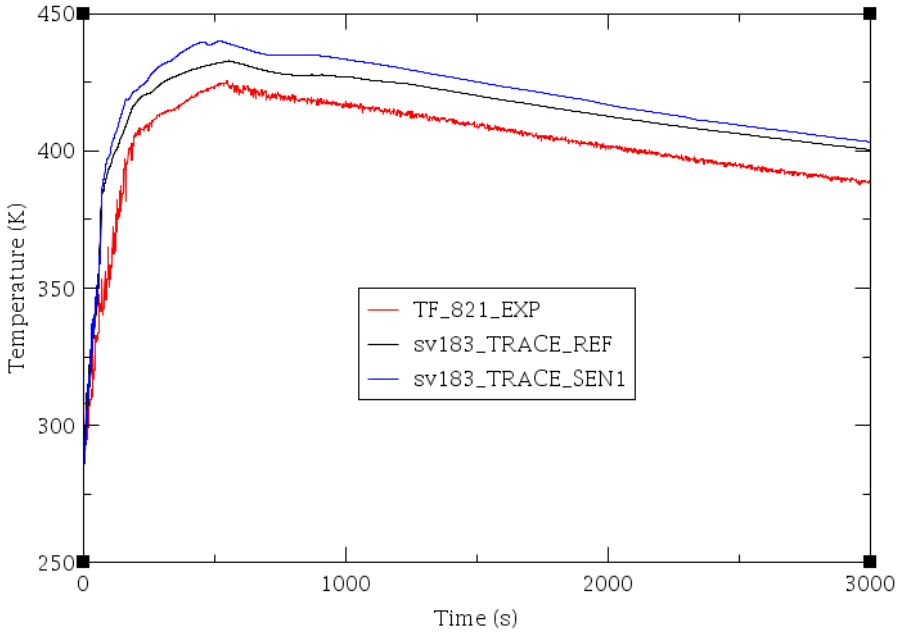

Figure 42 Experimental Data versus Code Calculation for TF-821 for REF and SEN1 Case

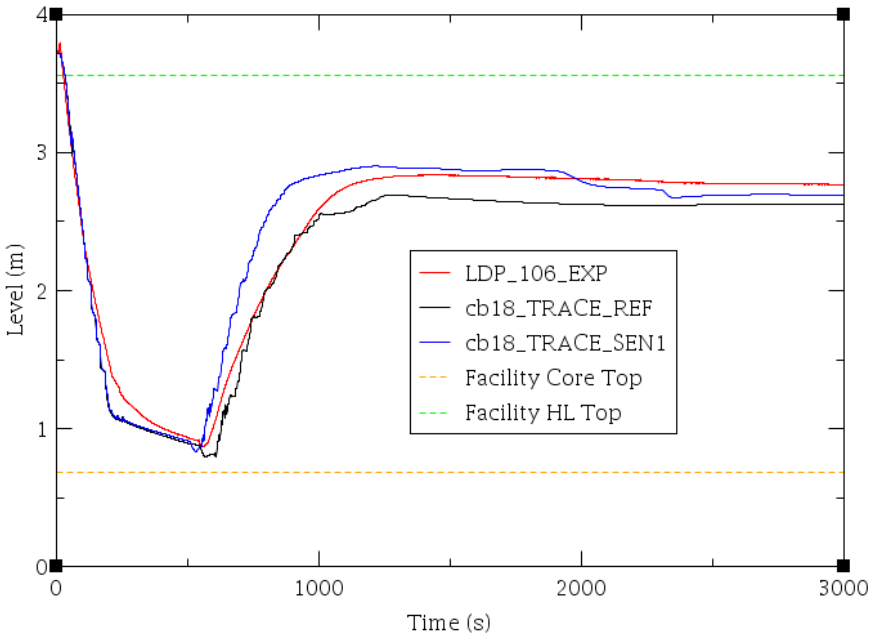

Figure 43 Experimental Data versus Code Calculation for RPV Level (LDP-106) for REF and SEN1 Case

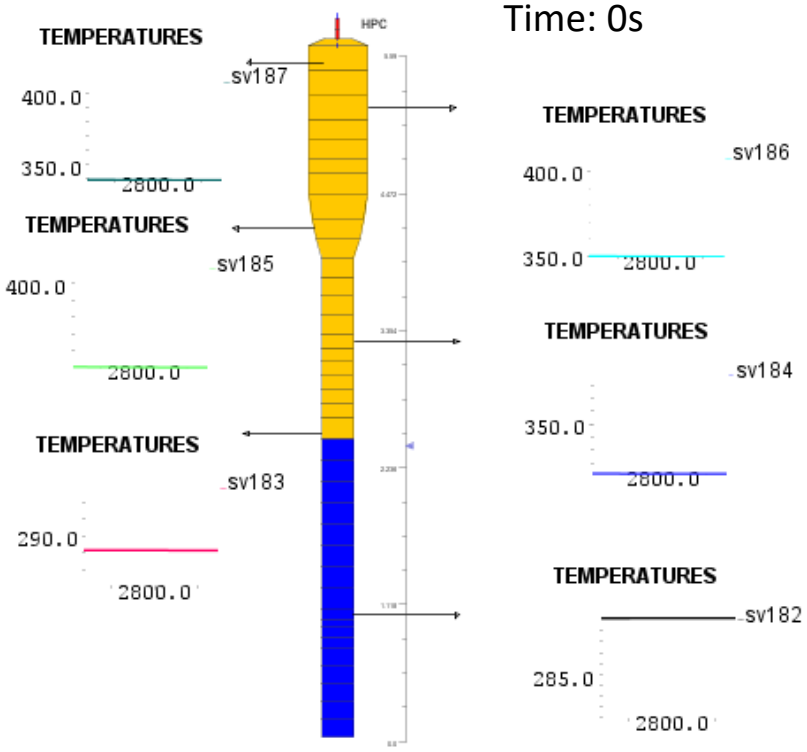

Figure 44 Fluid Condition and Temperature Visualization of the HPC, by using SNAP, at T=0s (REF Plot Reference)

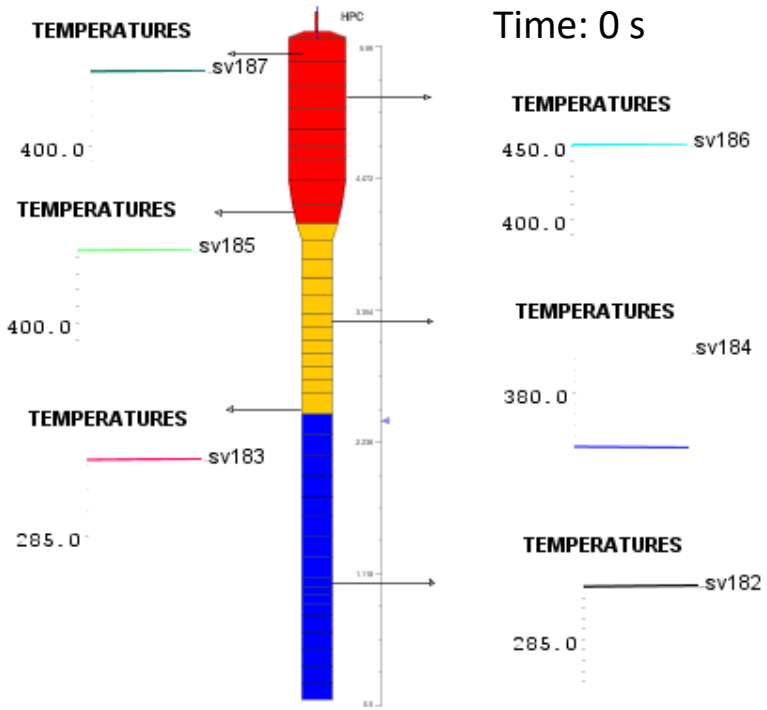

Figure 45 Fluid Condition and Temperature Visualization of the HPC, by using SNAP, at T=0s (SEN1 Plot Reference)

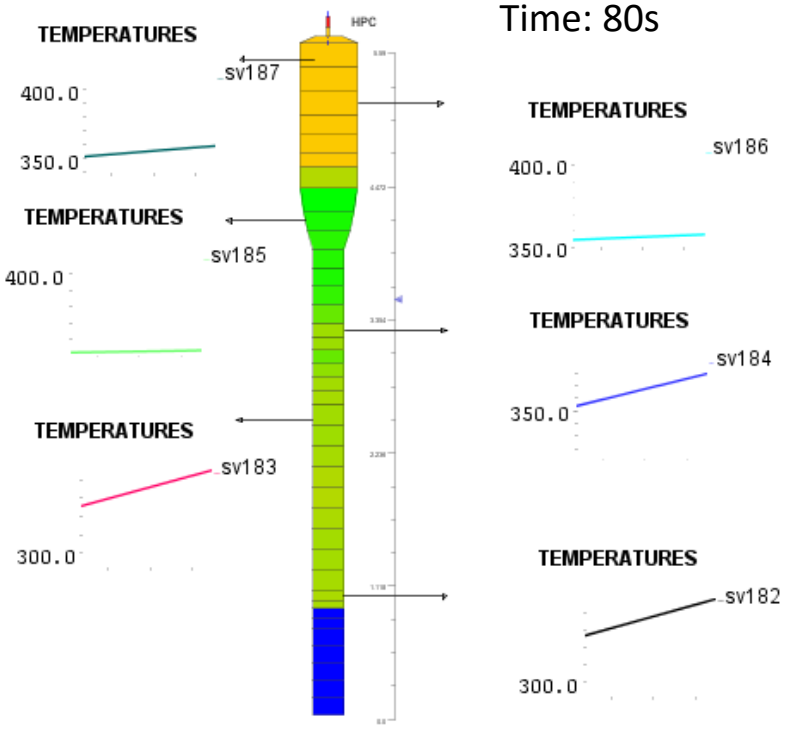

Figure 46 Fluid Condition and Temperature Visualization of the HPC, by using SNAP, at T=80s (REF Plot Reference)

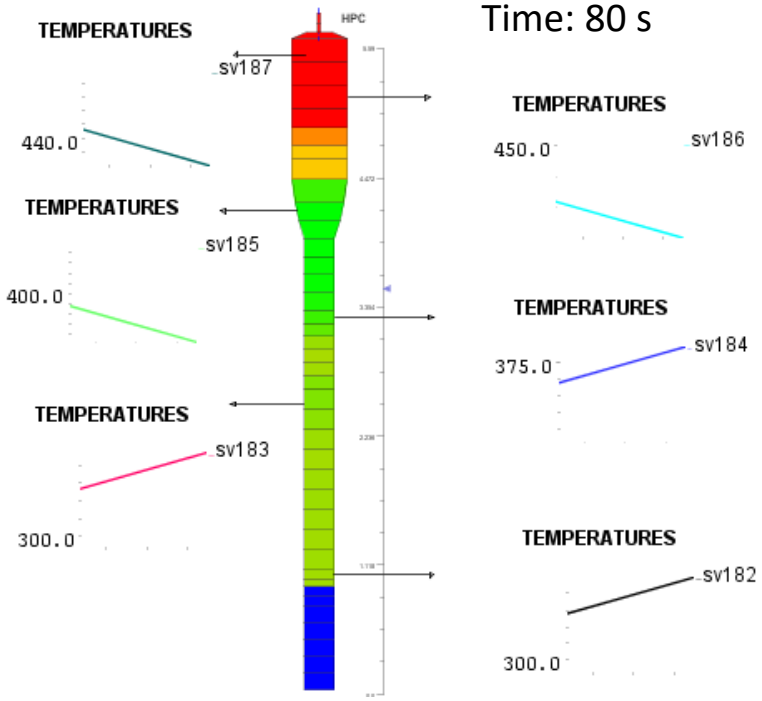

Figure 47 Fluid Condition and Temperature Visualization of the HPC, by using SNAP, at T=80s (SEN1 Plot Reference)

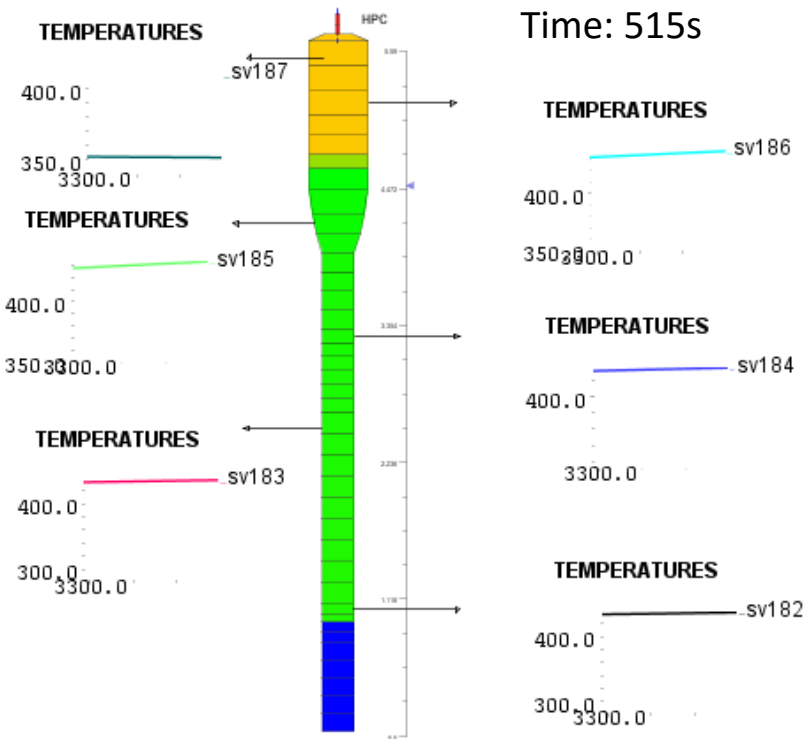

Figure 48 Fluid Condition and Temperature Visualization of the HPC, by using SNAP, at T=515s (REF Plot Reference)

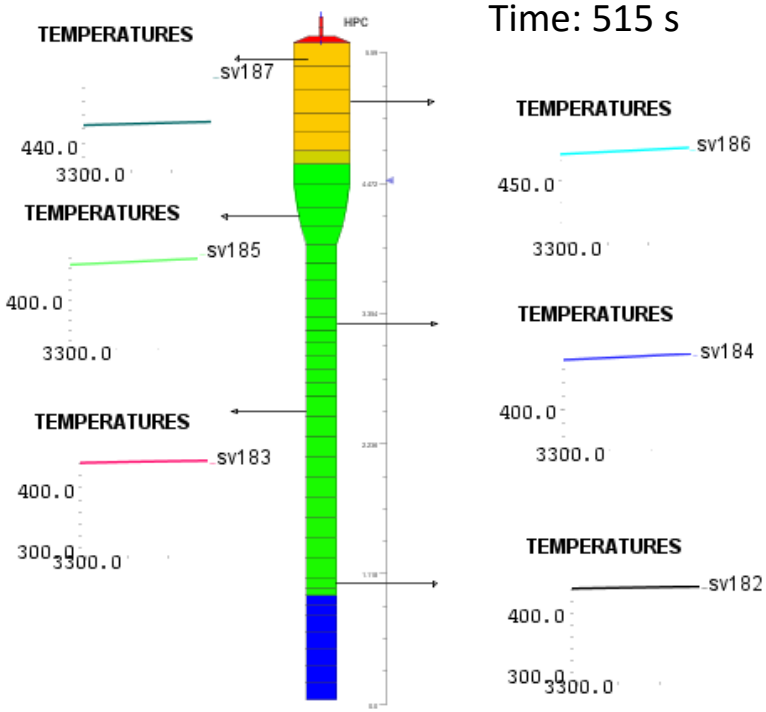

Figure 49 Fluid Condition and Temperature Visualization of the HPC, by using SNAP, at T=515s (SEN1 Plot Reference)

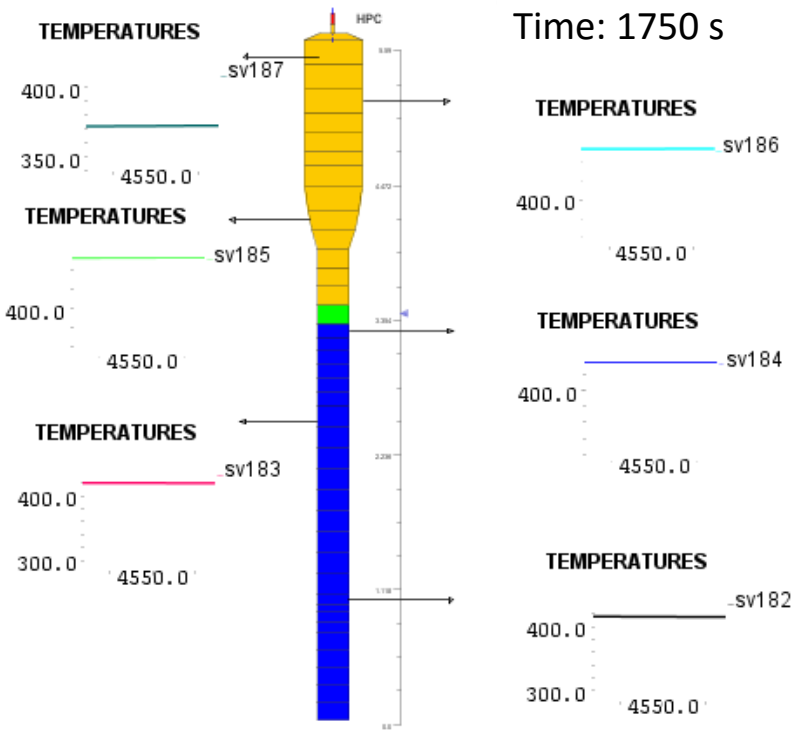

Figure 50 Fluid Condition and Temperature Visualization of the HPC, by using SNAP, at T=1750s (REF Plot Reference)

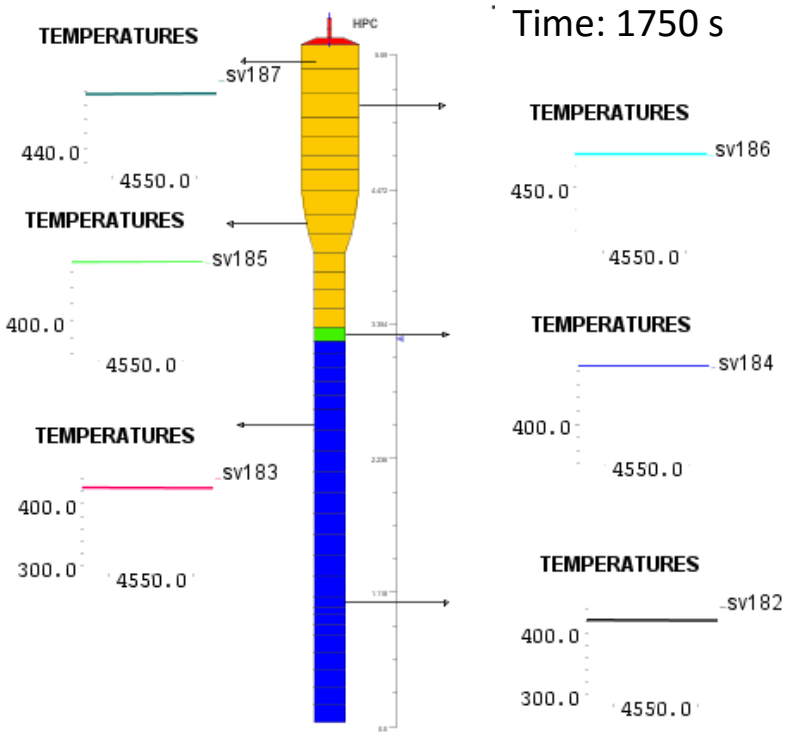

Figure 51 Fluid Condition and Temperature Visualization of the HPC, by using SNAP, at T=1750s (SEN1 Plot Reference)

The general qualitative conclusions of this revised analyses are in agreement with the results of the calculated data reported in the previous studies [12,13,14,16,20]. A better quantitative prediction of the TRAFE code is obtained with the REF analysis. Of particular interest is the analyses reported in the [12] where the application of the TRACE, RELAP5 Mod3.3 and RELAP5-3D code shows that the codes are able to qualitatively predict primary/containment coupling phenomena in the MASWLR tests. As it is shown in [13] and confirmed in [20] a detailed TRACE nodalization of the ADS lines, including the nodalization of the sparger, is necessary in order to have a better prediction of the calculated data as it is shown from better qualitative behavior of the RPV and HPC pressure obtained in the calculated data.

A matrix of phenomena observed test OSU-MASLWR-001 and TRACE code is shown in Table 13[3].

Table 13 Test versus Phenomena, TRACE Prediction vs Phenomena [43, 49-52]

Phenomenon	Experiment		TRACE code
	Phenomena	Measurement	Phenomena
Single-Phase Natural Circulation	+	+	+
Two-Phase Natural Circulation	+	NA	+
Heat Transfer in Covered Core	+	+	+
Distribution of Pressure Drop Through Primary System	+	+	+
Primary-Containment Coupling During Blowdown And Long Term Cooling	+	o	+
Structural Heat And Heat Losses	+	o	+
Break Flow	+	o	+
Behavior of Large Pool: Thermal Stratification (HPC)	+	+	+
Behavior of Large Pool: Natural Convection (HPC)	+	NA	NA*
Behavior of Large Pool: Steam Condensation (HPC)	+	NA	+
Effect of Non-Condensable Gases On Condensation Heat Transfer (HPC)	+	NA	+
Condensation on Containment Structures (HPC)	+	o	+
Behavior of Large Pool: Thermal Stratification (CPV)	+	+	+
Behavior of Large Pool: Natural Convection (CPV)	+	NA	NA*

**The natural circulation phenomena in HPC and CPV are not predicted by the TRACE code for the 1D nodalization strategy of the HPC and CPV. A 3D model, by using the vessel component, could permits the prediction of these phenomena.*

[3] *Experimental facility and code qualitative phenomena prediction evaluation:*

	+	o	NA	-
Experimental data	Phenomenon occurred in the test and it is directly measured	Phenomenon occurred in the test and it is indirectly measured	Phenomenon occurred during the test but there is no instrumentation to detect (lack of instrumentation)	Phenomenon not occurred in the test
Calculated data	Phenomenon is clearly predicted by the code **(Excellent/Reasonable)**	Phenomenon is partially predicted (i.e. the answer of the code is **reasonable** but closure code relation are not appropriate, etc)	Models are not appropriate to predict (i.e. nodalization strategy, etc) **(Minimal)**	Phenomenon is not predicted by the code **(Unqualified)**

3.4 Analyses of the OSU-MASLWR-002 Calculated Data

Starting from the TRACE calculations developed in previous analyses [11,13-16,18,23], the purpose of this section is to give an expanded revised analyses of the TRACE V5.0 code capability in predicting the natural circulation phenomena and heat exchange from primary to secondary side by helical SG in superheated condition, typical of the MASLWR design, by simulating the OSU-MASLWR-002 test.

In order to reach the BIC a pre-test phase has been conducted. The pre-test phase started at about 2295s before the SOT (-2295s) and the main facility procedures to reach the BIC characterizing that time window (from -2295s to 0s) have been implemented in the TRACE model. The facility configuration before the SOT of the OSU-MASLWR-002 test is reported in Table 14. The core power time evolution and the FW time evolution are imposed as boundary condition during this phase. The PRZ heaters are assumed to be in operation in order to maintain the primary pressure set-point; the HPC heaters are OFF. The ADS valves were closed.

Table 14 Facility Configuration Before the SOT of the OSU-MASLWR-002 Test

System	Facility Operation	TRACE Model Operation	Note
Core Heaters	ON	ON	-
PRZ Heaters	ON	ON	In order to maintain the primary pressure set-point.
Containment Heaters	OFF	OFF	-
Feed water	ON	ON	In order to remove the net primary power [primary power less ambient losses].

At SOT the TRACE code predicts a primary system in a sub-cooled condition with single-phase natural circulation. The primary pressure is at about 7.7 MPa and the PRZ heaters are set up to maintain the primary pressure at the fixed set point. The secondary fluid, circulating inside the helical coil tubes, removes the core power (minus the facility heat losses from the primary fluid) and goes out from the SG as superheated steam. The outlet SG secondary pressure is around 1.4 MPa. The ADS middle line valves, the ADS high line valves and the ADS sump recirculation line valves are closed. Since no helical coil heat transfer correlation have been implemented in the TRACE V5.0 Patch 3, in agreement with previous analyses [21, 22, 23, 43], the heat transfer area of the equivalent helical coil SG heat structure is incremented in order to reach the initial conditions of the OSU-MASLWR-002 test. Table 15 shows the SOT conditions of the TRACE model VS experimental data for the OSU-MASLWR-002 test.

During the simulation of the transient the core power is imposed as BIC and the PRZ heaters are ON in order to control the primary side pressure. The temperature and pressure of the FW fluid at the inlet of the SG are imposed as BIC. The time dependence of the pressure, at the outlet of the SG, and the time dependence of the FW mass flow rate are imposed as boundary condition as well. Fig. 52 shows the fluid condition and the temperature diagram of the TRACE model at the SOT.

Table 15 SOT Condition Predicted by the TRACE Code vs Experimental Data for the OSU-MASLWR-002 Test

Parameter	EXP	TRACE (REF)	TRACE (SEN)
Core Power (W)	80000	80000	80000
PRZ Pressure (Pa)	7745080	7697156	7697166
Core Outlet T(K)	504	504	504
Core Inlet T (Average) (K)	487	486	487
Primary Volumetric Flow Rate (m^3/s)	0.001	0.001	0.001
PRZ Level (m)	0.33	0.33	0.35
SG Inlet T (K)	292	292	292
SG Inlet P (average) (Pa)	1385980	1334900	1334900
SG Outlet P (Pa)	1428364	1428530	1428848
Secondary Mass Flow Rate (kg/s)	0.019	0.019	0.019
Average SG Outlet Temperature (K)	498	495	495

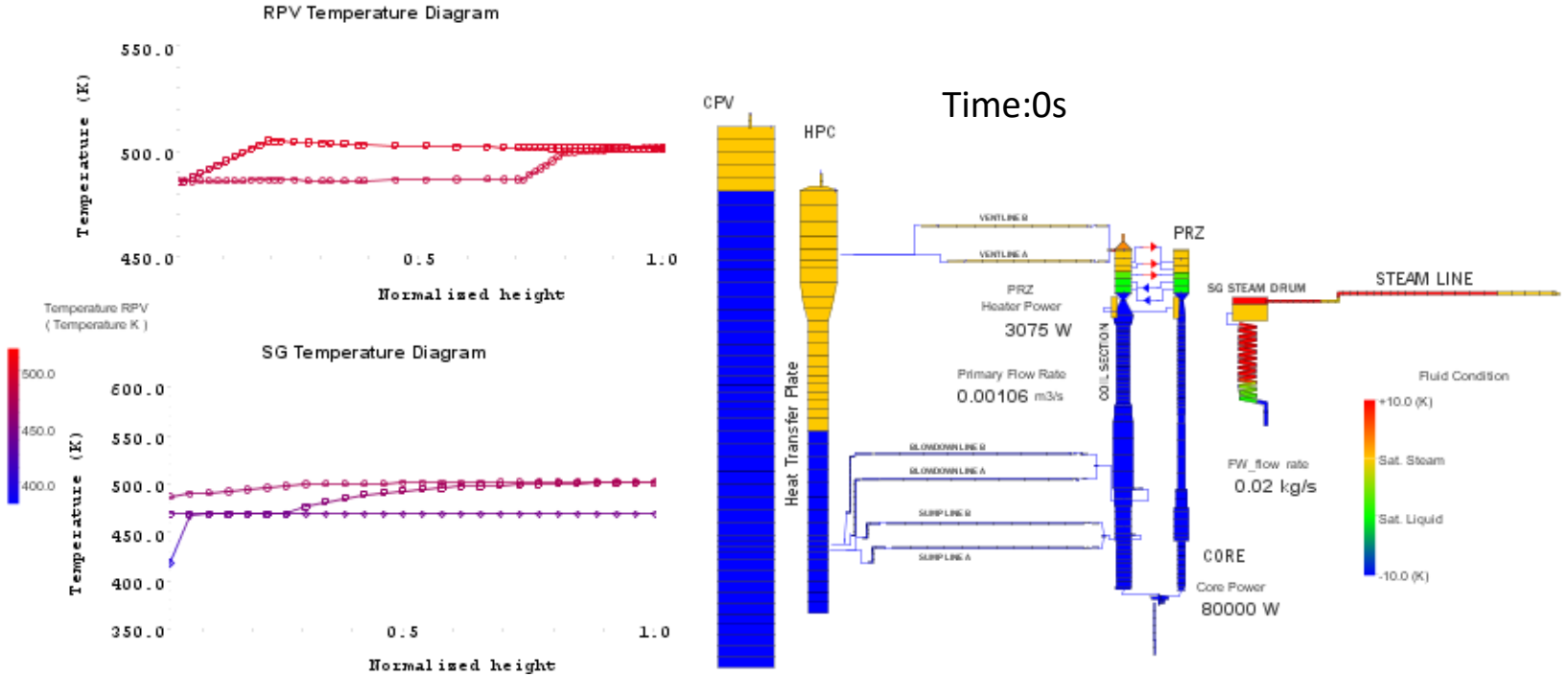

Figure 52 SNAP Animation Model Showing the SOT Condition of the TRACE Model (REF Plot Reference)

The core outlet and inlet temperatures are predicted by the TRACE code and shown in Fig. 53 and Fig. 54, respectively. The primary volumetric flow rate, and the difference between the core inlet and outlet fluid temperature (delta T core) are shown in Fig. 55 and Fig. 56, respectively. The inlet/outlet fluid core temperature calculations by TRACE show a qualitative agreement but a general overestimation compared with the experimental data. Therefore, in the TRACE simulation, the primary circuit stores more energy compared with the experimental data.

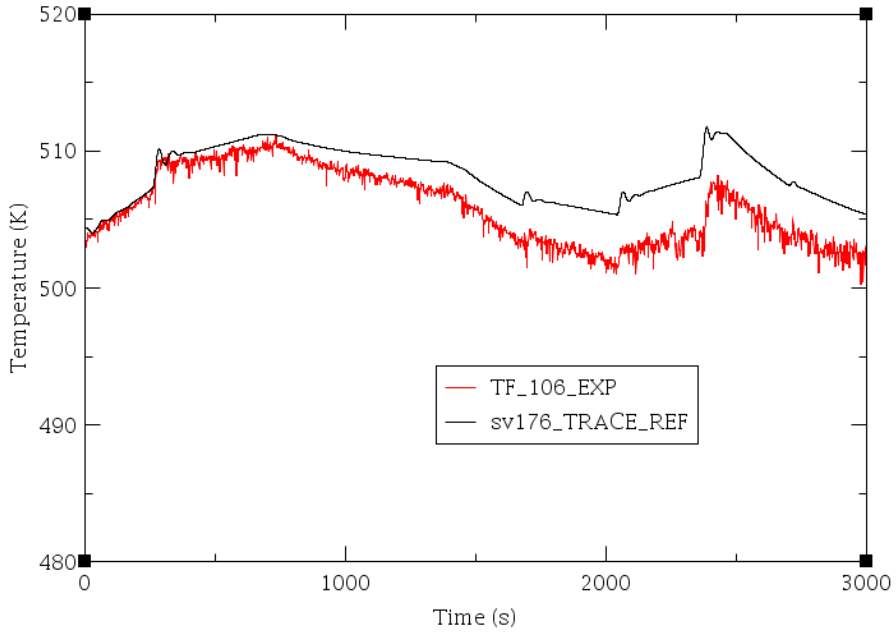

Figure 53 Experimental Data versus Code Calculations for Fluid Temperature at the Core Outlet (TF-106)

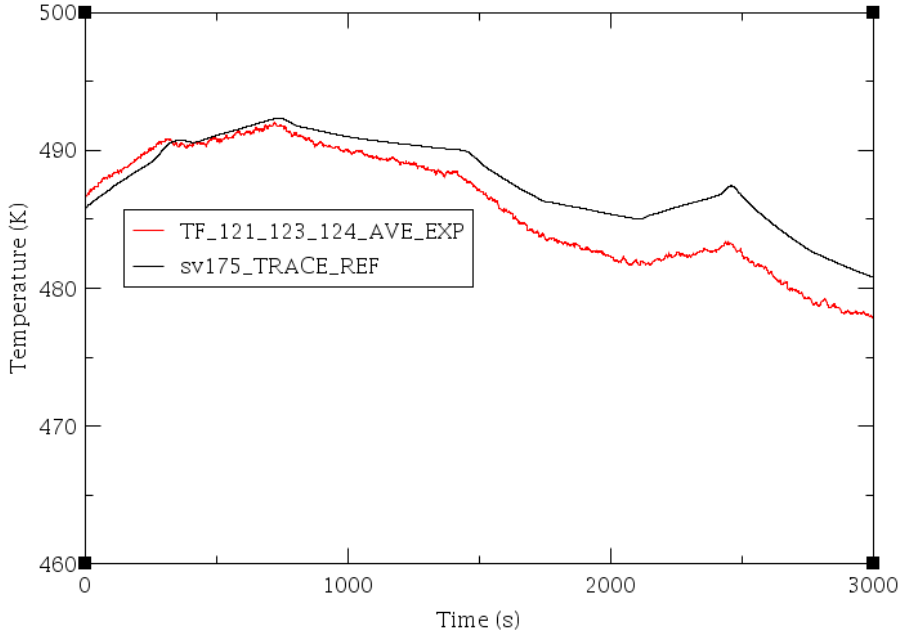

Figure 54 Experimental Data versus Code Calculations for Fluid Temperature at the Core Inlet (Average Value of TF 121, 123, 124)

The primary natural circulation volumetric flow rate behavior is qualitatively and quantitatively predicted by the code. It is important to note that previous discrepancies between experimental and calculated data by using a constant k loss coefficient at the core entrance (SEN case), are now not observed by using the new feature of the TRACE V 5.0 patch 3 code that allow to define flow Reynolds number-dependent loss coefficient (REF case).

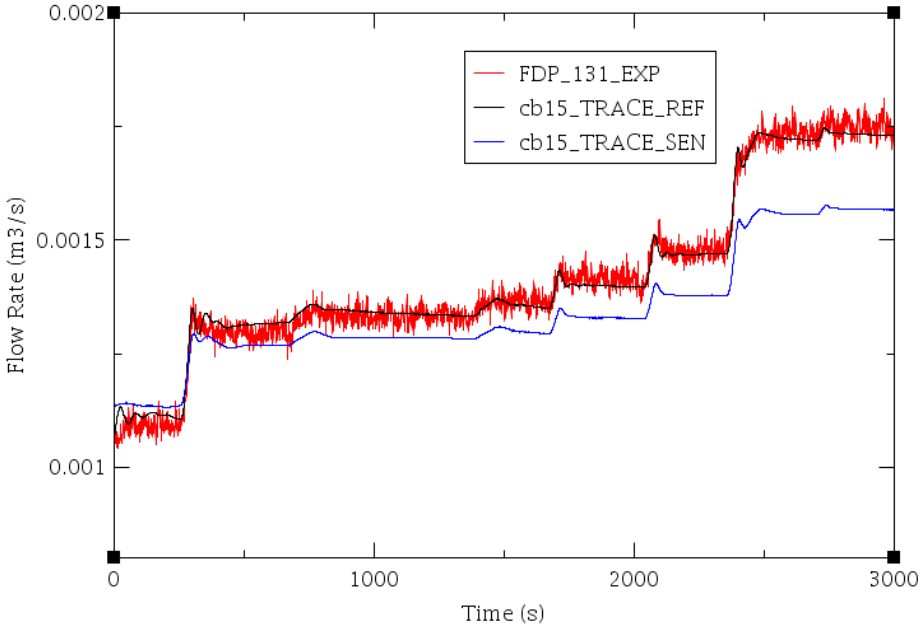

Figure 55 Experimental Data versus Code Calculations for Primary Volumetric Flow Rate (FDP-131)

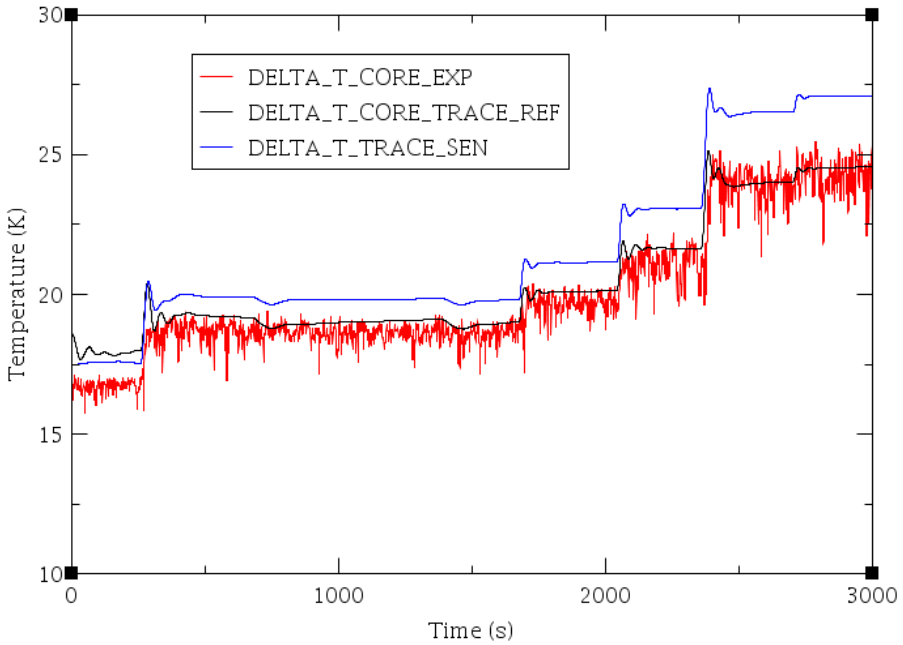

Figure 56 Experimental Data versus Code Calculations for Core Delta T

The core delta T time trend is coupled with the primary volumetric flow rate, the core power and the thermo physical condition of the primary fluid. An underestimation of the primary volumetric flow rate results in an overestimation of the delta T core (SEN case) by the TRACE code. The correct quantitative prediction of the primary volumetric flow rate determines a general correct quantitative prediction of the core delta T (REF case), Fig. 55 and 56.

The PRZ level is qualitatively predicted by the TRACE code, Fig. 57; the PRZ pressure behavior is predicted by the code as well, Fig. 58. Previous PRZ pressure discrepancies predicted by the TRACE V5 Patch 01 are now not predicted by the Patch 02 and Patch 03 results in a more stable prediction of PRZ pressure and level [16]. The general overestimation of the PRZ liquid level by the TRACE code is due to the general overestimation of the RPV temperatures.

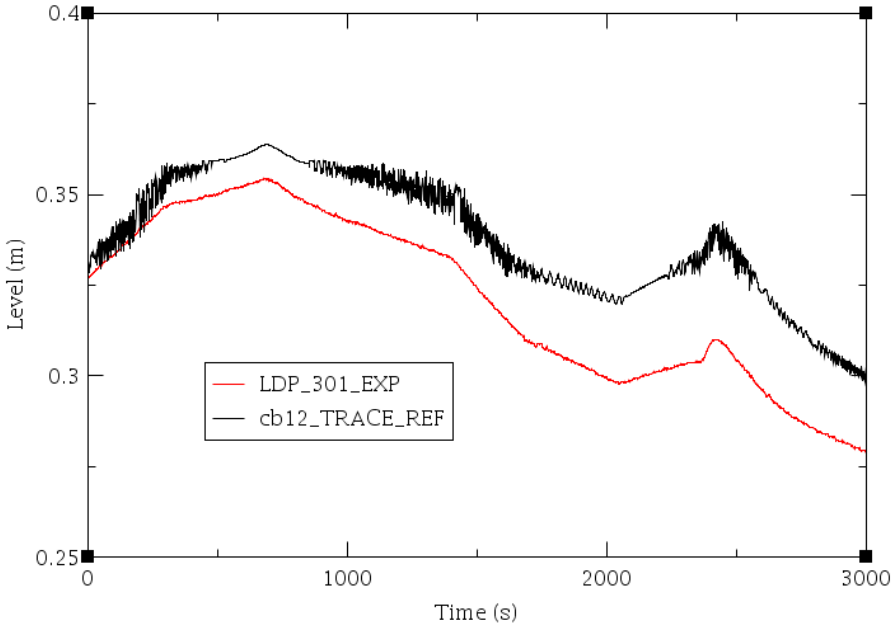

Figure 57 Experimental Data versus Code Calculations for PRZ Level

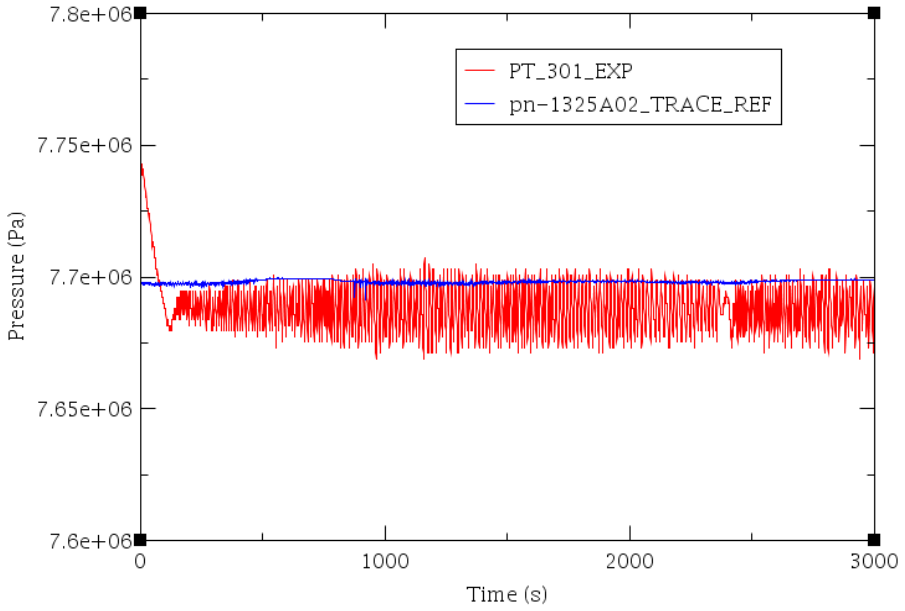

Figure 58 Experimental Data versus Code Calculations for PRZ Pressure

By analysing the experimental data, related to the flow temperature after the SG coils primary side section and the core inlet temperature, it is evident that the direct heat exchange, through the internal shell, between the fluid ascending the HL and the fluid descending the CL, is a crucial parameter for the evaluation of the core inlet temperature and therefore the core outlet temperature [18]. In fact, the experimental data show that, along the downcomer region, the fluid increases his temperature between the end of the SG primary side section and the core inlet. An overestimation or an underestimation of this phenomenon creates an increase or decrease of the core inlet temperature. The phenomenon is predicted by the TRACE model used. Fig. 59 shows the comparison between the experimental and calculated data for the difference of temperature between the fluid at the inlet of the core and the fluid at the exit of the SG primary side section.

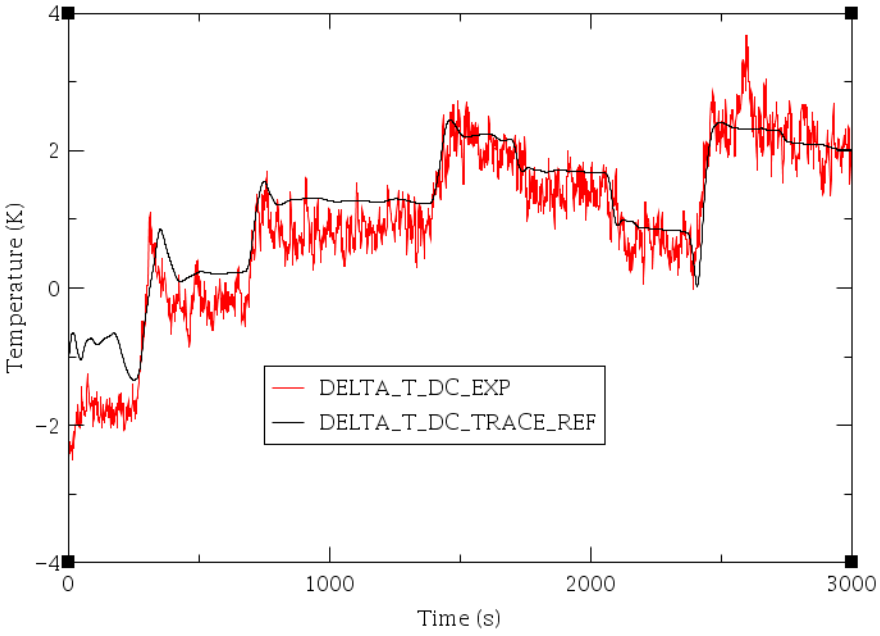

Figure 59 Experimental Data versus Code Calculations for the Difference of Fluid Temperature at the Inlet of the Core and at the Exit of the SG Primary Side

The SG heat transfer is qualitatively predicted by the TRACE code. The average fluid temperature at the outlet of the helical coils, Fig. 60, shows a qualitative agreement compared with the experimental data.

Fig. 61, developed by using SNAP, shows the RPV temperature profile for the OSU-MASLWR-002 test (2555s after the SOT). Fig. 62, also developed by using SNAP, shows the fluid temperature along the equivalent helical coil cells and the fluid temperature profile along the SG primary side section at 2555s after the SOT. From these figures it is possible to identify the subcooled, saturated and superheat region of the inner equivalent helical coil. In agreement with the experimental data, the secondary fluid enters subcooled at the bottom of the SG and boils off after travelling a certain length in the SG. In the TRACE model, in agreement with the experimental data, the steam will leave the SG superheated. As in the experimental data the slope of the MS superheat curve increases if the value of the core power increases and decreases if the value of the FW flow rate increases. In Fig.63 and 64, the condition of the TRACE model at 1000s and 2700s after the SOT are shown. Of particular interest is the reduction of the steam superheating region at 2700s after the SOT easily visualized by using SNAP.

As noted before, the inlet/outlet fluid core temperatures predicted by TRACE show a qualitative agreement but a general overestimation compared with the experimental data. This could be related to SG primary and secondary side heat transfer. One of the reasons could be an underestimation of the helical coil heat transfer coefficient during the different phases of the test. No specific helical coil heat transfer correlations have been implemented in the TRACE V5.0 Patch 3 used for this simulation. From the results of the previous analyses it is important to note the influence of the correct heat losses prediction [16]. Another important point to consider is the influence of the nodalization choice. The analyses of previous TRACE calculated data show that one of the reasons of the instability of the superheat condition of the fluid at the outlet of the SG, already observed in [11], is the equivalent SG model used to simulate the different group of helical coils. In particular, if the helical coils are modelled by only one “equivalent” vertical tube, a more stable fluid temperature at the outlet of the helical tubes is predicted by the code. The model with three different oblique or vertical tubes needs more investigations in order to study the possible instability conditions predicted by the code [18].

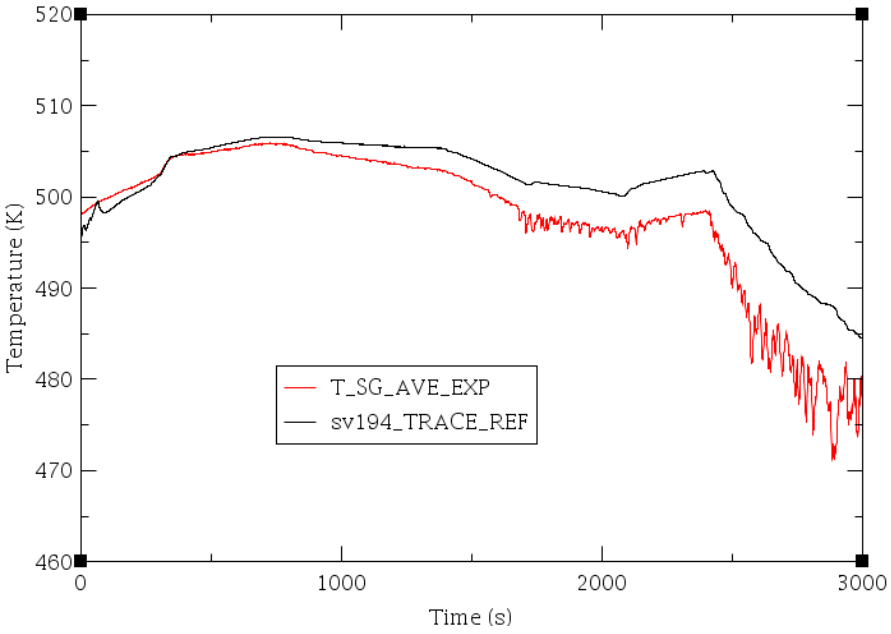

Figure 60 Experimental Data versus Code Calculations for the Average Fluid Temperature at the SG Coil Outlet

A matrix of phenomena observed in test OSU-MASLWR-002 and TRACE code is shown in Table 16[3].

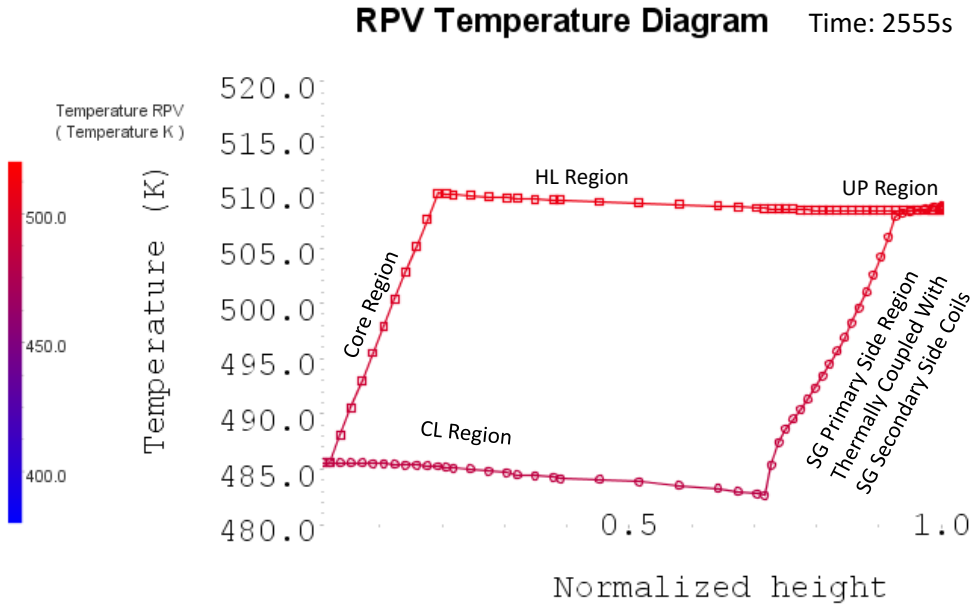

Figure 61 RPV Temperature Profile for the OSU-MASLWR-002 Test (2555s after the SOT)

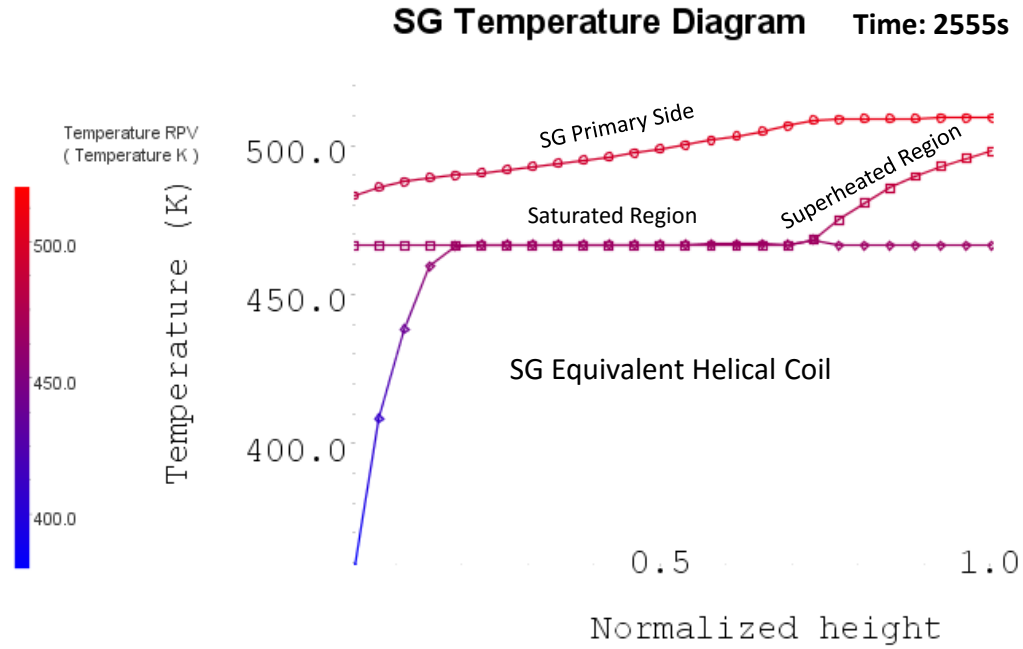

Figure 62 SG Primary Side and Equivalent Helical Coil Temperature Diagram for the OSU-MASLWR-002 Test (2555s after SOT)

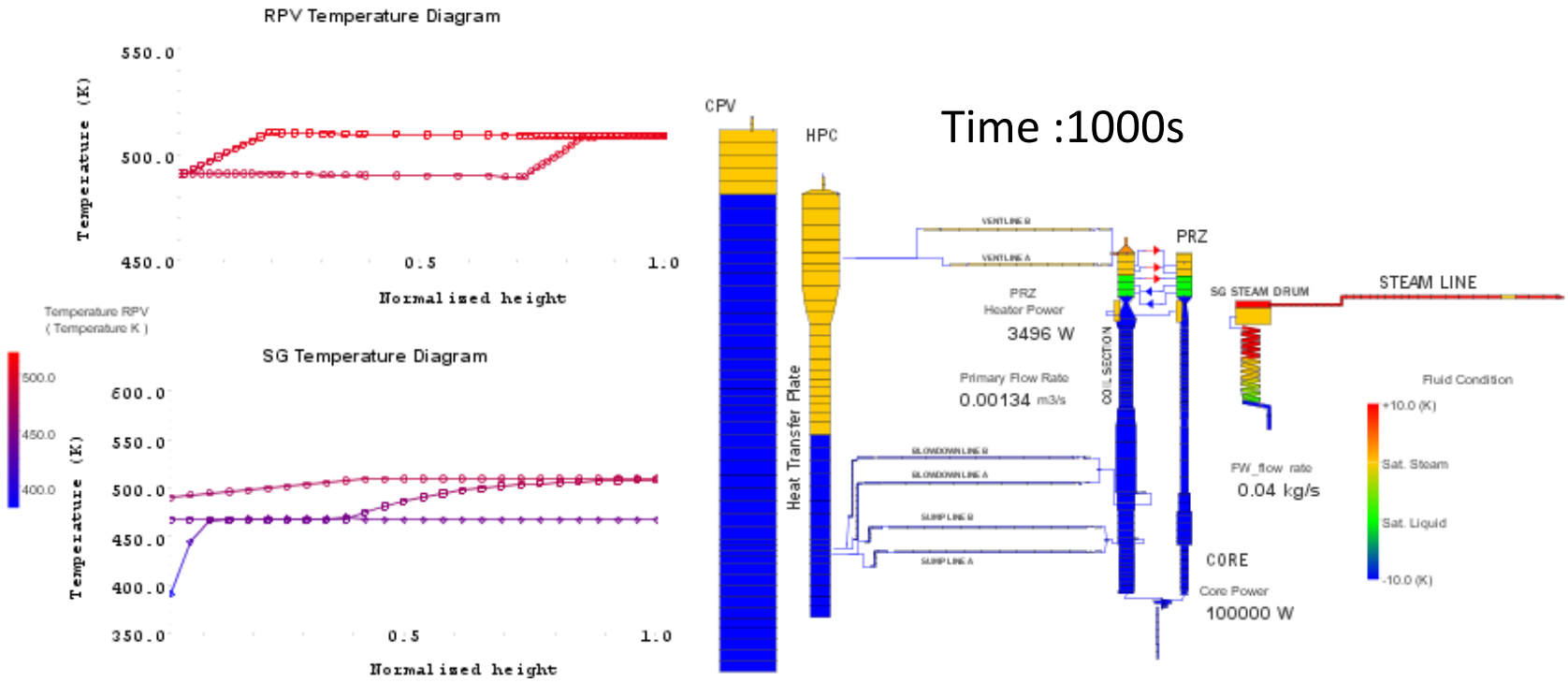

Figure 63 SNAP Animation Model Showing the Condition of the TRACE Model 1000s after the SOT

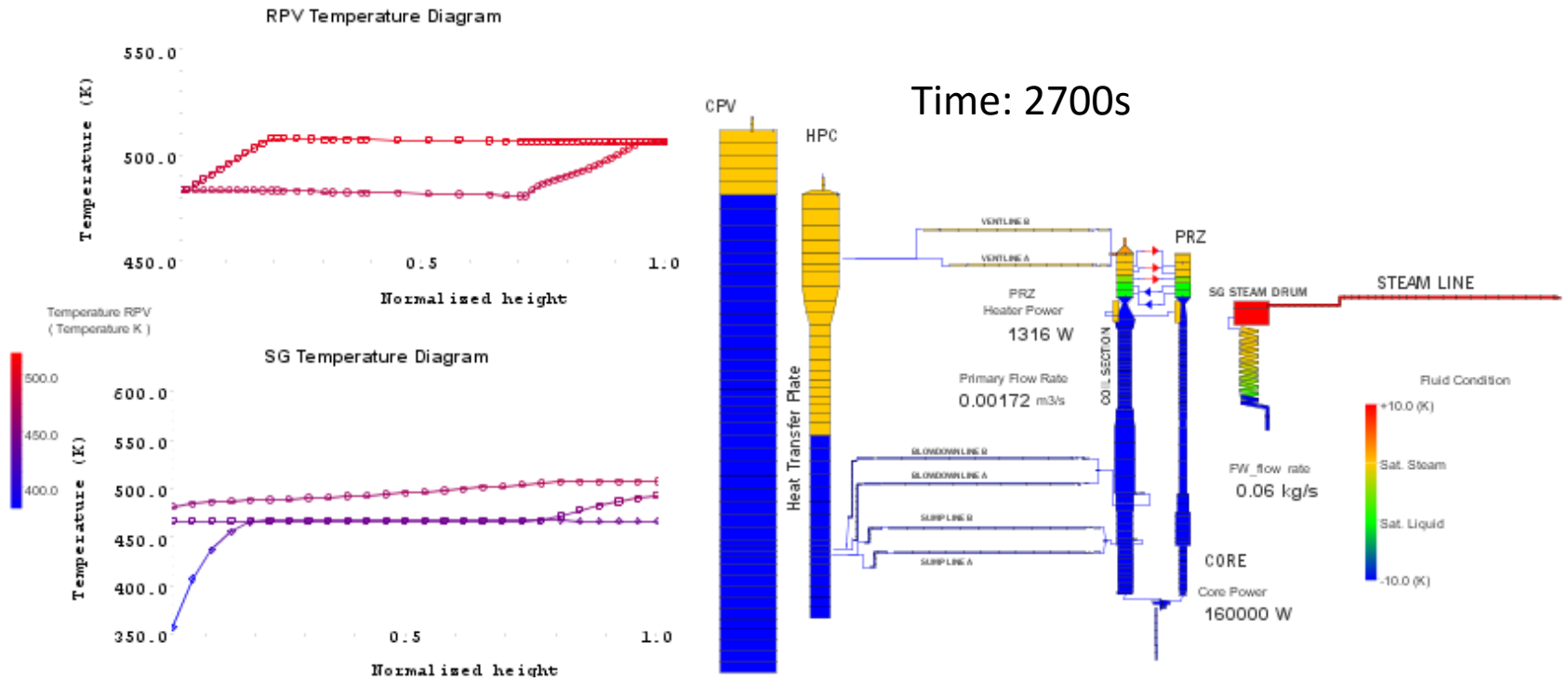

Figure 64 SNAP Animation Model Showing the Condition of the TRACE Model 2700s after the SOT

Table 16 Main Phenomena vs Facility and vs TRACE[3] [43, 49-52]

Phenomenon	Experiment		TRACE code
	Phenomena	Measurement	Phenomena
Single-phase Natural Circulation	+	+	+
Heat Transfer in Covered Core	+	+	+
By Pass Heat Transfer	+	+	+
Distribution of Pressure Drop Through Primary System	+	+	+
Heat Transfer in SG Primary Side	+	+	+
Structural Heat and Heat Losses	+	o	+
Heat Transfer in SG Secondary Side	+	+	o*
Steam Superheated on Secondary Side	+	+	+

**The heat transfer in SG secondary side is partially predicted by the code because no helical coil heat transfer correlation has been implemented in the TRACE V5.0 Patch 3.*

4. CONCLUSIONS

The TRACE code has been used to predict two tests from the MASLWR integral pressure reactor test facility at Oregon State University. This activity has been conducted in a collaboration among the ENEA, the Department of Energy of the University of Palermo, the Gruppo di Ricerca Nucleare San Piero a Grado (GRNSPG) of University of Pisa, the Department of Nuclear Engineering and Radiation Health Physics of the Oregon State University and NuScale Power Inc.. In particular the OSU-MASLWR-001 test, an inadvertent actuation of one submerged ADS valve, investigates the primary/containment coupling in design basis accident condition; the OSU-MASLWR-002 test, a natural circulation test, investigates the primary system flow rates and secondary side steam superheat for a variety of core power levels and feed water flow rates.

The analysis of the OSU-MASLWR-001 test show that the TRACE code is able to qualitatively predict the single and two-phase natural circulation and primary/containment coupling phenomena characterizing the test. The sub-cooled, saturated, and single phase blowdown are reasonably predicted by the code. The refill of the core, permitting its cooling, is reasonably predicted as well. In agreement with the experimental data the RPV level water calculated by TRACE never fell below the upper part of the core during the blowdown following the middle valve opening. The results of the TRACE calculations show a general over prediction of primary side pressure and temperatures compared with the experimental data. It is thought that this could be due to a combination of selection of vent valve discharge coefficients and condensation models applied to the inside surface of the containment. A more detailed 3D HPC model, by using the “vessel component”, may provide a better quantitative estimation of the HPC temperatures. In this way it is possible to simulate the natural circulation and the mixing phenomena in the upper part of the HPC.

The analyses of the OSU-MASLWR-002 test shows that the TRACE code is able to qualitatively predict natural circulation phenomena and heat exchange from primary to secondary side. The calculated results show a general qualitative agreement with the experimental data. An overestimation of the inlet/outlet core temperature is predicted by the code. This could be related to SG primary and secondary side heat transfer. One of the reasons could be an underestimation of the helical coil heat transfer coefficient during the different phases of the test. No specific helical coil heat transfer correlations have been implemented in the TRACE V5.0 Patch 3 used for this simulation. From the results of the previous analyses it is important to consider the influence of the correct heat losses prediction. Another important point to note is the influence of the nodalization choice. The analyses of previous TRACE calculations show that one of the reasons of the instability of the superheat condition of the fluid at the outlet of the SG, already observed in [11], is the equivalent SG model used to simulate the different group of helical coils. In particular, if the helical coils are modelled by only one “equivalent” vertical tube, a more stable fluid temperature at the outlet of the helical tubes is predicted by the code. The model with three different oblique or vertical tubes needs more investigations in order to study the possible instability conditions predicted by the code [18]. The primary natural circulation volumetric flow rate behavior is qualitatively and quantitatively predicted by the TRACE code. It is important to consider that previous discrepancies between experimental and calculated data by using a constant k loss coefficient at the core entrance are now not observed by using the new feature of the TRACE V 5.0 patch 3 code that contain flow Reynolds number-dependent loss coefficients.

The activity here presented consists in a qualitative accuracy assessment of the TRACE code. The TRACE code is judged to be able to reasonable predict the phenomena of interest of the selected tests. Since the qualitative assessment of the TRACE code is fulfilled, a quantitative assessment of the TRACE accuracy is envisaged to have a complete independent assessment. The quantitative accuracy evaluation method selected is the Fast Fourier Transform Based Methods [47,53,54].

5. REFERENCES

1. Modro, S. M., Fisher, J. E., Weaver, K. D., Reyes, J. N., Jr., Groome, J. T., Babka, P., Carlson, T. M., *Multi-Application Small Light Water Reactor final report, DOE Nuclear Energy Research Initiative Final Report*, Idaho National Engineering and Environmental Laboratory, December 2003.

2. Reyes, J. N., Jr., *Integral system experiment scaling methodology*, Annex 11, Natural circulation in water cooled nuclear power plants phenomena, models, and methodology for system reliability assessments, IAEA-TECDOC-1474, November 2005.

3. Reyes, J.N., Jr., Groome, J., Woods, B. G., Young, E., Abel, K., Yao, Y., Yoo, J. Y., 2007, *Testing of the Multi Application Small Light Water Reactor (MASLWR) passive safety systems*, Nuclear Engineering and Design 237 (2007) 1999-2005.

4. Reyes, J. N., Jr., King, J., *Scaling analysis for the OSU integral system test facility*, Department of Nuclear Engineering Oregon State University 116 Radiation Center Corvallis, OR 97331-5902 NERI Project 99-0129, Prepared For U.S. Department of Energy, 2003.

5. *An integrated structure and scaling methodology for severe accident technical issue resolution*, NUREG/CR-5809.

6. Zuber, N., *Appendix D:* Hierarchical, Two-Tiered scaling analysis, An integrated structure and scaling methodology for severe accident technical issue resolution, U.S Nuclear Regulatory Commission, Washington, D.C. 20555, NUREG/CR-5809, November 1991.

7. Galvin, M. R., 2007, *OSU MASLWR test facility modification description report*, IAEA Contract Number USA-13386, Oregon State University, November 19, 2007.

8. IAEA TECDOD-1474: *Natural circulation in water cooled nuclear power plants phenomena, models, and methodology for system reliability assessments*, International Atomic Energy Agency, Vienna, November 2005.

9. http://www.nuscalepower.com/our-technology.

10. Reyes, J., *NuScale plant safety in response to extreme events*, Nuclear Technology, Vol 178, May 2012.

11. Mascari, F., Woods, B.G., Adorni, M., *Analysis, by TRACE code, of natural circulation phenomena in the MASLWR-OSU-002 test*, Proceedings of the International Conference Nuclear Energy for New Europe 2008, Portoroz, Slovenia, September 8–11.

12. Pottorf, J., Mascari, F., Woods, B.G., *TRACE, RELAP5 Mod 3.3 and RELAP5-3D code comparison of OSU-MASLWR-001 test*, 2009 ANS Winter Meeting and Nuclear Technology Expo. Transactions of the ANS. ISSN: 0003-018X, 2009, Volume 101.

13. Mascari, F., Vella, G., Woods, B. G., Adorni, M., D'Auria, F., *Analysis of the OSU-MASLWR natural circulation phenomena using TRACE code*, IAEA, organized in cooperation with the OECD Nuclear Energy Agency and the European Commission, Technical meeting on "Application of Deterministic Best Estimate Safety Analysis", University of Pisa, Pisa, Italy, 21–25 September, 2009.

14. Mascari, F., PhD Thesis on "*Natural circulation and phenomenology of boron dilution in the pressurzied water reactors (circolazione naturale e fenomenologie di boron dilution in reattori ad acqua in pressione)*". University of Palermo, 2010.

15. Mascari, F., Vella, G., Woods, B.G., Welter, K., Pottorf, J., Young, E., Adorni, M., D'Auria, F., *Sensitivity analysis of the MASLWR helical coil steam generator using TRACE*, Proceedings of the International Conference Nuclear Energy for New Europe 2009 Bled, Slovenia, September 14-17.

16. Mascari, F., Vella, G., Woods, B.G., D'Auria, F., *Analysis of the Multi-Application Small Light-Water Reactor (MASLWR) design natural circulation phenomena*, Proceedings of ICAPP 2011, Nice, France, May 2-5, 2011.

17. Mascari, F., Vella, G., Woods, B.G., *TRACE Code Analyses for the IAEA ICSP on integral PWR design natural circulation flow stability and thermo-hydraulic coupling of containment and primary system during accidents*, Proceedings of the ASME 2011 Small Modular Reactors Symposium, September 28-30, 2011, Washington, DC, USA.

18. Mascari, F., Vella, G., Woods, B.G., Welter, K., Pottorf, J., Young, E., Adorni, M., D'Auria, F., *Sensitivity analysis of the MASLWR helical coil steam generator using TRACE*, Nuclear Engineering and Design 241 (2011) 1137–1144.

19. Mascari, F., Vella, G., Woods, B.G., D'Auria, F., *Analyses of The OSU-MASLWR experimental test facility*, Hindawi Publishing Corporation Science and Technology of Nuclear Installations Volume 2012, Article ID 528241, 19 pages doi:10.1155/2012/528241.

20. Mascari, F., Vella, G., Woods, B.G., Welter, K., D'Auria F., *Analysis of primary/containment coupling phenomena characterizing the MASLWR design during a SBLOCA scenario*, Nuclear Power Plants, InTech, 2012.

21. Mascari, F., Richiusa, M.L., Vella, G., Woods, B. G., Welter, K., F. D'Auria, *Analysis of the OSU-MASLWR-003A natural circulation test by using the TRACE code*, Advances In Thermal Hydraulics (ATH '12) Conference, November 11-15, 2012, San Diego, California.

22. Mascari, F., Richiusa, M.L., Vella, G., Woods, B.G., Welter, K., D'Auria, F., *TRACE analysis of the MASLWR primary/containment coupling phenomena in beyond design accident scenario*, Proceedings of the NURETH 15 Conference, Pisa 13- 17 2013, Italy.

23. Mascari, F., De Rosa, F., Polidori, M., Colletti, A.M., Costa, A.M., Richiusa, M.L., Vella, G., Woods, B.G., Welter, K., D'Auria, F., *Analyses of the TRACE V5 capability for the simulation of natural circulation and primary/containment coupling in BDBA condition Typical of the MASLWR*, Proceedings of ASME 2014 Small Modular Reactor Symposium, Washington DC, USA, April 15-17, 2014.

24. Mascari, F., Woods, B.G, Adorni, M., Analysis, by TRACE code, of *natural circulation phenomena in the MASLWR-OSU-002 Test, performed in the OSU MASLWR facility*, Spring Camp Meeting 2008, May 28-30 2008 Pisa, Italy.

25. Mascari, F., Vella, G., Woods, B.G., Welter, K., D'Auria, F., *Analyses of the OSU-MASLWR natural circulation phenomena by using TRACE code*, Spring 2012 CAMP, May 30 - June 1, Ljubljana, Slovenia, 2012.

26. Mascari, F., Richiusa, M.L., Vella, G., Woods, B.G., Welter, K., D'Auria, F., *Analysis of the OSU-MASLWR-003A natural circulation test by using the TRACE code*, Fall 2012 CAMP Meeting, November 7-9, 2012, Washington D.C. USA.

27. Mascari, F., Richiusa, M.L., Vella, G., Woods, B.G., Welter, K., D'Auria, F., *TRACE analysis of the MASLWR primary/containment coupling phenomena in beyond design accident scenario*, 2013 Spring CAMP Meeting, May 8-10, Pisa, Italia.

28. Mascari, F., Vella, G., *IAEA International collaborative standard problem on integral PWR design natural circulation flow stability and thermo-hydraulic coupling of containment and primary system during accidents*, 2013 Spring CAMP meeting, 8-10 May, Pisa, Italia.

29. Mascari, F., Colletti, A.M., Costa, A.M., Richiusa, M.L., De Rosa, F., Woods, B.G., Welter, K., D'Auria, F., Vella, G., *Analyses of natural circulation phenomena typical of the MASLWR by using the TRACE V5 code*, Fall 2013 CAMP Meeting, November 6 - 8, 2013, Washington, D.C. USA.

30. Mascari, F., Woods, B.G., Welter, K., D'Auria F., Vella, G., *Analyses of OSU-MASLWR-001 and 002 test updated analyses for the in progress NUREG on "Analysis of the OSU-MASLWR 001 and 002 test by using the TRACE code"*, FALL 2014 CAMP Meeting, 22-24, October, Rockville MD, USA.

31. Mascari, F., Woods, B. G., Vella, G., *Analyses of the IAEA ICSP Test 2 by Using TRACE Code*, FALL 2014 CAMP Meeting, 22-24, October, Rockville MD, USA.

32. Mascari, F., Woods, B.G., Welter, K., Vella G., D'Auria F., De Rosa, F., *Analyses of natural circulation phenomena typical of the MASLWR by using the TRACE V5 code*, 2015 SPRING CAMP Meeting, Prague, Czech Republic, May 27 - 29, 2015.

33. Woods, B. G., Mascari, F., 2009, *Plan for an IAEA international collaborative standard problem on integral PWR design natural circulation flow stability and thermo-hydraulic coupling of containment and primary system during accidents*, Department of Nuclear Engineering and Radiation Health Physics, Oregon State University, prepared for IAEA.

34. Woods, B. G., Galvin M. R., Bowser C. Jordan, *Problem specification for the IAEA international collaborative standard problem on integral PWR design natural circulation flow stability and thermo-hydraulic coupling of containment and primary system during accident*, DRAFT.

35. Weiss, A., Bowser, J., Galvin, M., Woods, B., OSU MASLWR drawings, 2010.

36. Choi, J.H., *Second Workshop of IAEA ICSP on "Integral PWR design natural circulation flow stability and thermo-hydraulic coupling of containment and primary system during accidents"*, Presentation, 21-23 March 2011, Vienna, Austria.

37. Mascari, F., Vella, G., 2011, *IAEA international collaborative standard problem on integral PWR design natural circulation flow stability and thermo-hydraulic coupling of containment and primary system during accidents double blind calculation results*, Dipartimento dell'Energia, Sezione di Ingegneria Nucleare, Prepared for International Atomic Energy Agency P.O. Box 100 Wagramer Strasse 5 A-1400 Vienna, Austria (February 2011).

38. Mascari, F., Vella, G., *IAEA international collaborative standard problem on integral PWR design natural circulation flow stability and thermo-hydraulic coupling of containment and primary system during accidents double blind calculation results*, II Technical Meeting IAEA ICSP, 21-23 March 2011, presentation.

39. Mascari, F., Vella, G., *IAEA international collaborative standard problem on integral PWR design natural circulation flow stability and thermo-hydraulic coupling of containment and primary system during accidents- blind calculation results*, University of Palermo - Dipartimento Dell'Energia - Sezione Ingegneria Nucleare, Prepared for International Atomic Energy Agency.

40. Mascari, F., Vella, G., *IAEA international collaborative standard problem on integral PWR design natural circulation flow stability and thermo-hydraulic coupling of containment and primary system during accidents – blind calculation results*, III Technical Meeting IAEA ICSP, 27-30 March 2012. https://www.iaea.org/NuclearPower/Downloadable/Meetings/2012/2012-03-27-30-WS-Korea/11-UNIPA_MASCARI.pdf

41. Mascari, F., Vella, G., *IAEA international collaborative standard problem on integral PWR design natural circulation flow stability and thermo-hydraulic coupling of containment and primary system during accidents-open calculation results*, University of Palermo-Dipartimento Dell'Energia- Sezione Ingegneria Nucleare, Prepared for International Atomic Energy Agency, 2013.

42. Mascari, F., Vella, G., *IAEA international collaborative standard problem on integral PWR design natural circulation flow stability and thermo-hydraulic coupling of containment and primary system during accidents- open calculation results-,* Fourth Workshop for the ICSP on Integral Water Cooled Reactor Designs, Pisa 25-28 February 2013, Italy. https://www.iaea.org/NuclearPower/Downloadable/Meetings/2013/2013-02-25-02-28-WS-NPTD/8.UNIPA.pdf

43. IAEA-TECDOC-1733: *Evaluation of advanced thermohydraulic system codes for design and safety analysis of integral type reactors*, International Atomic Energy Agency, Vienna, February 2014.

44. TRACE V5.0, 2008. *Theory and User's Manuals*. Division of System Analysis, Office of Nuclear Regulatory Research, U.S. Nuclear Regulatory Commission, Washington, DC.

45. *Symbolic Nuclear Analysis Package (SNAP)*, 2007. Users Manual. Applied Programming Technology, Inc., Bloomsburg, PA.

46. Staudenmeier, J., *TRACE reactor system analysis code*, MIT Presentation, Safety Margins and Systems Analysis Branch, Office of Nuclear Regulatory Research, U.S. Nuclear Regulatory Commission (2004).

47. NUREG/IA-0155: D'Auria, F., Frogheri, M., Giannotti, W., *RELAP5/Mod 3.2 Post Test Analysis and Accuracy Quantification of SPES Test SP-SB-04*, (1999).

48. Bonuccelli, M., D'Auria, F., Debrecin, N., Galassi, G. M., *A methodology for the qualification of thermalhydraulic code nodalizations*, Proc. of NURETH-6 Conference, Grenoble, France, October 5–8, 1993.

49. CSNI *integral test facility validation matrix for the assessment of thermal-hydraulic codes for LWR LOCA and transients*, NEA/CSNI/R(96)17.

50. *Relevant thermal hydraulic aspects of advanced reactor design*, Status Report, OCDE/GD(97)8, NEA/CSNI/R(1996)22.

51. IAEA-TECDOC-1624: *Passive safety systems and natural circulation in water cooled nuclear power plants*, International Atomic Energy Agency, Vienna, November, 2009.

52. IAEA-TECDOC-1677: *Natural circulation phenomena and modelling for advanced water cooled reactors*, International Atomic Energy Agency, Vienna, March, 2012.

53. Prosek, A., Leskovar, M., Mavko, B., *Quantitative assessment with improved fast Fourier transform based method by signal mirroring*, Nuclear Engineering and Design 238 (2008) 2668–2677.

54. Prošek, A., Leskovar, M., *Use of FFTBM by signal mirroring for sensitivity study*, Annals of Nuclear Energy 76 (2015) 253–262.

6. APPENDIX A: EXPERIMENTAL DATA VERSUS CODE CALCULATION FOR THE OSU-MASLWR-001 TEST

In this Appendix A the comparison between the REF and SEN1 calculated data and experimental data related to the OSU-MASLWR-001 test, presented in the section 3.3, have been presented considering all the main parameters of interest.

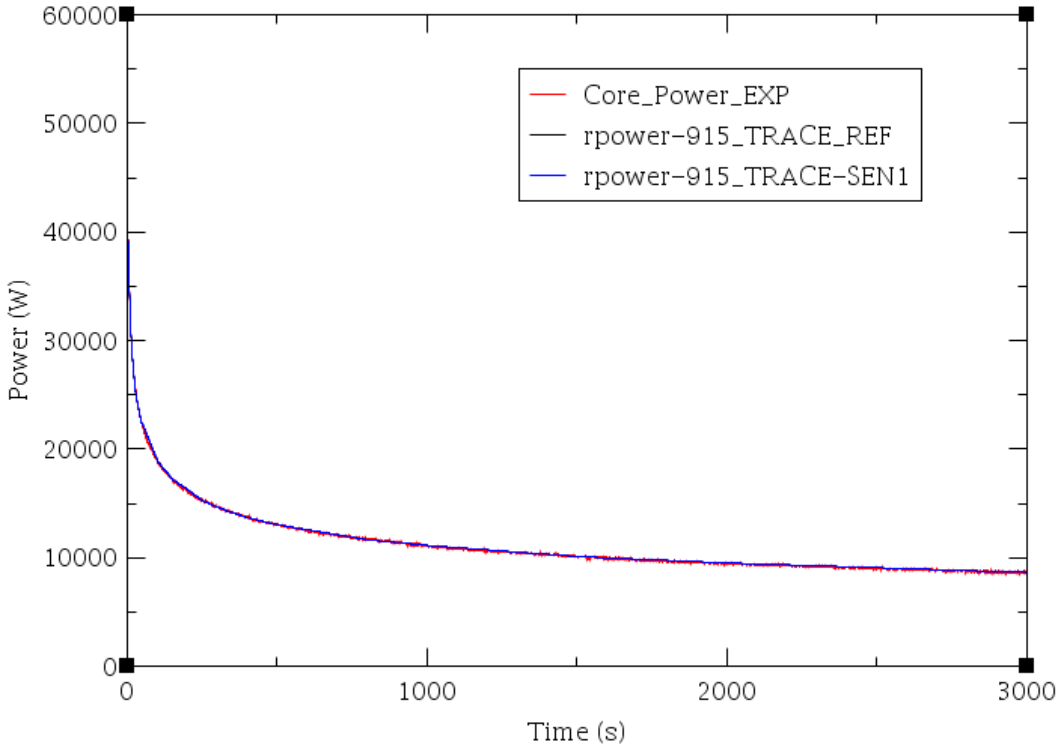

Figure A-1 Experimental Data versus Code Calculations for Core Power (KW 101-102)

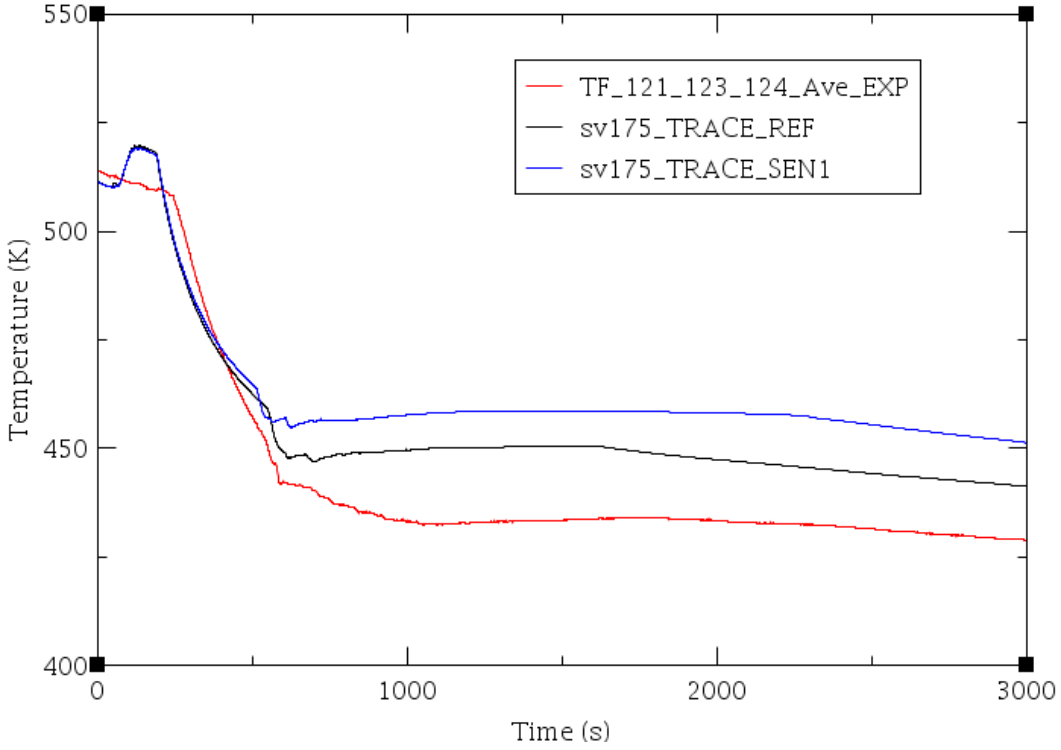

Figure A-2 Experimental Data versus Code Calculations for the Average Value of TF 121-123-124

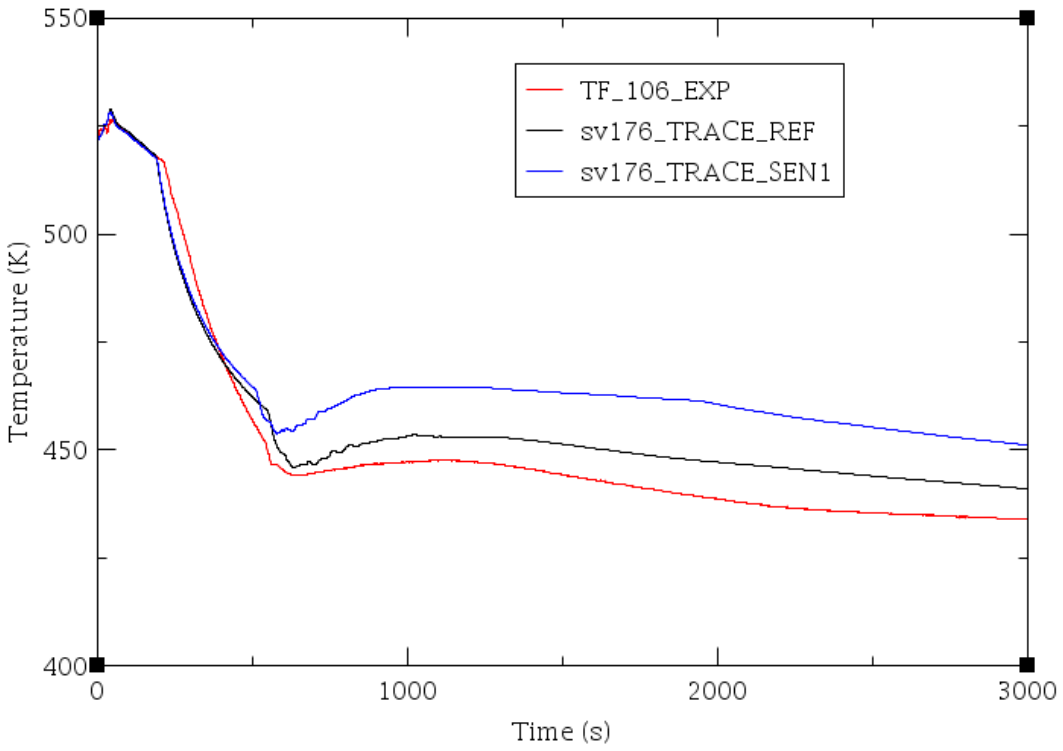

Figure A-3 Experimental Data versus Code Calculations for TF-106

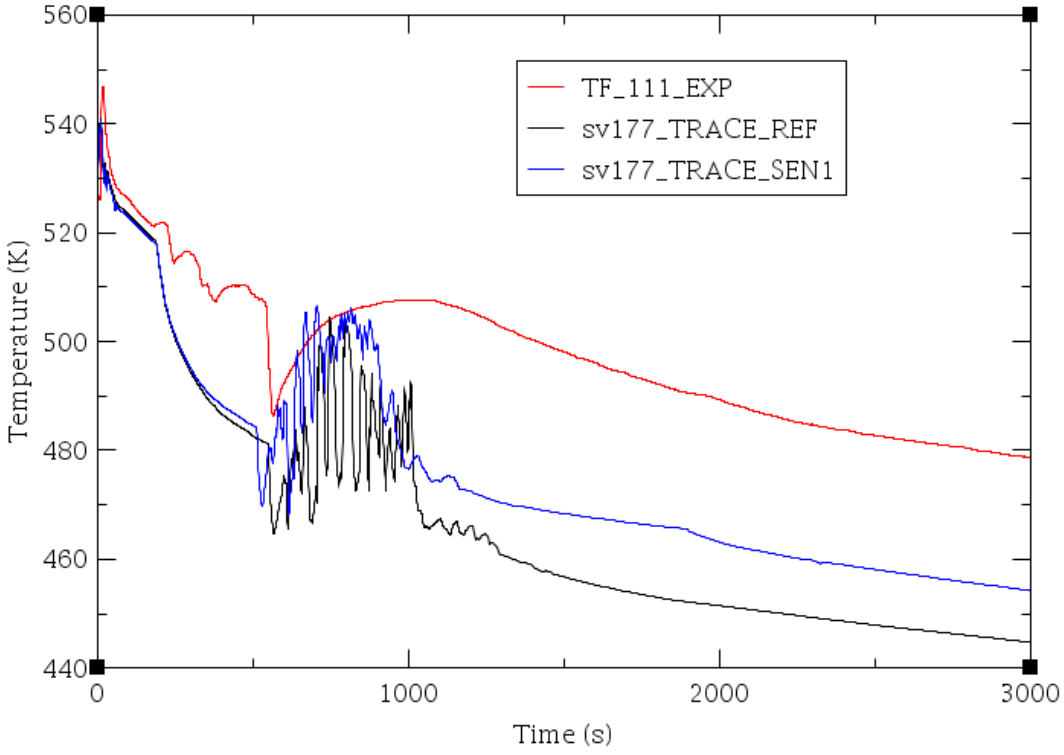

Figure A-4 Experimental Data versus Code Calculations for TF-111

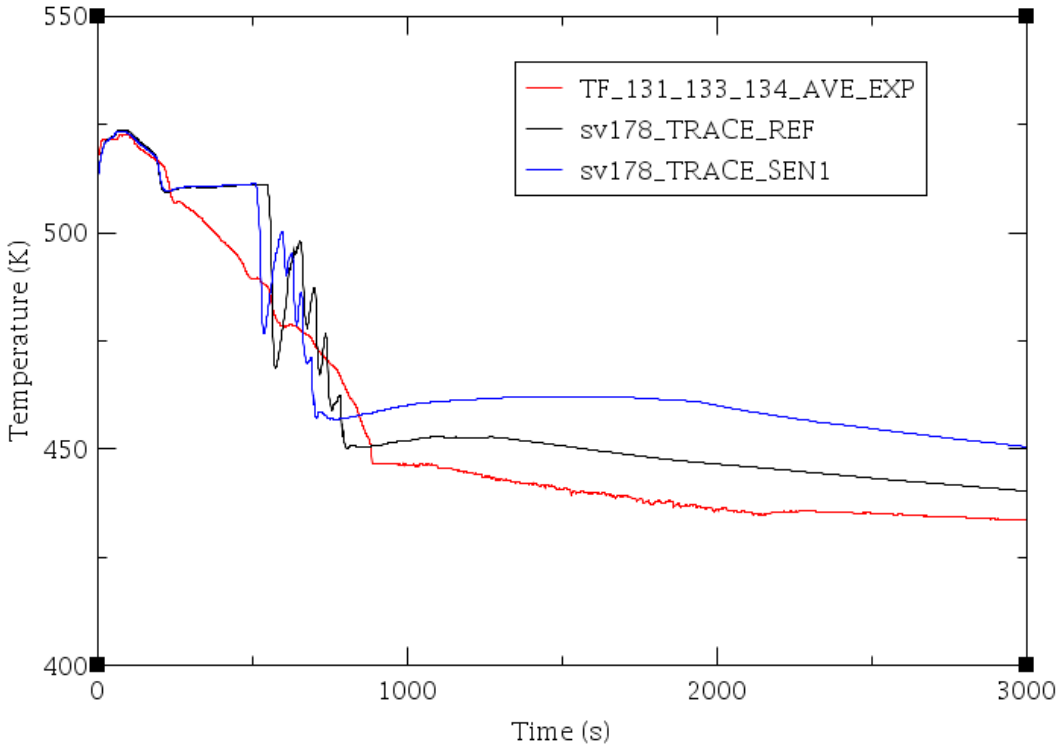

Figure A-5 Experimental Data versus Code Calculations for the Average Value of TF 131-133-134

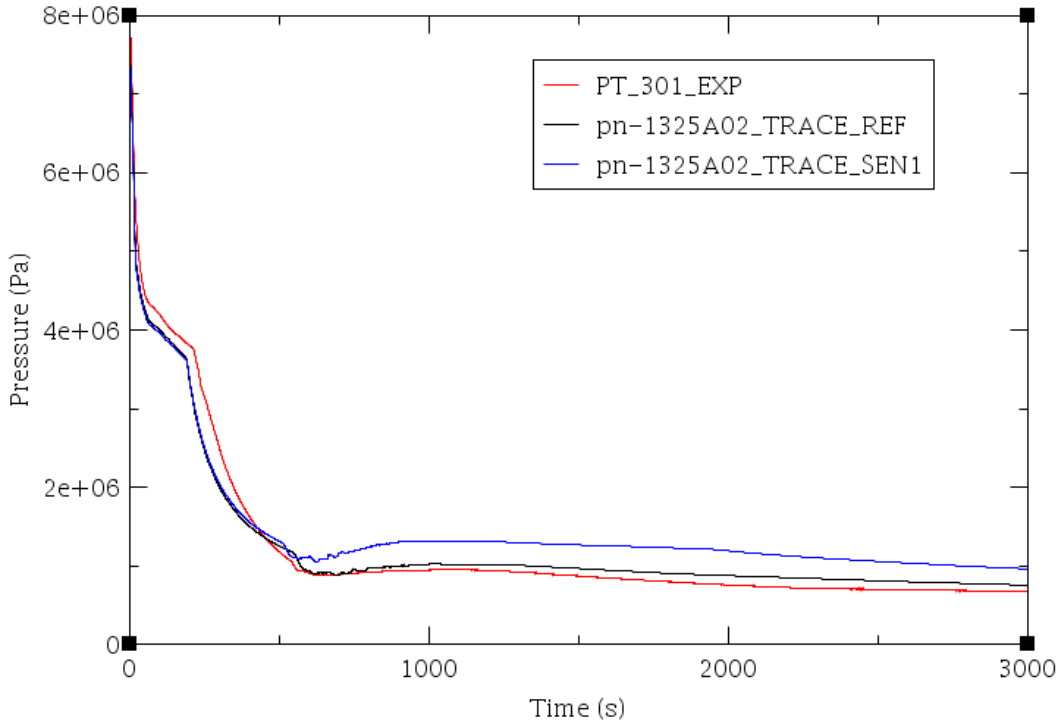

Figure A-6 Experimental Data versus Code Calculations for PT-301

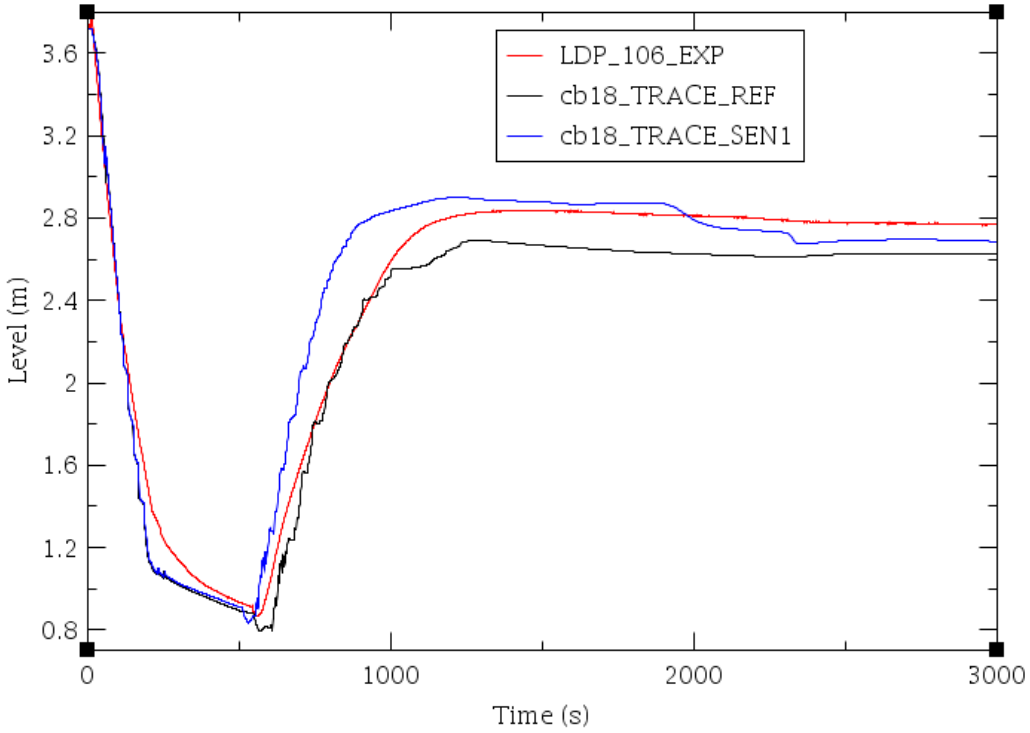

Figure A-7 Experimental Data versus Code Calculations for LDP-106

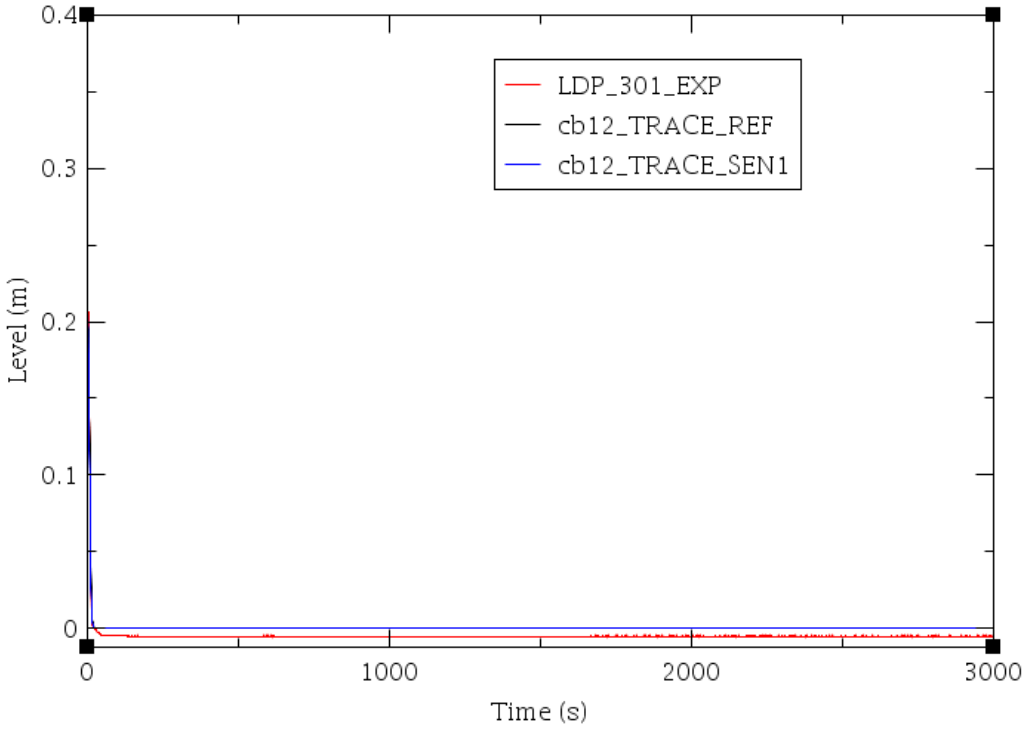

Figure A-8 Experimental Data versus Code Calculations for LDP-301

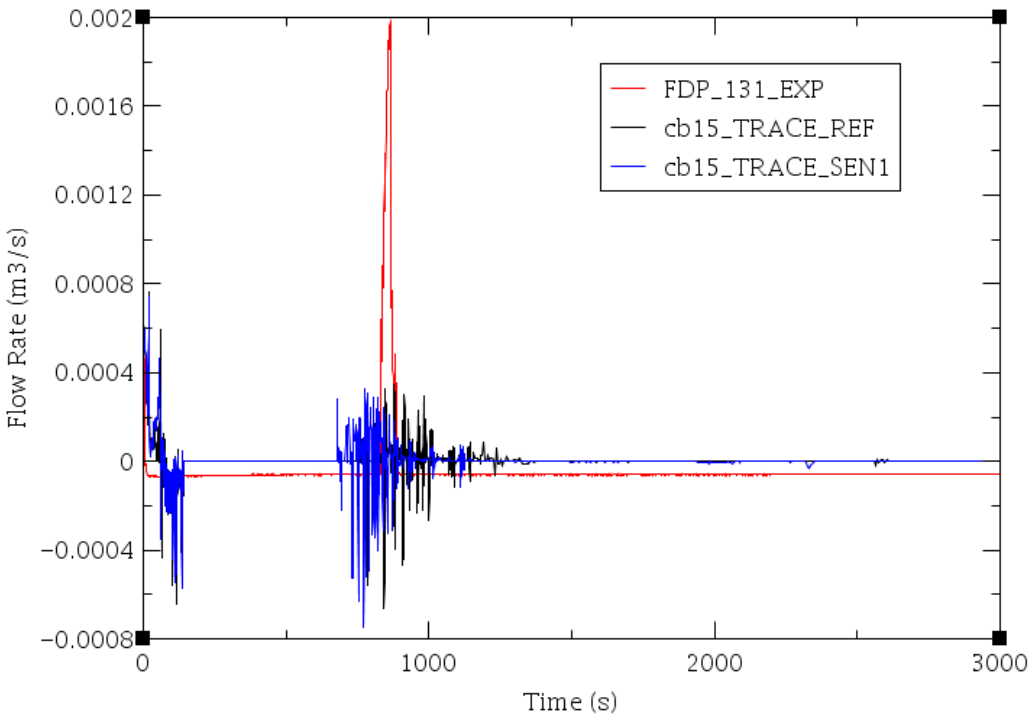

Figure A-9 Experimental Data versus Code Calculations for FDP-131

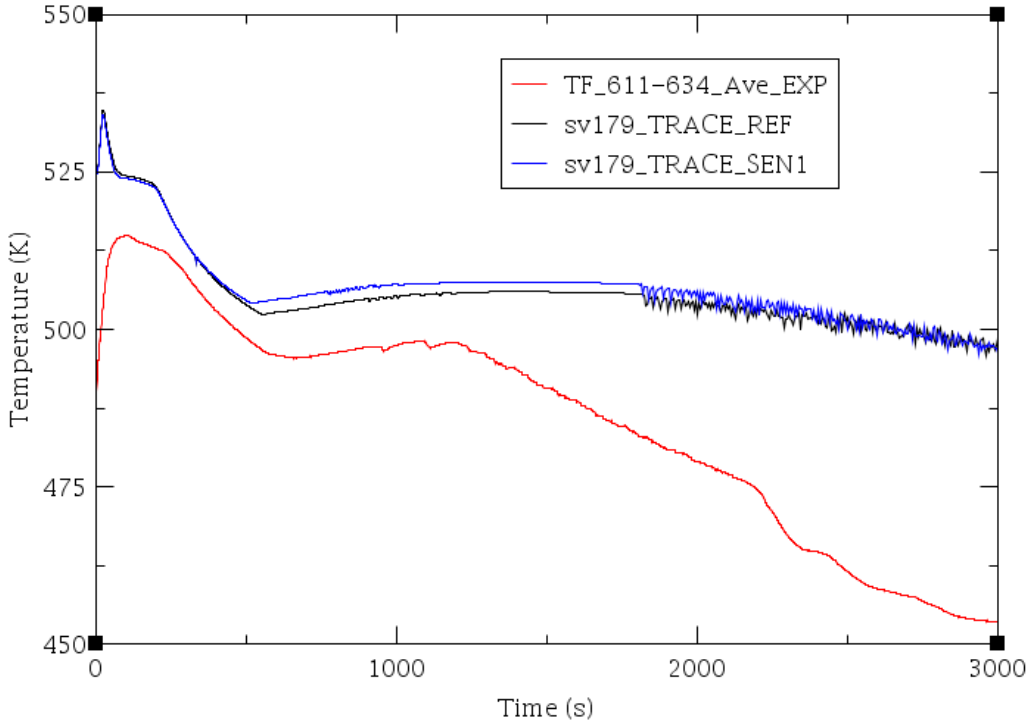

Figure A-10 Experimental Data versus Code Calculations for the Average Value of TF 611 to 634

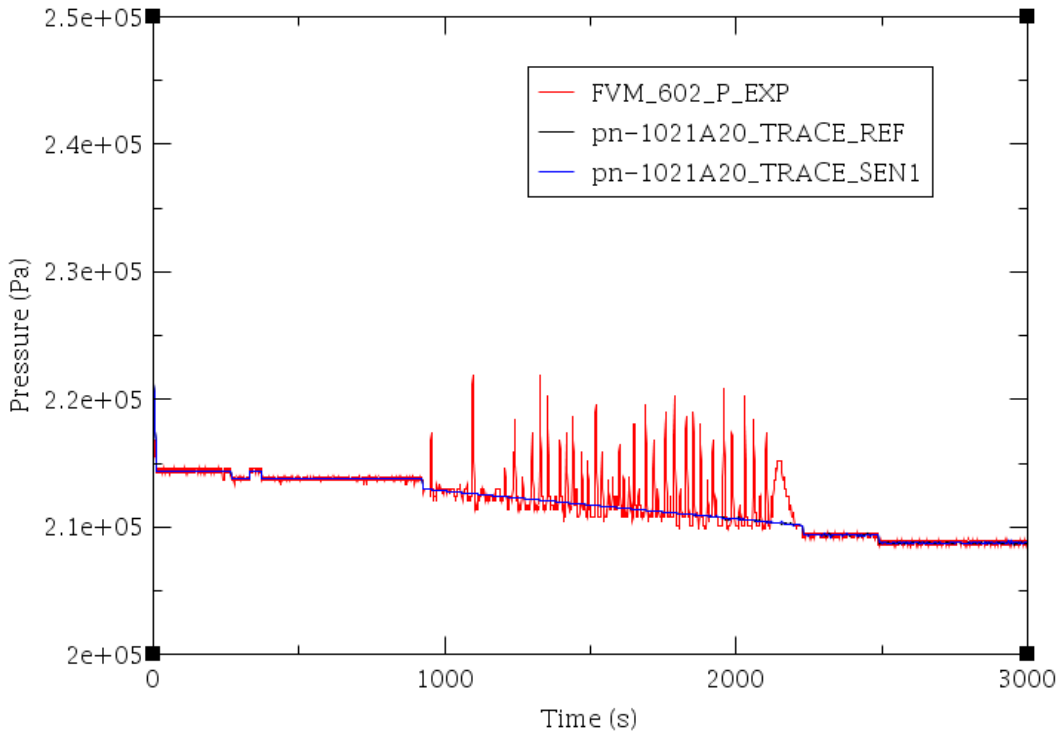

Figure A-11 Experimental Data versus Code Calculations for FVM-602-P

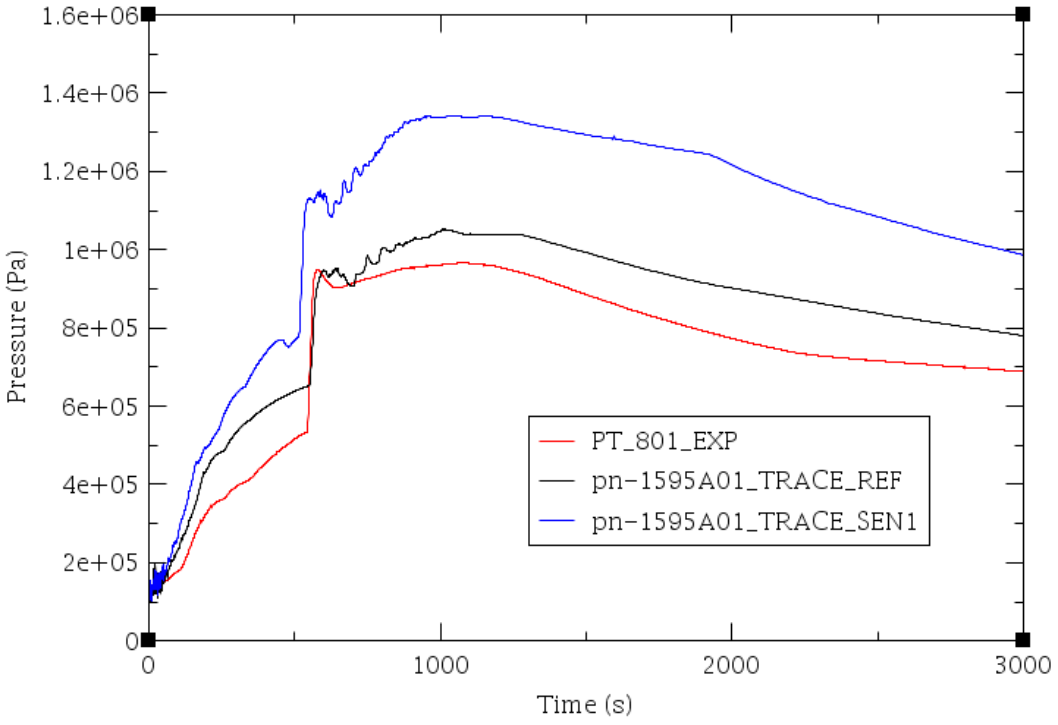

Figure A-12 Experimental Data versus Code Calculations for PT-801

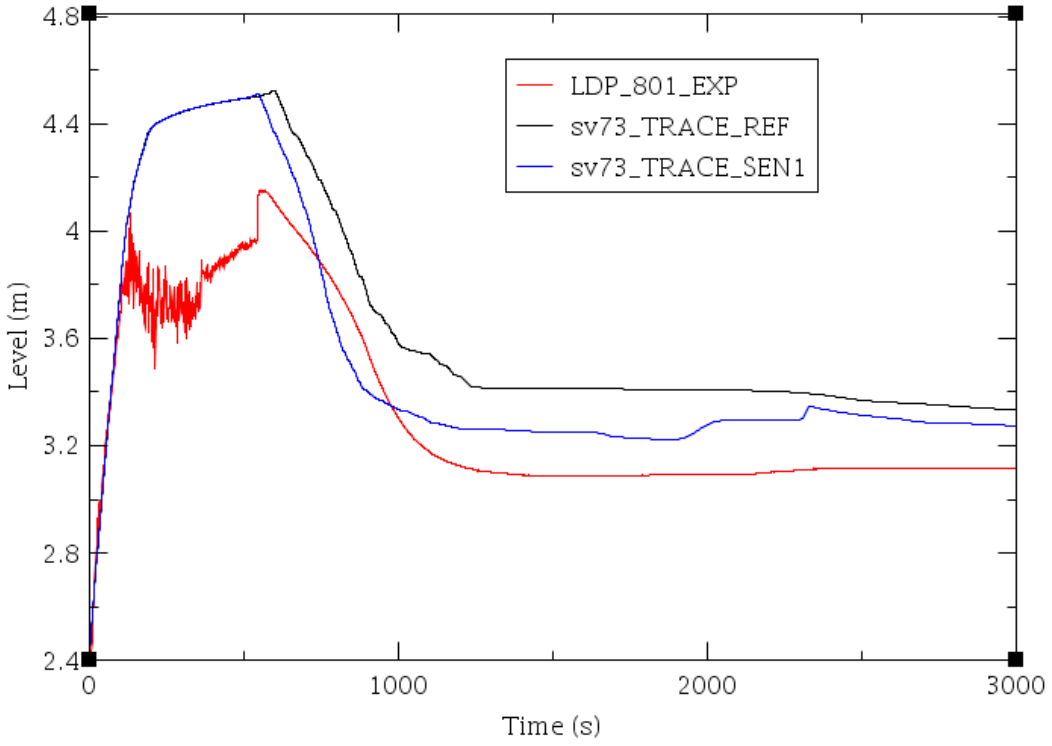

Figure A-13 Experimental Data versus Code Calculations for LDP-801

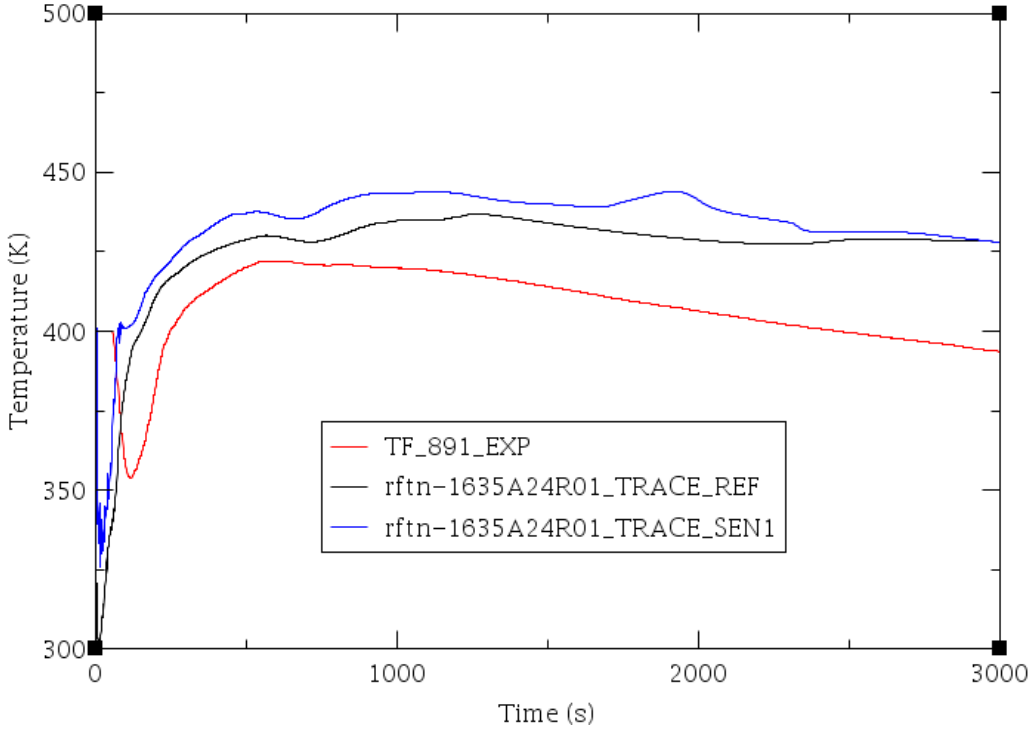

Figure A-14 Experimental Data versus Code Calculations for TF-891

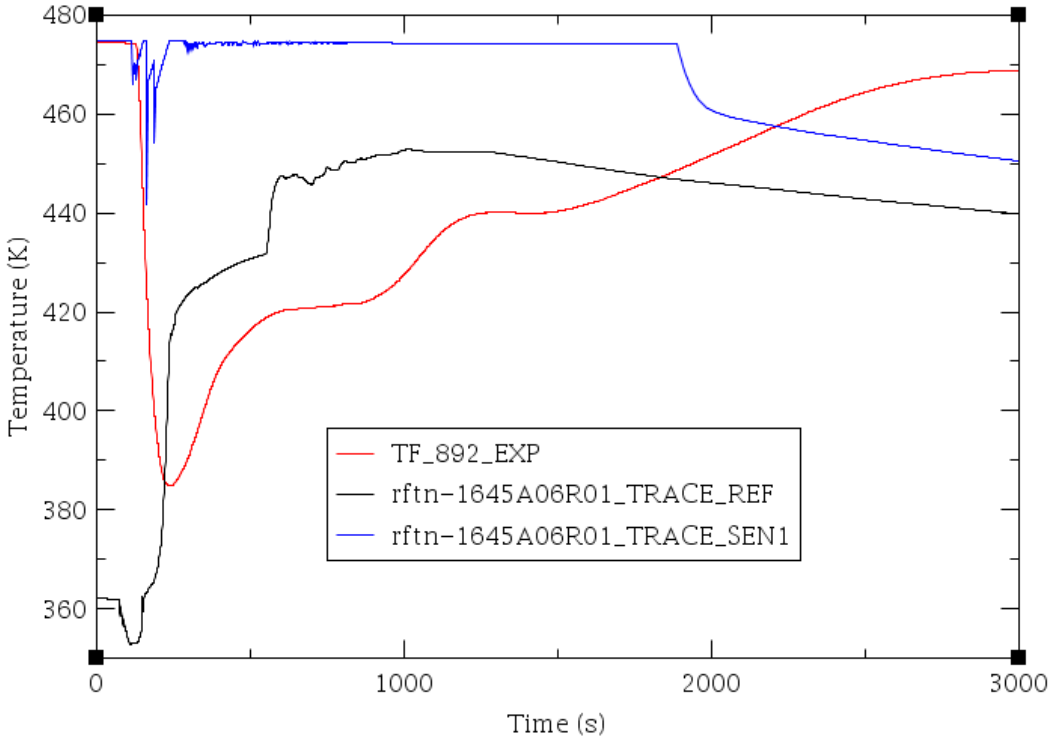

Figure A-15 Experimental Data versus Code Calculations for TF-892

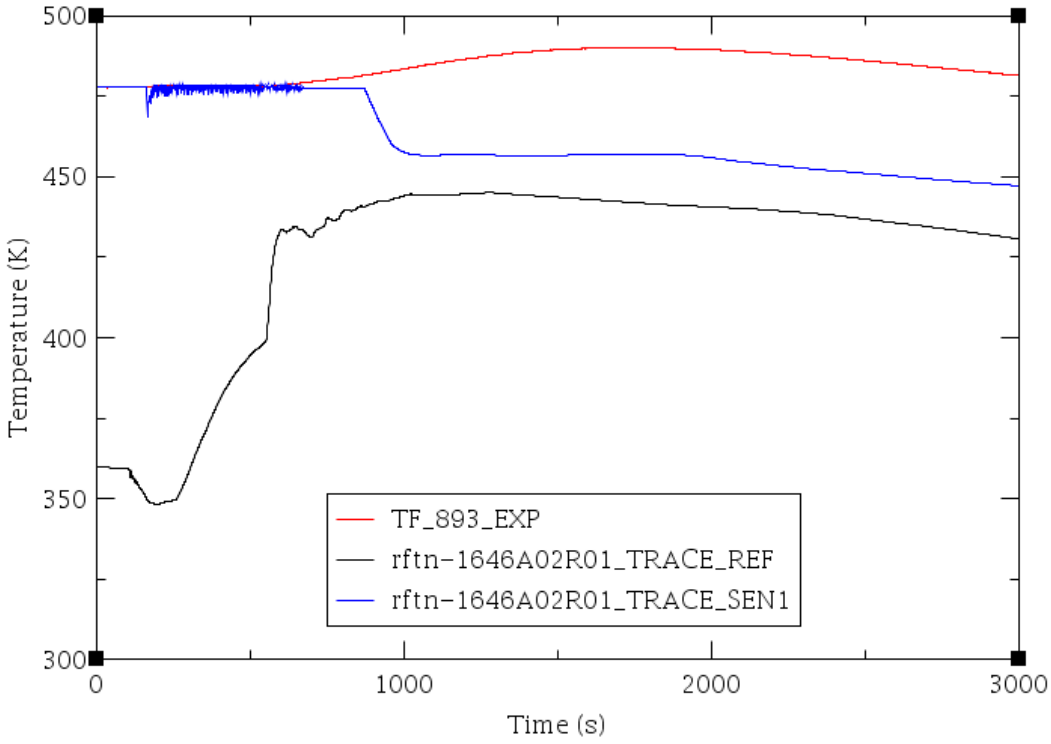

Figure A-16 Experimental Data versus Code Calculations for TF-893

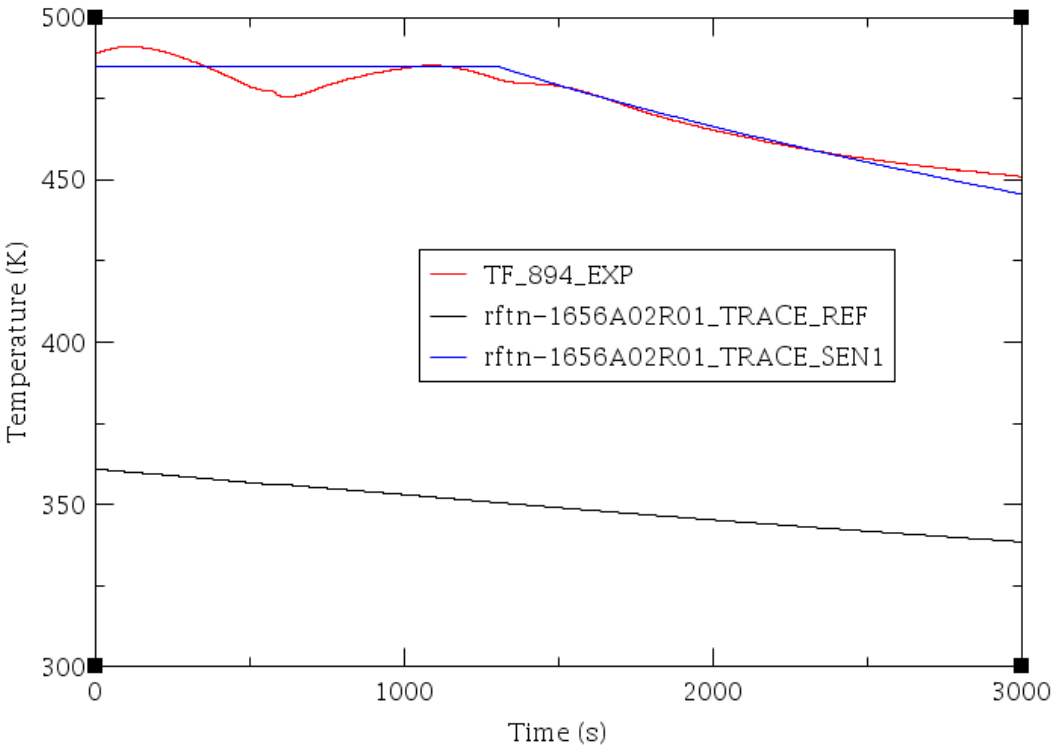

Figure A-17 Experimental Data versus Code Calculations for TF-894

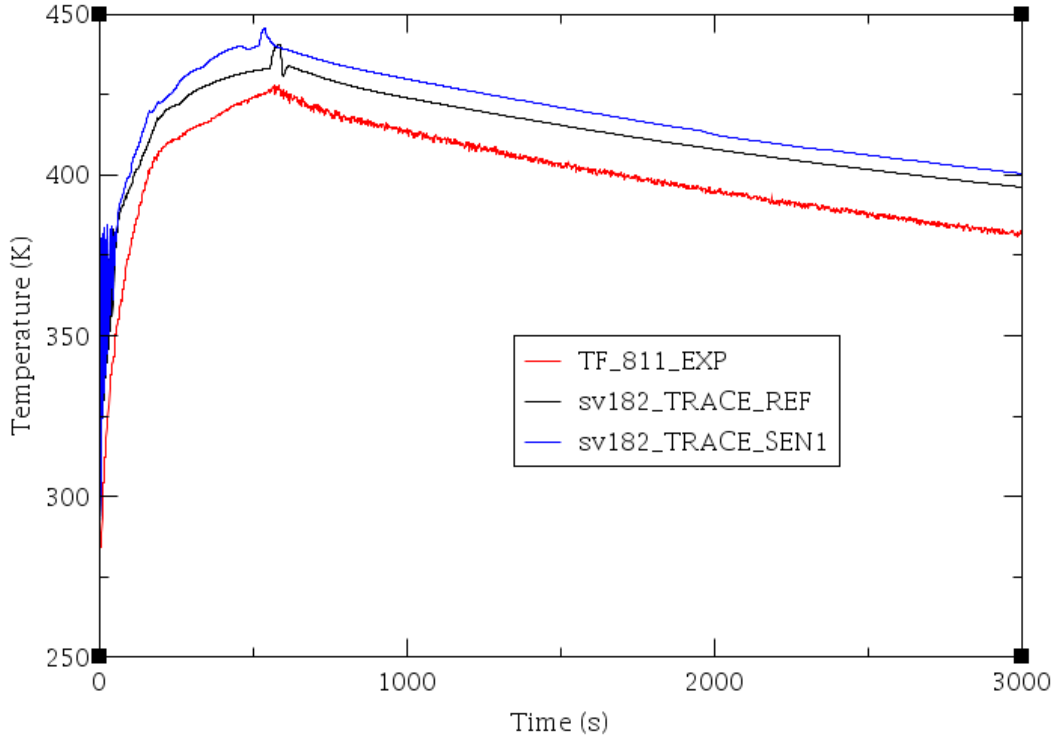

Figure A-18 Experimental Data versus Code Calculations for TF-811

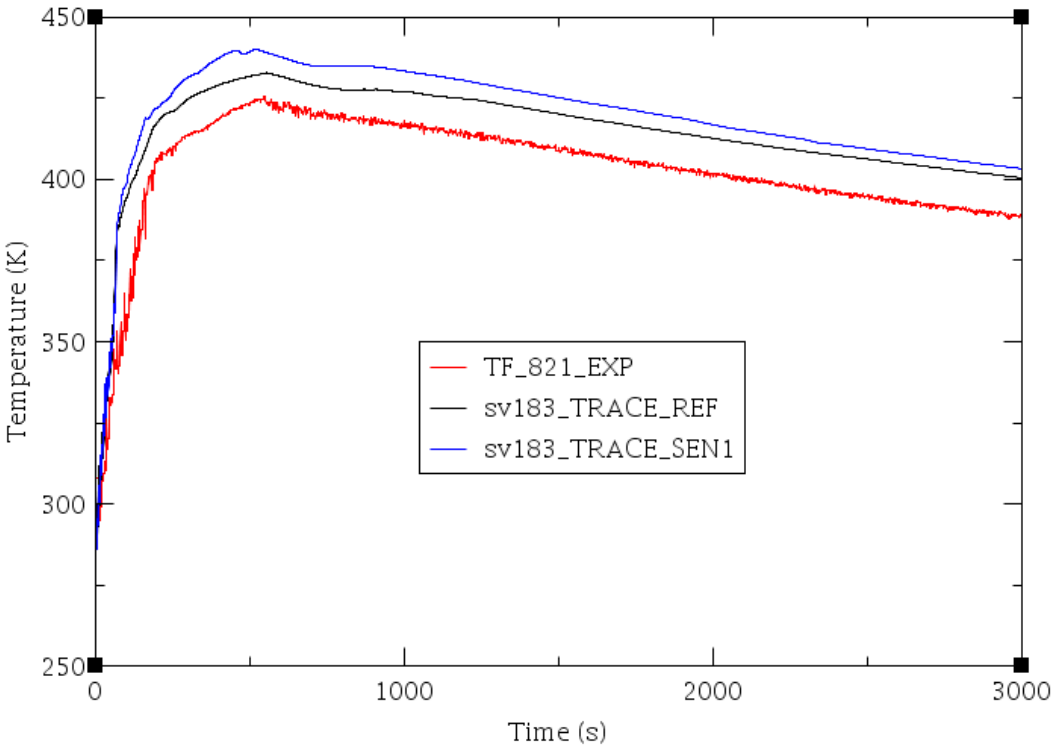

Figure A-19 Experimental Data versus Code Calculations for TF-821

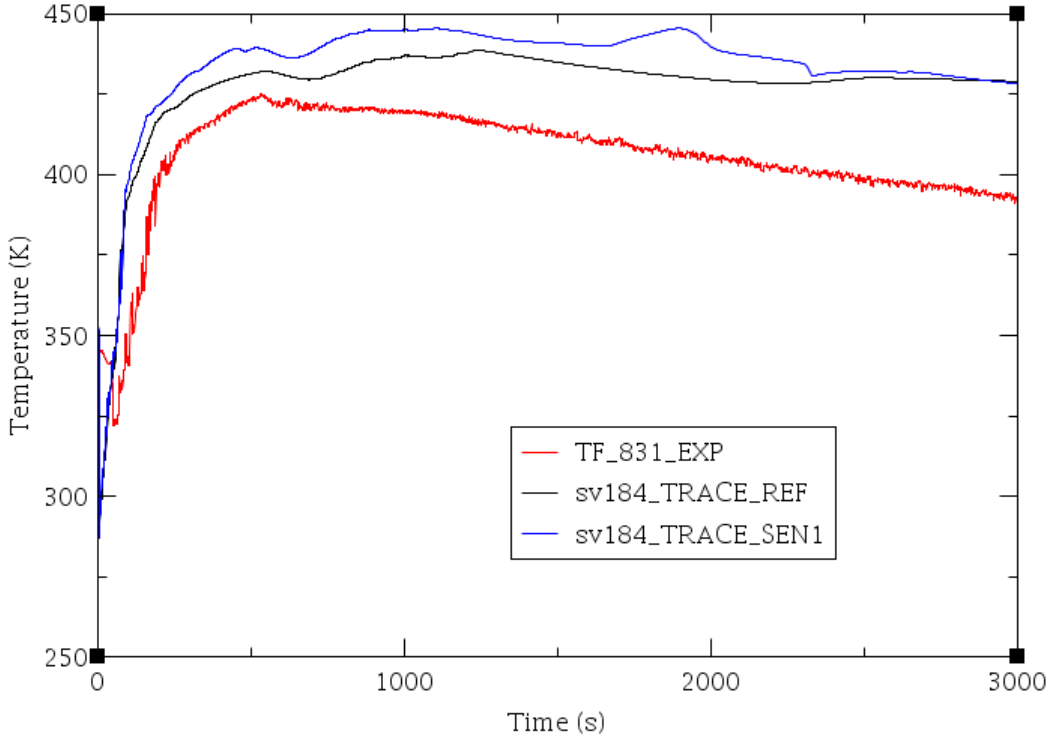

Figure A-20 Experimental Data versus Code Calculations for TF-831

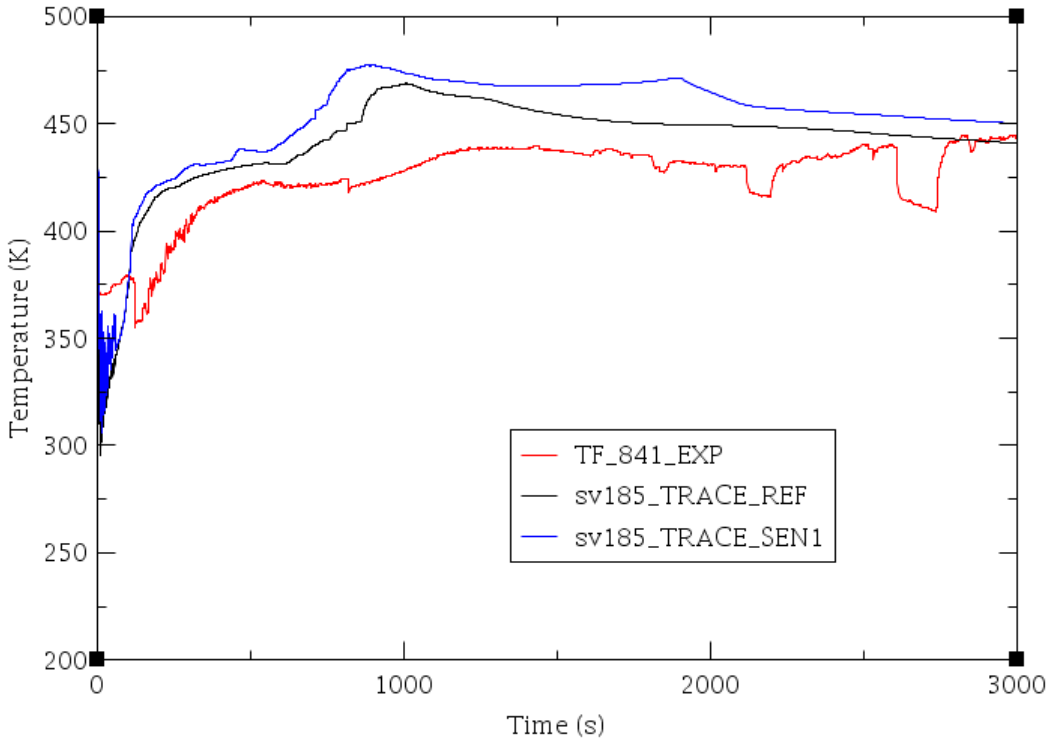

Figure A-21 Experimental Data versus Code Calculations for TF-841

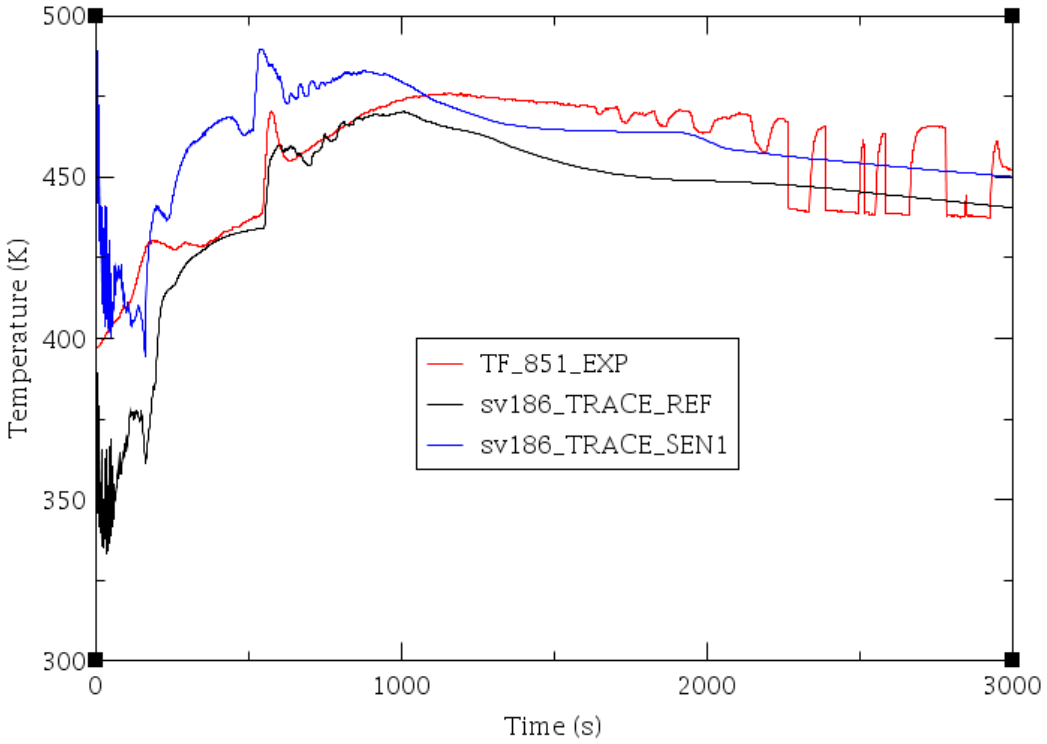

Figure A-22 Experimental Data versus Code Calculations for TF-851

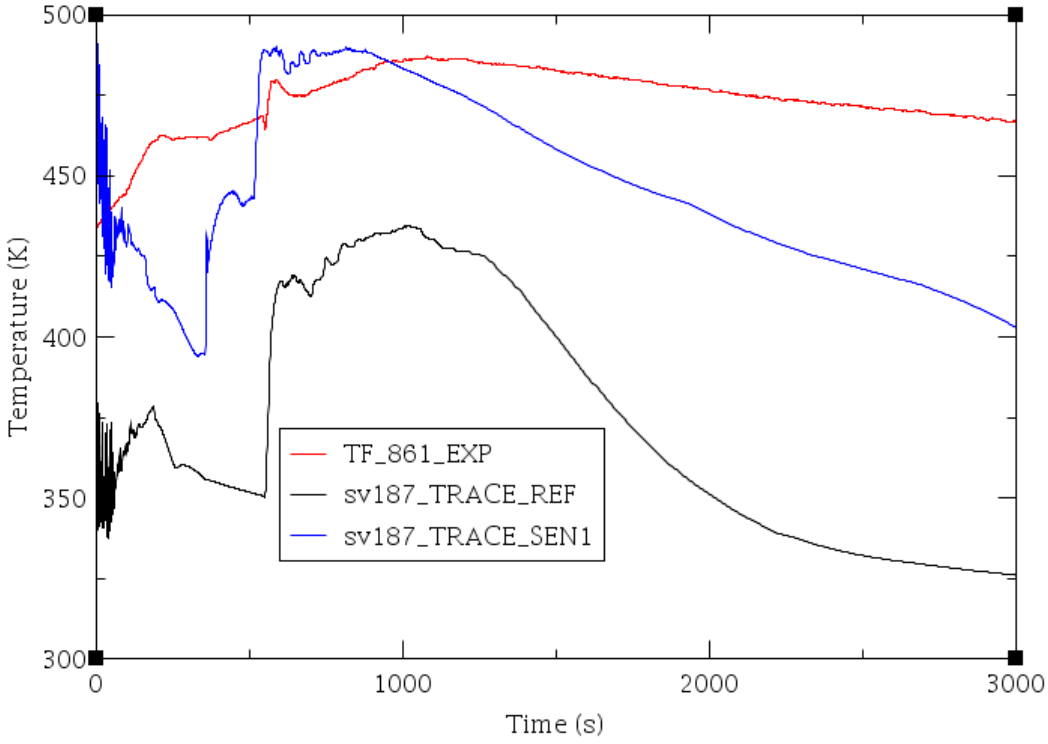

Figure A-23 Experimental Data versus Code Calculations for TF-861

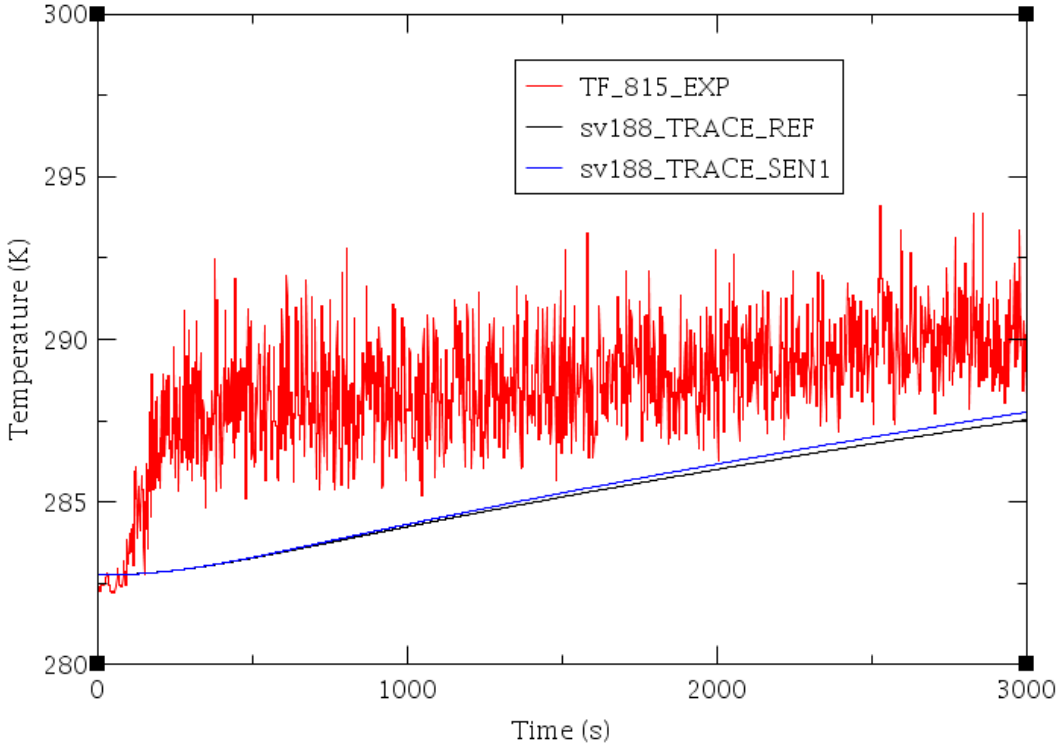

Figure A-24 Experimental Data versus Code Calculations for TF-815

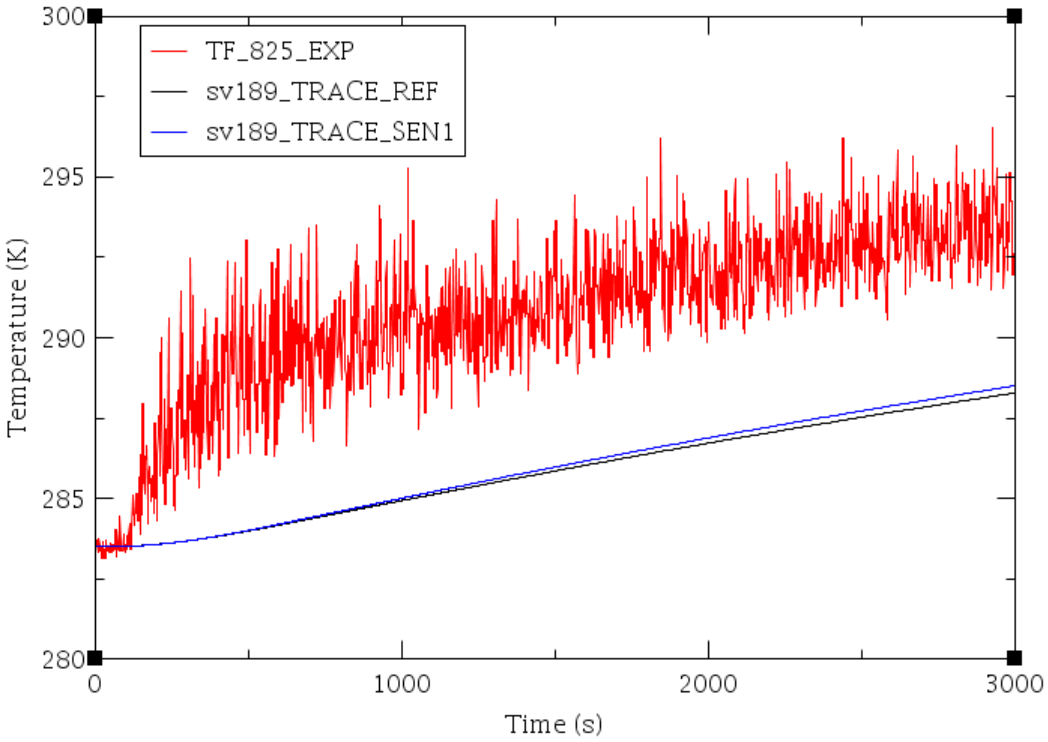

Figure A-25 Experimental Data versus Code Calculations for TF-825

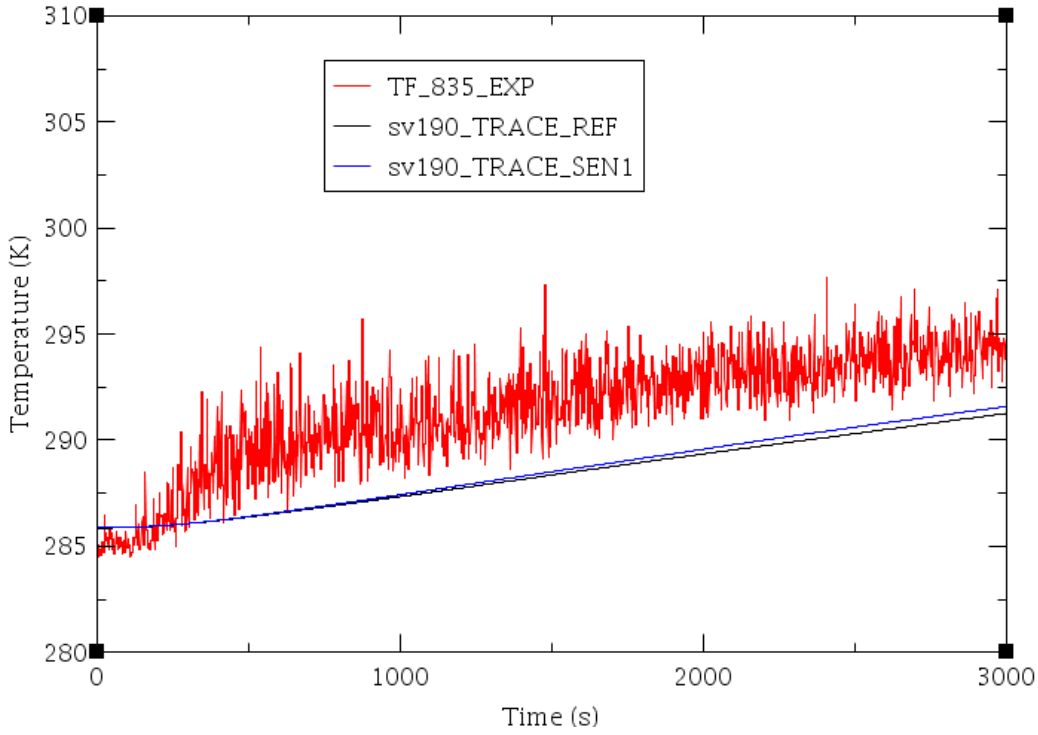

Figure A-26 Experimental Data versus Code Calculations for TF-835

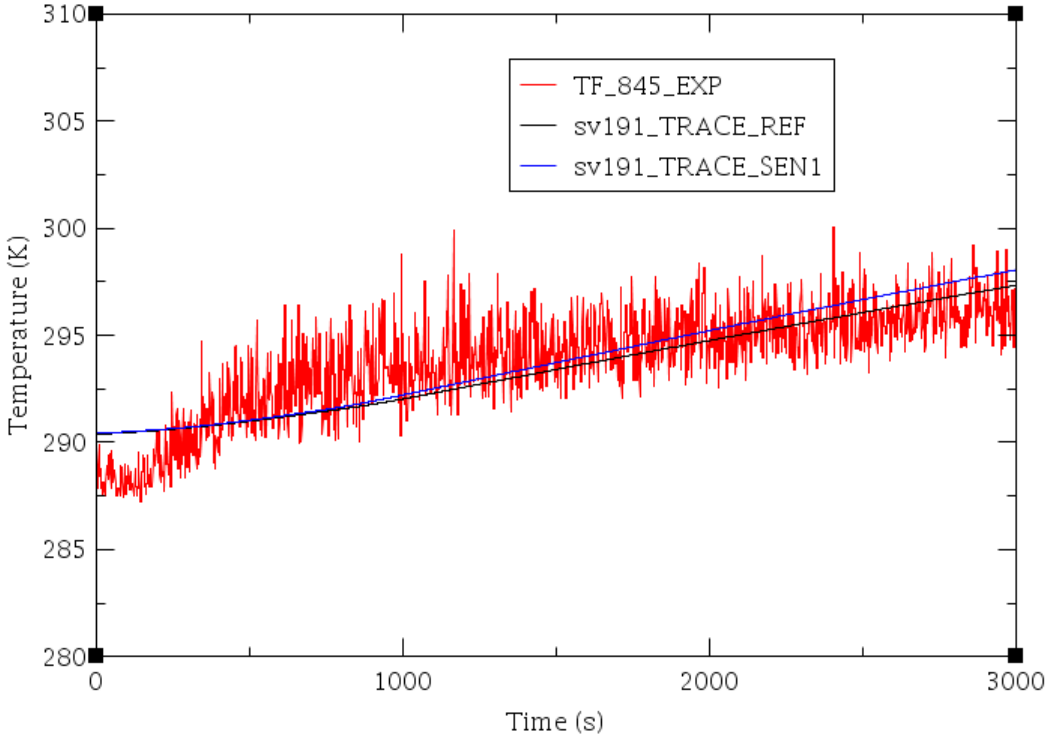

Figure A-27 Experimental Data versus Code Calculations for TF-845

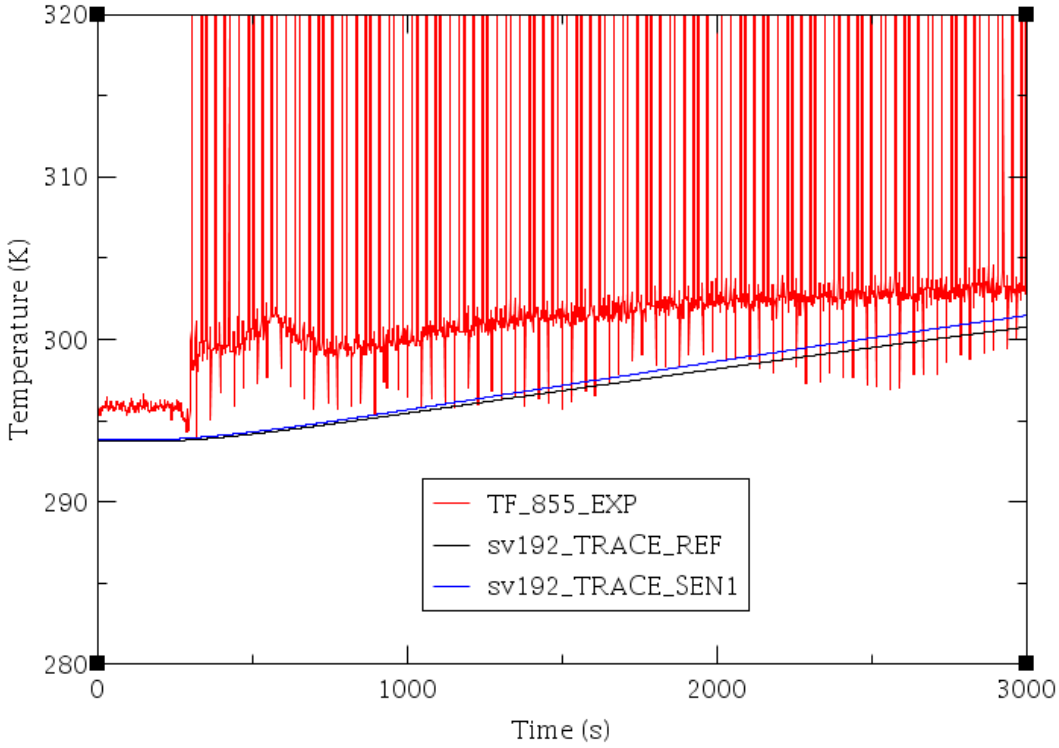

Figure A-28 Experimental Data versus Code Calculations for TF-855

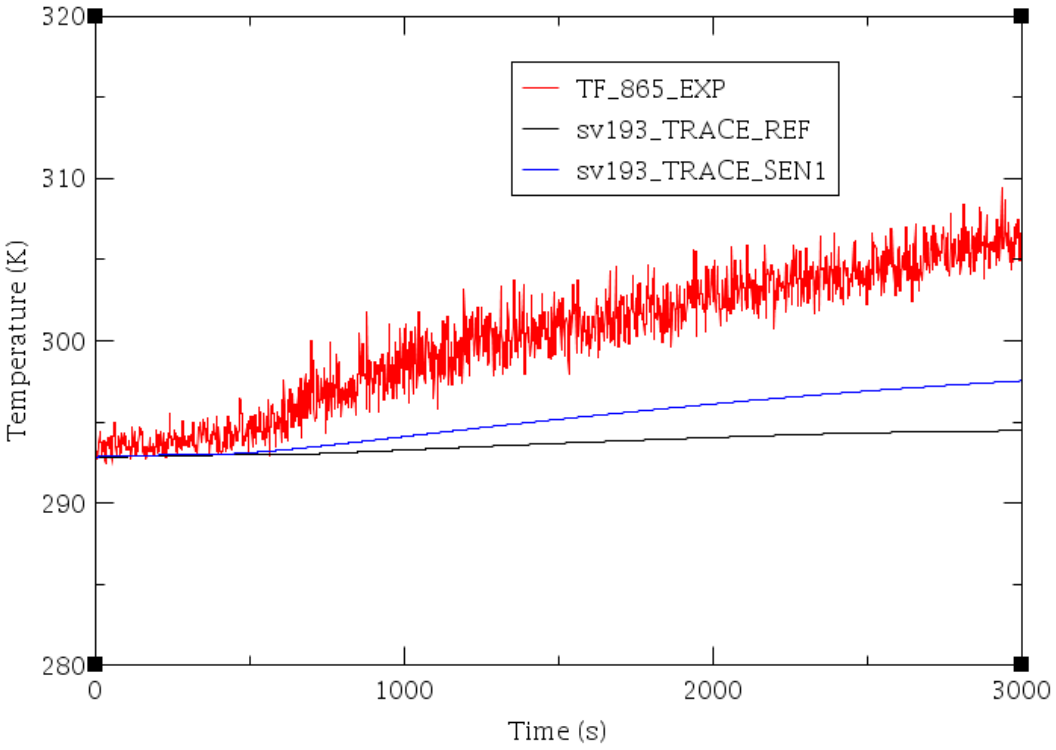

Figure A-29 Experimental Data versus Code Calculations for TF-865

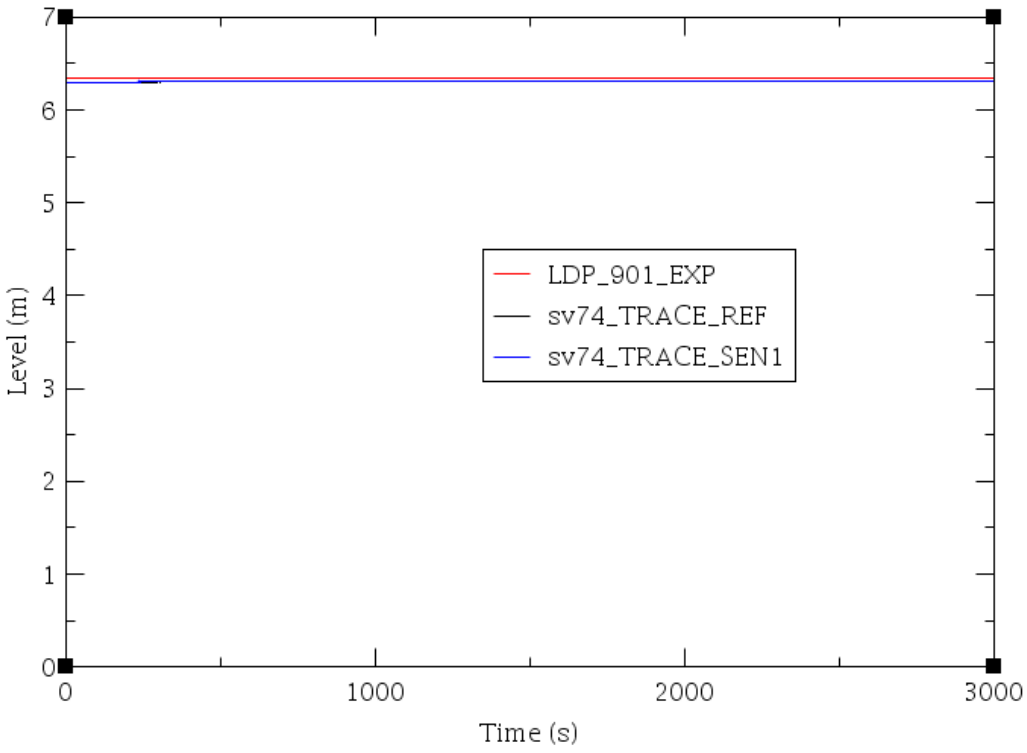

Figure A-30 Experimental Data versus Code Calculations for LDP-901

7. APPENDIX B: EXPERIMENTAL DATA VERSUS CODE CALCULATION FOR THE OSU-MASLWR-002 TEST

In this Appendix B the comparison between the REF and SEN calculated data and experimental data related to the OSU-MASLWR-002 test, presented in the section 3.4, have been presented considering all the main parameters of interest.

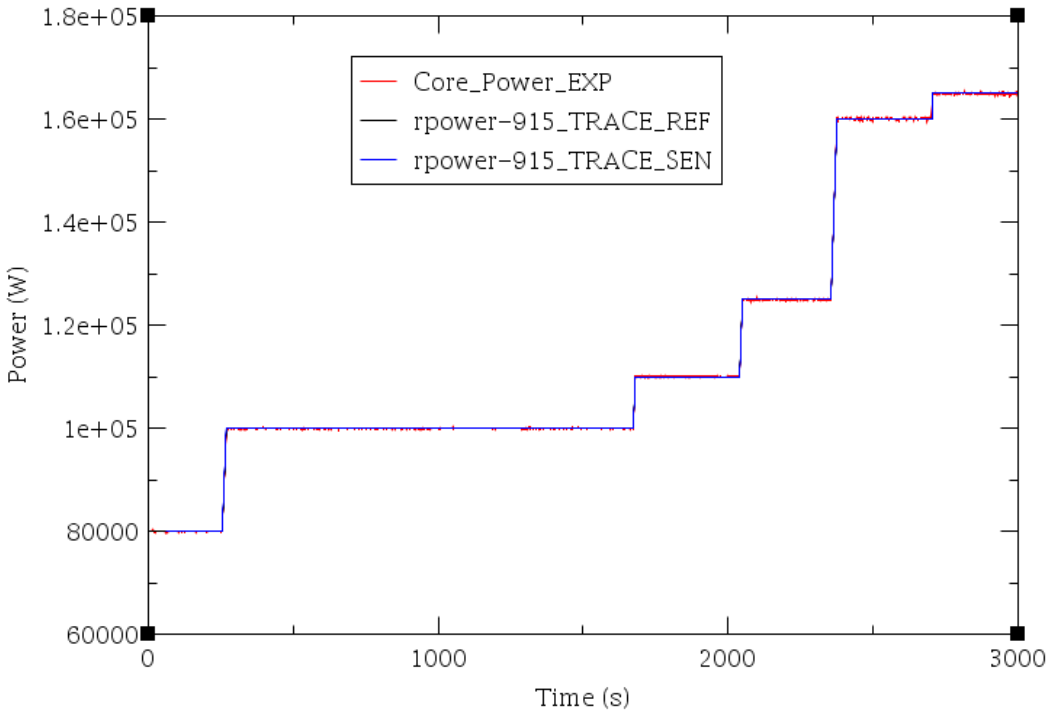

Figure B-1 Experimental Data versus Code Calculations for Core Power (KW-101-102)

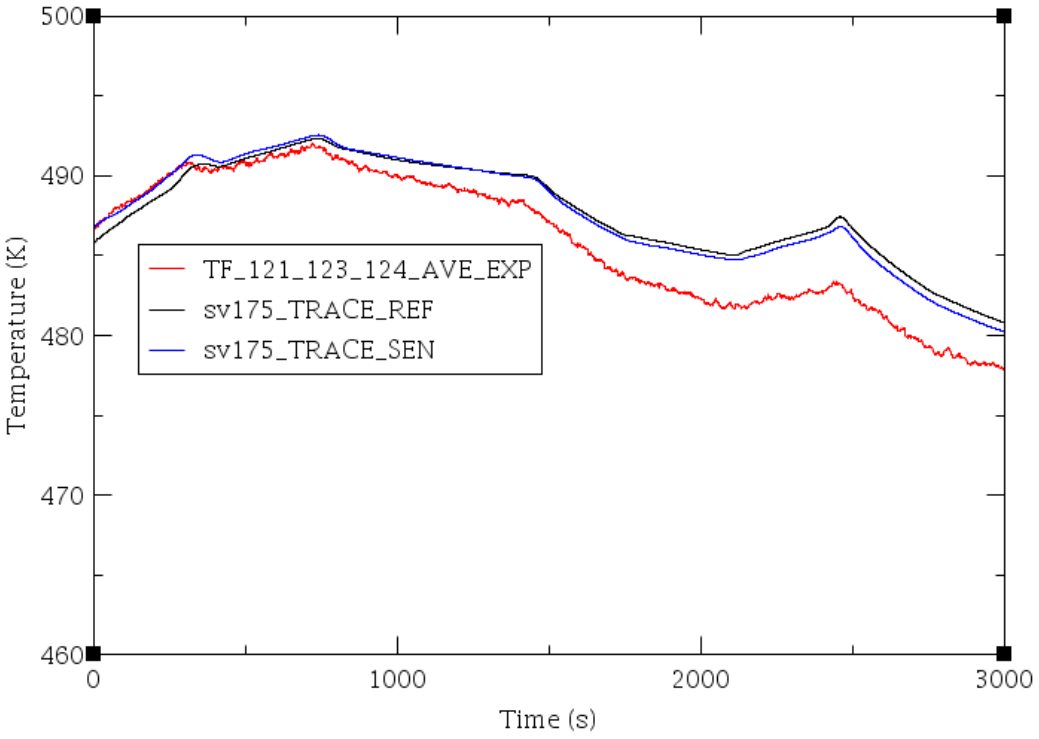

Figure B-2 Experimental Data versus Code Calculations for the Average Value of TF 121, 123, 124

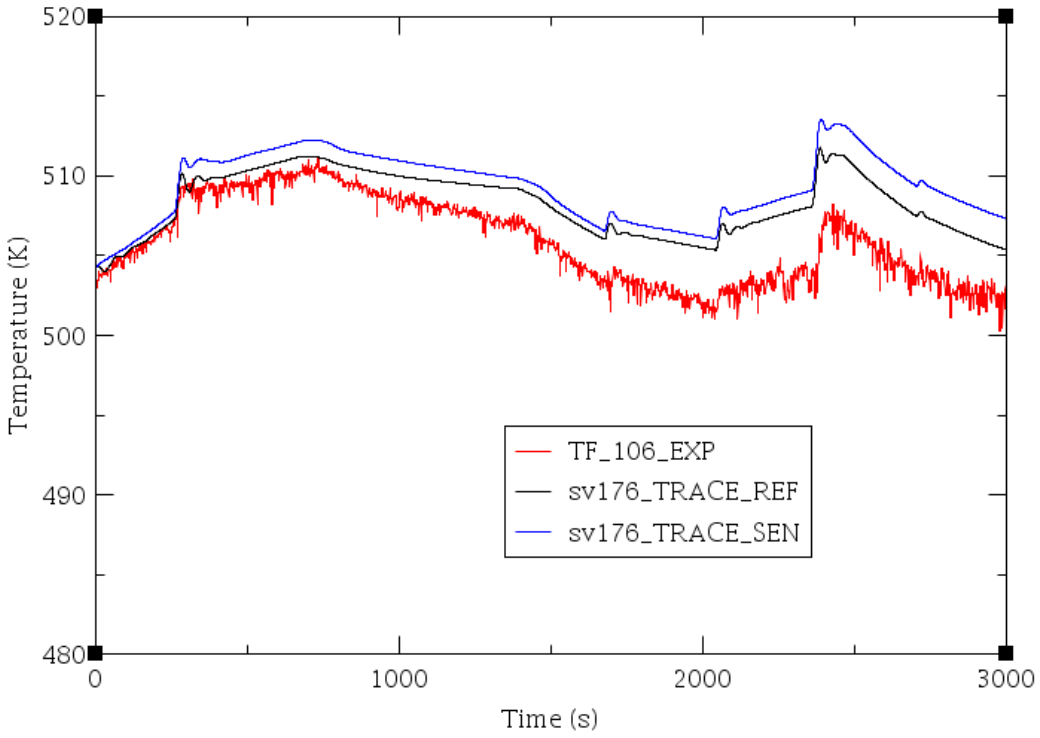

Figure B-3 Experimental Data versus Code Calculations for TF-106

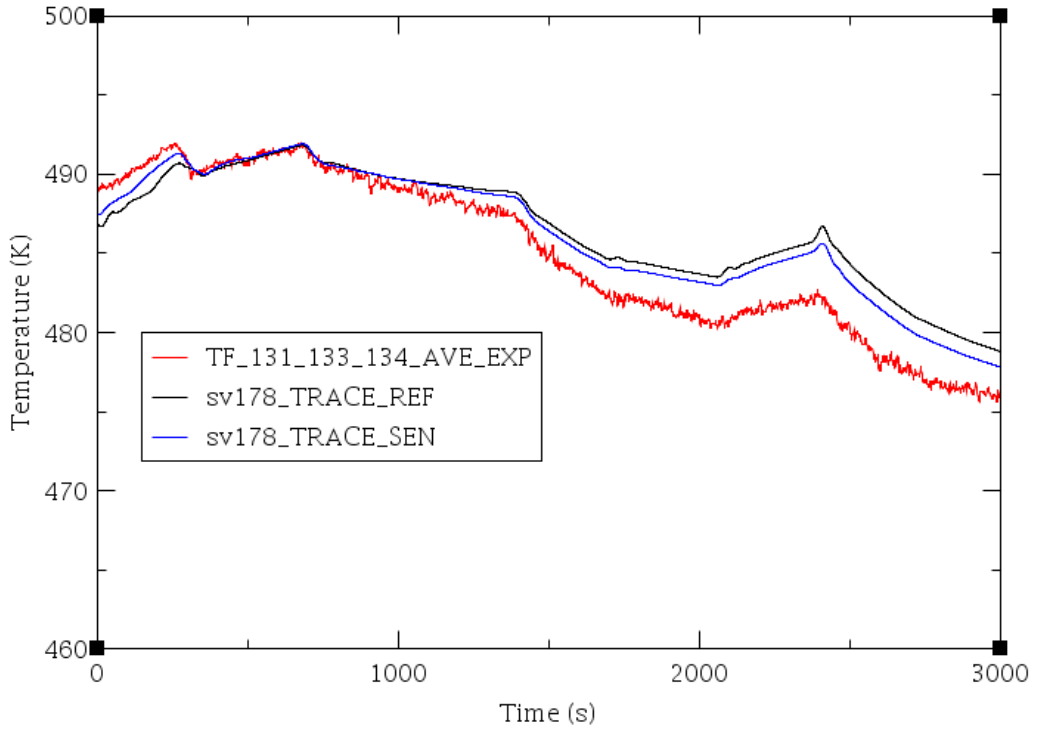

Figure B-4 Experimental Data versus Code Calculations for the Average Value of TF-131-133-134

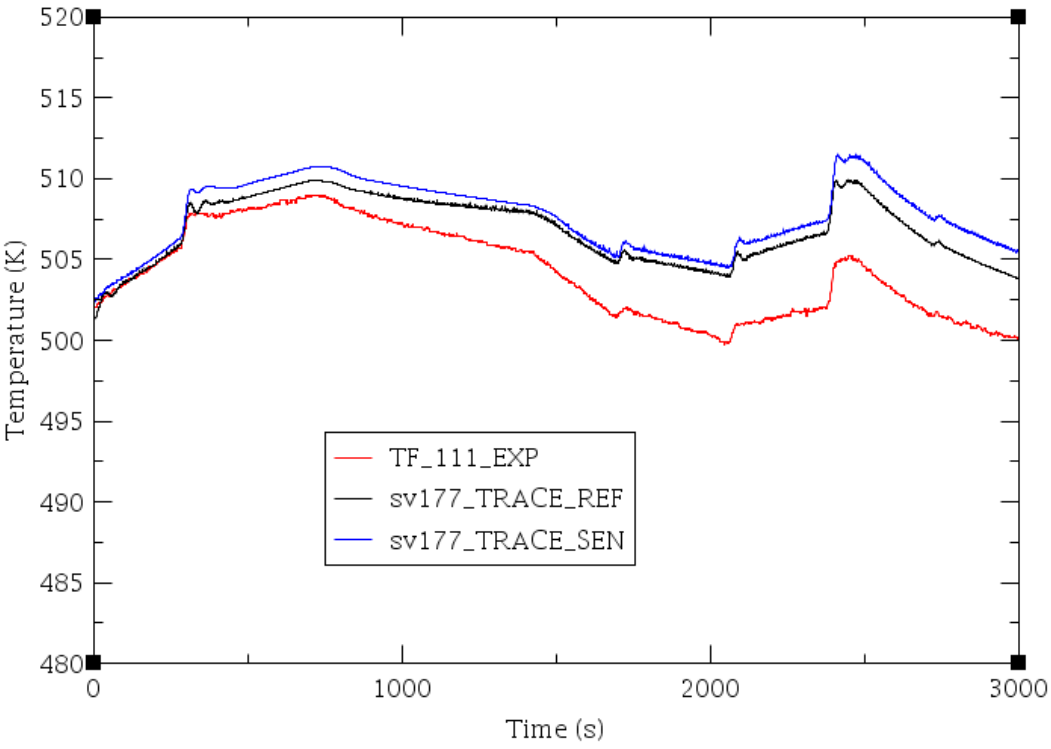

Figure B-5 Experimental Data versus Code Calculations for TF-111

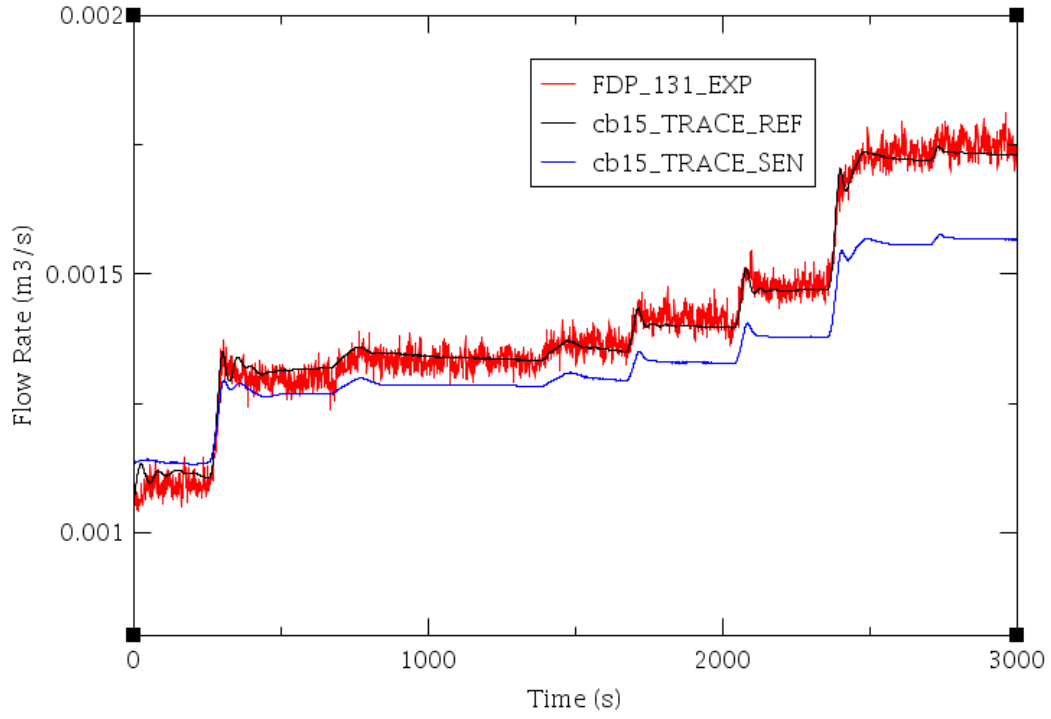

Figure B-6 Experimental Data versus Code Calculations for FDP-131

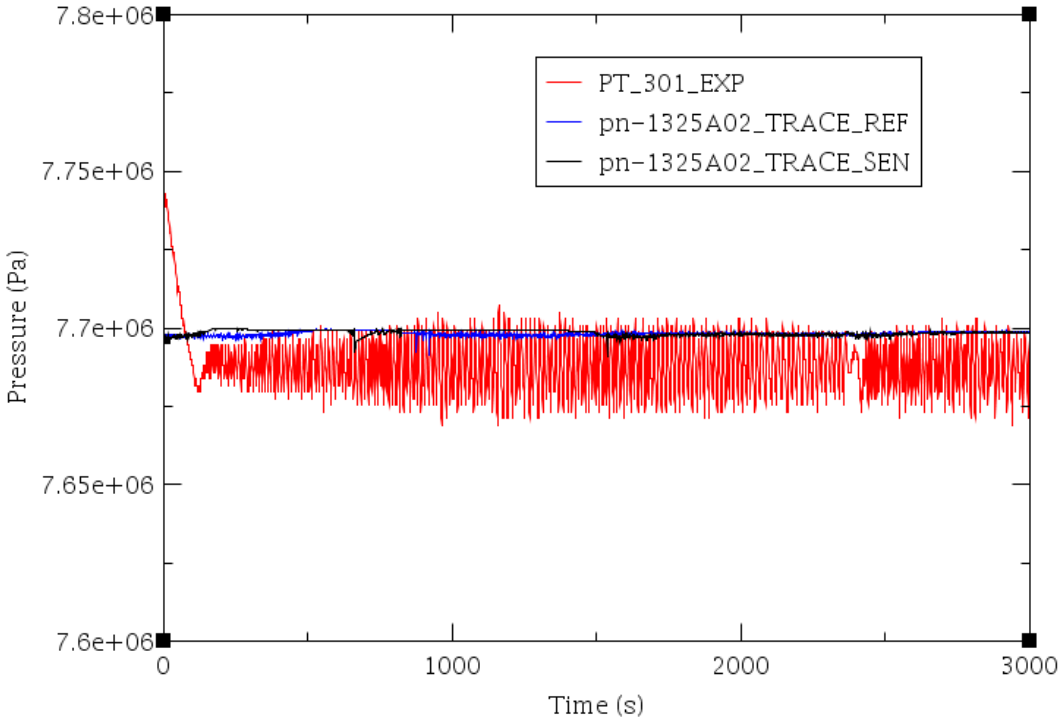

Figure B-7 Experimental Data versus Code Calculations for PT-301

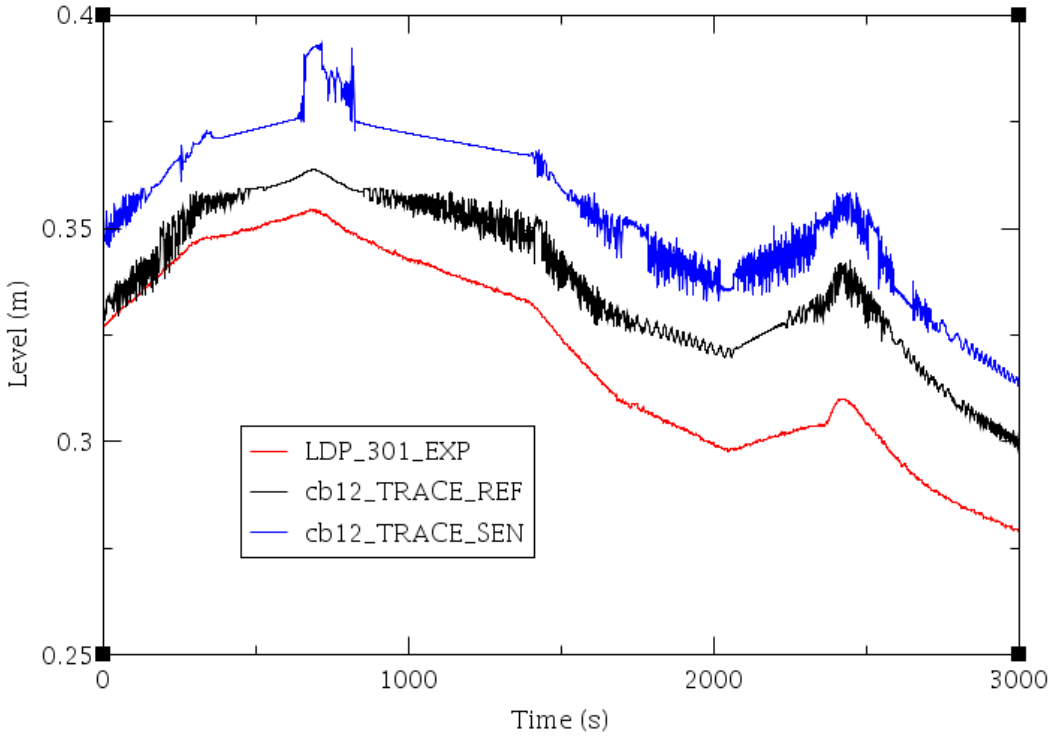

Figure B-8 Experimental Data versus Code Calculations for LDP-301

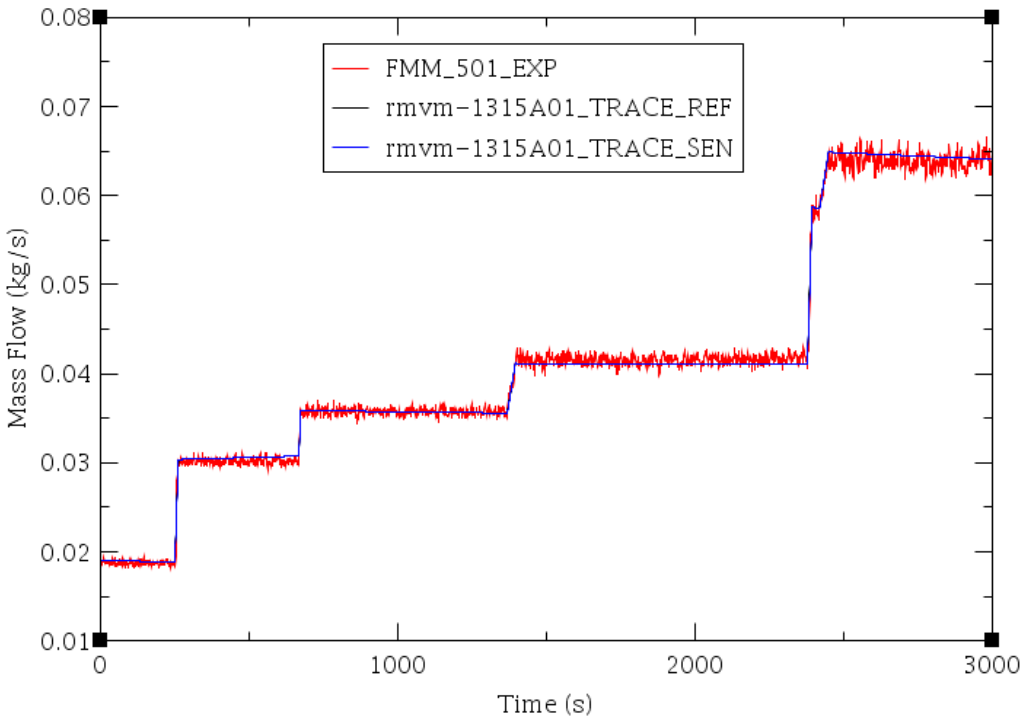

Figure B-9 Experimental Data versus Code Calculations for FMM-501

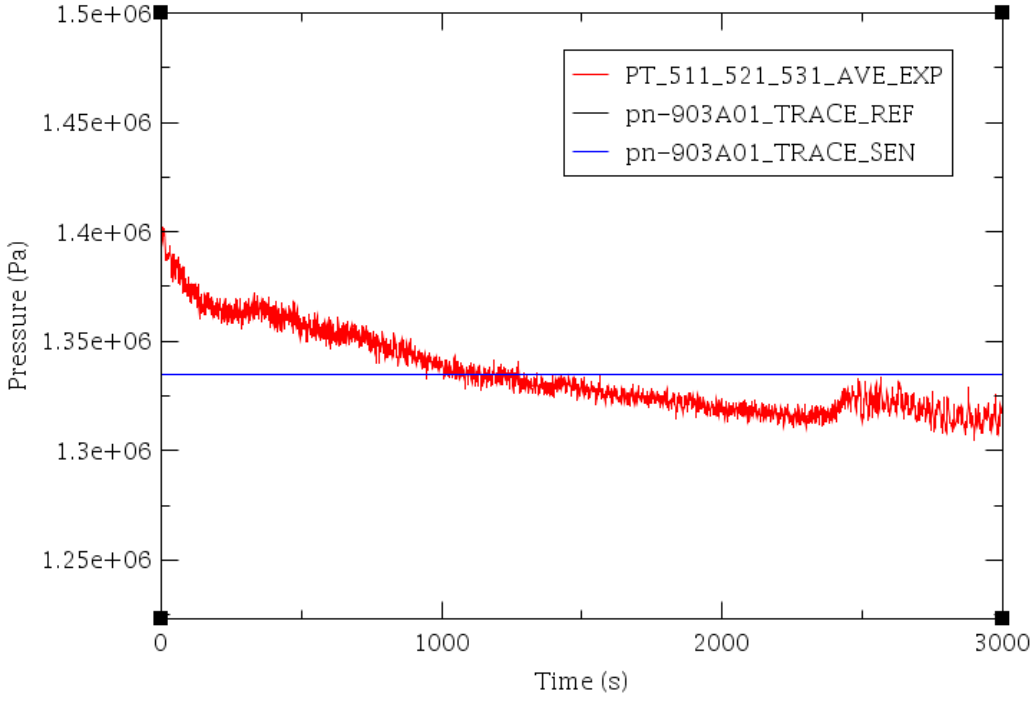

Figure B-10 Experimental Data versus Code Calculations for the Average Value of PT-511-521-531

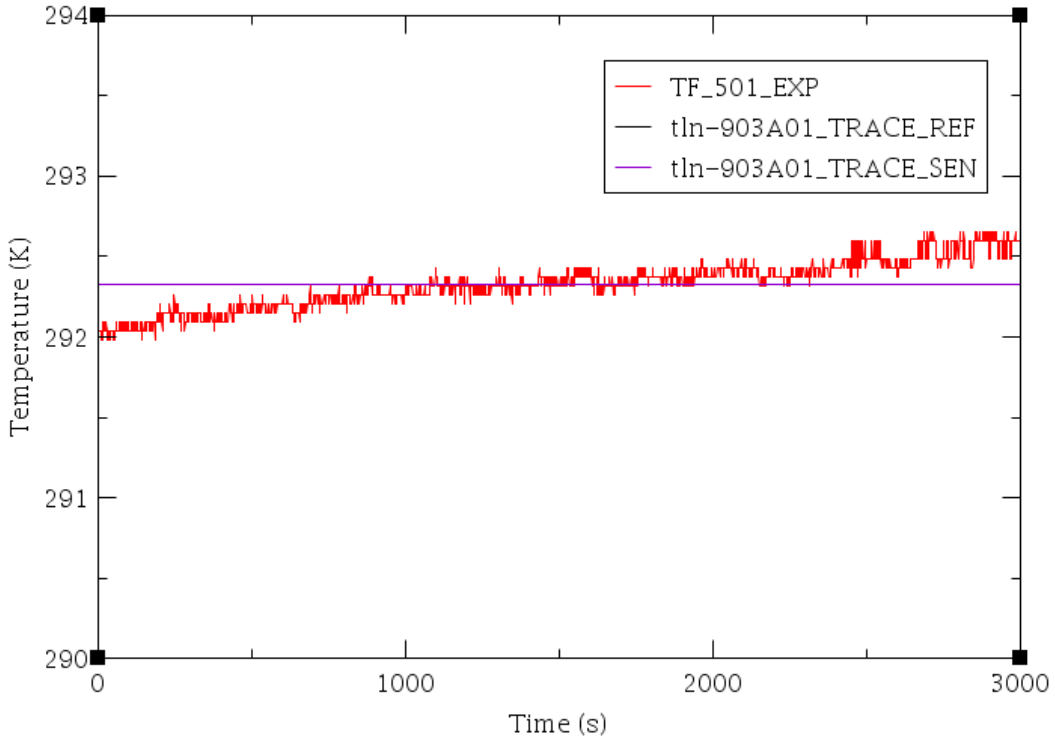

Figure B-11 Experimental Data versus Code Calculations for TF-501

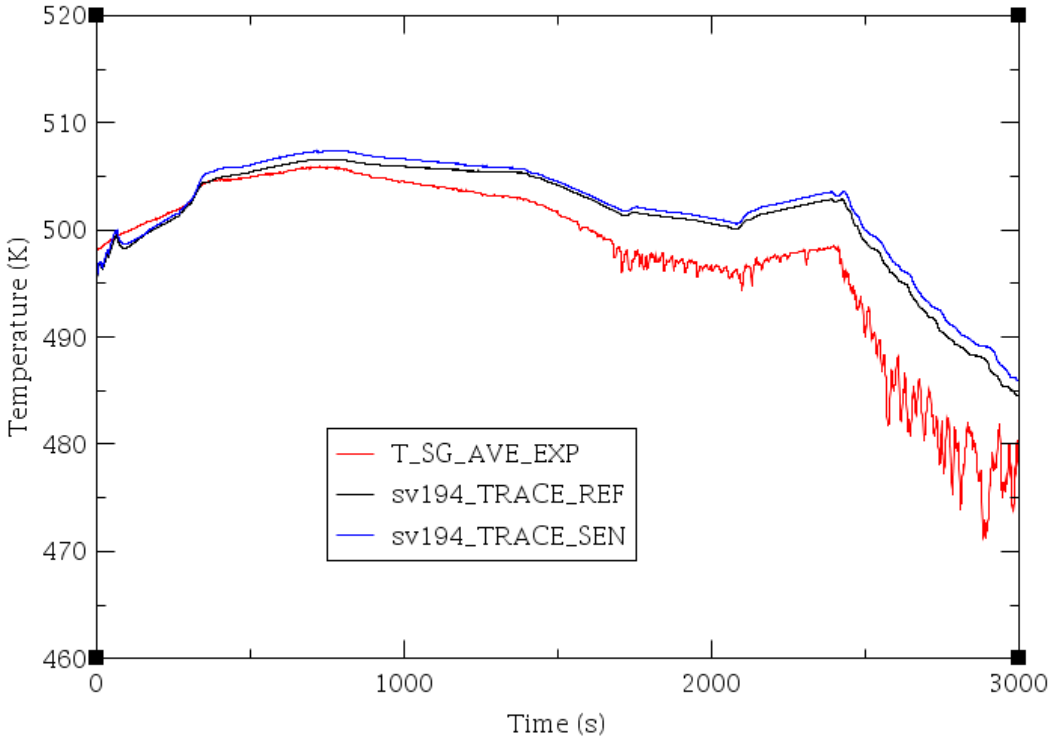

Figure B-12 Experimental Data versus Code Calculations for the Average Value of T_SG outlet (611-634)

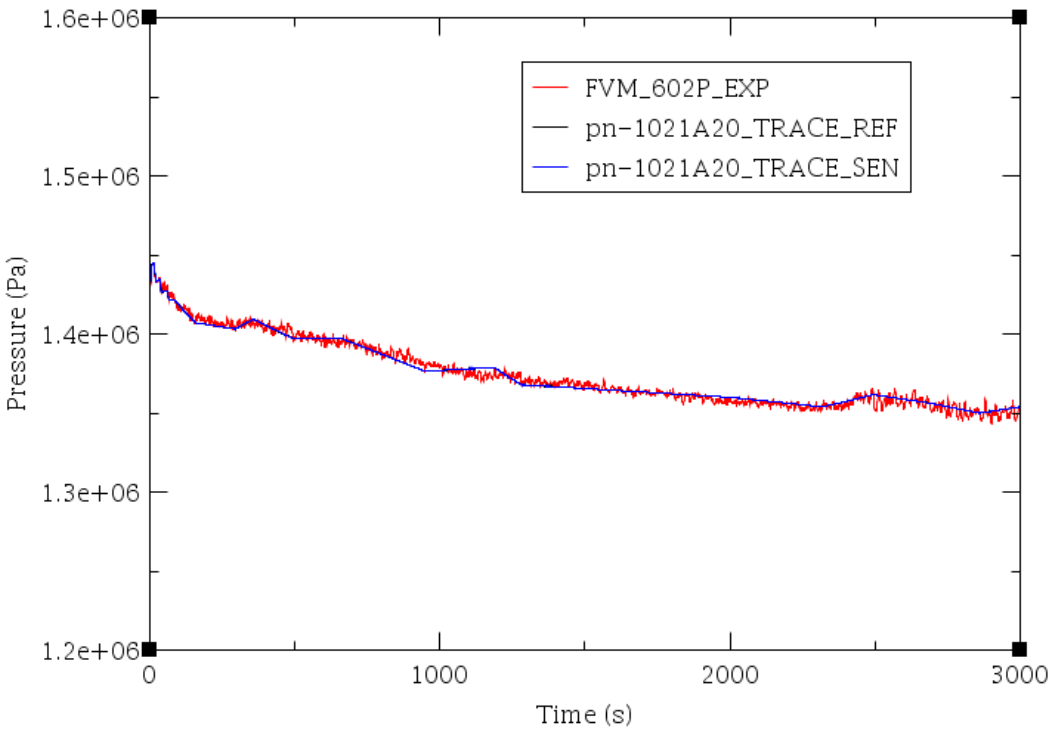

Figure B-13 Experimental Data versus Code Calculations for FVM-602 P